Theses   Electronic Theses and Dissertations

12-2015

Numerical Validation of Cooling Performance of Phase Change Materials Integrated Into Heat Sinks for Electronics Cooling

Shaimaa Mohamed Abu Ayyan

Follow this and additional works at: https://scholarworks.uaeu.ac.ae/all_theses

Part of the Mechanical Engineering Commons

Recommended Citation

United Arab Emirates University

College of Engineering

Department of Mechanical Engineering

NUMERICAL VALIDATION OF COOLING PERFORMANCE OF PHASE CHANGE MATERIALS INTEGRATED INTO HEAT SINKS FOR ELECTRONICS COOLING

Shaimaa Mohamed Abu Ayyan

This thesis is submitted in partial fulfilment of the requirements for the degree of Master of Science in Mechanical Engineering

Under the Supervision of Dr. Mohammad O. Hamdan

December 2015

Declaration of Original Work

I, Shaimaa Mohamed Abu Ayyan, the undersigned, a graduate student at the United Arab Emirates University (UAEU), and the author of this thesis entitled "*Numerical validation of cooling performance of phase change materials integrated into heat sinks for electronics cooling*", hereby, solemnly declare that this thesis is my own original research work that has been done and prepared by me under the supervision of Dr. Mohammad O. Hamdan, in the College of Engineering at UAEU. This work has not previously been presented or published, or formed the basis for the award of any academic degree, diploma or a similar title at this or any other university. Any materials borrowed from other sources (whether published or unpublished) and relied upon or included in my thesis have been properly cited and acknowledged in accordance with appropriate academic conventions. I further declare that there is no potential conflict of interest with respect to the research, data collection, authorship, presentation and/or publication of this thesis.

Student's Signature: _____   Date: _____

Advisory Committee

1) Advisor: Dr. Mohammad O. Hamdan

Title: Associate Professor

Department of Mechanical Engineering

College of Engineering, UAE University

2) Co-advisor: Dr. Ahmed Hassan

Title: Assistant Professor

Department of Architectural Engineering

College of Engineering, UAE University

Approval of the Master Thesis

This Master Thesis is approved by the following Examining Committee Members:

1) Advisor (Committee Chair): Dr. Mohammad O. Hamdan

   Title: Associate Professor

   Department of Mechanical Engineering

   College of Engineering, UAE University

   Signature _____   Date _____

2) Member: Dr. Ahmed Hassan

   Title: Assistant Professor

   Department of Architectural Engineering

   College of Engineering, UAE University

   Signature _____   Date _____

3) Member: Dr. Emad Elnajjar

   Title: Associate Professor

   Department of Mechanical Engineering

   College of Engineering, UAE University

   Signature _____   Date _____

4) Member (External Examiner): Professor Phillip Eames

   Title: Professor

   Department of Mechanical Engineering

   Institution: University of Loughborough

   Signature _____   Date _____

This Master Thesis is accepted by:

Dean of the College of Engineering: Professor Mohsen Sherif

Signature _____   Date _____

Dean of the College of the Graduate Studies: Professor Nagi T. Wakim

Signature _____   Date _____

Copy ____ of ____

Abstract

This study aims to analyze the cooling performance of phase change materials (PCMs) integrated into metallic heat sinks (HSs) both experimentally and numerically. For the experimental part of the study, a test setup has been constructed to test PCM integrated heat sinks. The heat sinks are prepared as metallic containments having fins with fixed inter-fin spacing. The volume between the heat sink fins is filled with PCM namely: a paraffin wax, salt hydrate-calcium chloride and milk-fat, then the whole system is sealed for testing under various heat loads at 4W, 6W, 8W and 10W. Four modes of operation are experimentally tested in this study: HS under natural convection, HS integrated with PCM under natural convection, HS under forced convection, and HS integrated with PCM under forced ventilation. The temperature of heat generating surface and the heat sink surface are monitored over time to evaluate the PCM thermal performance. From the results, the time lag and temperature drop in case of with PCM compared to without PCM shows the cooling effect of adding PCM under both natural and forced ventilation modes of heat removal. It found that inclusion of each of the three types of PCM into heat sinks with natural convection shows higher temperature drop (up-to 15 °C) in first 15 min of heating than inclusion of fan (forced convection) without PCM. However, the combination of both the fan ventilation and the PCM always maintain the lower temperature other three modes. This leads to conclusion that implementing a PCM in the heat sink will be very useful in thermal management of the electronic device and the application is more suitable under cyclic thermal loading conditions since in all cases the PCM completes melting in certain time and then shows a temperature rise. It is recommended to use forced convection combined with PCM filled in HS to increase the cooling effect while using PCM will be recommended for short time operation or cyclic operation such as switching operations where PCM can be regenerated to solid during off duty cycle to be ready for the next cycle of heat absorption. It is also recommended to use PCM integrated into a HS to provide a backup passive cooling support especially in case of failure of the fan system during operation as an additional safety cover. For the numerical part of the study, a three dimensional transient heat transfer numerical model using commercial ANSYS CFD software is developed and is validated against the experimental results. Next the numerical model is used to optimize the heat sink geometry, the PCM amount and the

cooling-heating response in order to identify potential applications in electronic packaging in terms of temperature drop and charging-discharging cycle time. From parametric study, it is observed that a narrow melting point, not mixing of the PCM, good thermal conductivity, higher density, rectangular fin type and a reasonable package size are optimum for the temperature control of electronic devices employing heat sink with PCM.

Title and Abstract (in Arabic)

التحقق العددي من صحة الأداء العملي للمواد المتحولة حالتها الفيزيائية من الصلبة إلى السائلة، والمعبئة في المصارف الحرارية خلال استخدامها في عملية تبريد الأجهزة الكهربائية

الملخص

الهدف من هذه الأطروحة هو إجراء التحليل العملي والعددي لاختبار أداء المواد المتحوّلة حالتها الفيزيائيّة من الحالة الصلبة إلى الحالة السائلة (Phase change material) في عملية تبريد الأجهزة الكهربائية من خلال دمجها في مصارف الحرارة المعدنية (Heat sink).

بالنسبة للجزء التجريبي للدراسة؛ فقد تمّ إعداد الجهاز بطريقة تتناسب مع طريقة إجراء تقييمات مختلفة للمواد المتحولة حالتها الفيزيائية، والمعبئة في مصارف الحرارة المعدنية. وقد تمّ إعداد مصارف الحرارة المستخدمة في هذه الدراسة على هيئة أحواض فلزية تمتص الحرارة، مع احتوائها على عدد محدد من الزعانف المعدنية على أبعاد متساوية من بعضها البعض. ثمّ تم تعبئة الفراغ بين هذه الزعانف بالمواد المتحولة حالتها الفيزيائيًا؛ وهي كالآتي: شمع البارافين (Paraffin Wax)، وملح كلوريد هيدرات الكالسيوم (Calcium Chloride Hydrate)، والحليب الدسم (Milk-Fat). تم تعريض النظام بأكمله لأحمال حرارية: 4 و6 و8 و10 وحدات أحمال حرارية. ثم تم اختبار أربعة أساليب تجريبيًا في هذه الدراسة، وهي كالآتي: مصارف حرارية معرضة لتهوية الطبيعية، ومصارف حرارية معبئة بالمواد المتحولة حالتها الفيزيائية معرّضة لتهوية القسرية، ومصارف حرارية معرّضة لتهوية القسرية، ومصارف حرارية معبئة بالمواد المتحولة حالتها الفيزيائية معرّضة لتهوية القسرية. وبعد ذلك تم رصد درجة حرارة السطح المولّد للحرارة والسطح المشتت للحرارة مع مرور الوقت لتقييم أداء المواد المتحولة حالتها الفيزيائيّة حراريًا.

بالنسبة للجزء العددي للدراسة، فقد تم تطوير نموذج عددي ثلاثي الأبعاد، يحاكي النظام الذي تم استخدامه تجريبيًا في نقل الحرارة وذلك باستخدام برنامج تحليل عددي (ANSYS)؛ ليتم التحقق من النتائج التجريبية المستخرجة مسبقًا. بجانب ذلك تم استخدام النموذج العددي لتحسين هندسة المصارف الحراريّة، واختيار أفضل كمية مستخدمة من المواد المتحولة حالتها الفيزيائية

للحصول على أفضل النتائج في عملية التبريد؛ من أجل تحديد التطبيقات المحتمل استخدام هذا النظام فيها بطريقة فعّالة.

ومن خلال النتائج: تبيّن وجود انخفاض في الفارق الزمني، ودرجة الحرارة في حالة استخدام المواد المتحولة حالتها الفيزيائية مقارنة مع عدم استخدامها. كما ظهر تأثير التبريد وإزالة الحرارة خلال استخدام هذه المواد وتعريض المصارف الحرارية مختلف وسائط التهوية (الطبيعية والقسرية). وأظهرت النتائج أن تعبئة كل من الأنواع الثلاثة السابق ذكرها من المواد المتحولة حالتها الفيزيائية في المصارف الحرارية في حالة التهوية الطبيعية يظهر أعلى انخفاض في درجة الحرارة (يصل إلى 15 درجة حرارية) في أول 15 دقيقة من التدفئة مقارنة مع استخدام المراوح كتهوية قسرية من دون استخدام المواد المتحولة. ولكن استخدام هذه المواد لفترات طويلة أظهر ارتفاعًا في درجات الحرارة مقارنة مع نتائج التبريد في حال استخدام المواد ذاتها لفترة زمنية أقصر. ومع ذلك، فإنه تبين أن الجمع بين كل من مراوح التهوية، واستخدام المواد المتحولة يعطي نتائجًا أفضل في خفض درجة حرارة الأجهزة.

وفي الختام، ينصح باستخدام التهوية القسرية من خلال المراوح جنبًا إلى جنب مع المواد المتحولة حالتها الفزيائية في المصارف الماصّة للحرارة؛ لزيادة تأثير التبريد أثناء الاستخدام. كما يتمّ التوصية باستخدام هذا النظام في التطبيقات قصيرة المدى الزمني، أو إجراء التشغيل الدوري لها حتى تتمكن هذه المواد من العودة إلى حالتها الصلبة خلال دورة توقفها عن العمل؛ مما يتيح هذا التحوّل إمكانية الاستعداد للدورة المقبلة من امتصاص الحرارة. كما توصي الدراسة باستخدام هذه المواد ودمجها في المصارف الماصّة للحرارة لتوفير نسخة احتياطية بمثابة غطاء سلامة إضافي لدعم التبريد، وإزالة الحرارة خصوصًا في حال فشل نظام المراوح المستخدم للتبريد خلال هذه العملية.

مفاهيم البحث الرئيسية: المواد المتحولة حالتها الفيزيائية، أنظمة تبريد، الأجهزة الكهربائية، مصارف الحرارة.

Acknowledgements

Dedication

To my beloved husband

To my respected father & mother

To my family

To my "Jouri"

Table of Contents

List of Tables

List of Figures

List of Abbreviations

List of symbols

A	Area (m^2)
C_p	Specific heat (J/kg K)
C_v	Constant volume specific heat (J/mol K)
h	Heat transfer coefficient
H	Height (m)
I	Current (Amp.)
k	Thermal conductivity (W/m °C)
L	Length (m)
$\dot{m}$	Mass flow rate (kg/sec)
m	Mass (kg)
Nu	Nusselt Number
n	Number of Fins
P_{atm}	Atmosphere pressure (Pa)
Pr	Prandtl number
$\dot{Q}$	Heat transfer rate (W/sec)
q	Heat transfer flux (W/m^2)
Re	Reynolds number
T	Temperature (° C)
t	Thickness (m)
V	Voltage (V)
W	Width (m)

Greek symbols

η Efficiency

μ Dynamic viscosity

ν Kinematic Viscosity

ρ Density

Abbreviation

AC	Alternative current
AlSiC	Silicon carbide in aluminum matrix
CFD	Computational fluid dynamic
DAQ	Data acquisition
DC	Direct current
DSC	Differential scanning calorimetric
Dymalloy	Diamond in copper-silver alloy matrix
FEM	Finite element
HS	Heat sink
IC	Integrated circuit
LABVIEW	Laboratory Virtual Instrument Engineering Workbench
LHTMS	Latent Heat Thermal Management System
PCM	Phase change material
WOPCM	Without Phase change material
WPCM	Without Phase change material

Subscripts

atm	Atmosphere
Avg.	Average

b	Base
F	Fin
F	Forced
h.g.	Heat gain
h.l.	Heat loss
H.S.	Heat Sink
in	Inside
L	liquid
N	Natural
out	Outside
S	Solid
Tot	Total

Chapter 1: Introduction

1.1 Objectives of the thesis

The objective of this work is to design and optimize a novel heat sink (HS) containing phase change materials (PCMs) for thermal management of electronic devices subject to higher heat loads. To achieve this objective, various PCMs are integrated to the HS. PCMs are considered a suitable candidate to enhance HS performance due to their nature of isothermal heat absorption at the phase transition temperature.

The method adopted is to exploit PCM-integrated HS mechanism in order to restrict the integrated circuit (IC) temperature under allowable limit for safe electronic performance, and to increase the time lag to reach the peak temperature in order to protect the IC from failure during a cyclic operation such as diode switching.

The study investigates and optimizes the HS performance for cooling the electronic packaging by integrating PCMs through temperature drop and time lag for different power inputs to a heat generating surface. The experiments are used to validate the numerical simulation, while the validated numerical model is utilized to optimize the constructed integrated PCM heat sink.

1.2 Thesis Methodology

In order to have a better understanding of PCM cooling performance in electronics packaging, both experimental and numerical simulation methodologies are adopted. The Numerical simulation is executed under different design parameters in order to observe and evaluate the cooling performance of different types of PCMs.

The numerical simulation is conducted using finite volume ANSYS-Fluent software (version 15) and results are validated experimentally. The validated numerical model is used to better understand how different parameters affect PCM heat sink system performance. The numerical parameters to be examined in this thesis are:

- Different heat generating power inputs.

- Different PCM types

- Different amounts of PCM

- Different HS geometries and designs

- Improved thermal properties (i.e. thermal conductivity)

For the experimental work, rectangular HSs with internal fins are filled with solid-liquid PCMs and are subjected to heat loads through electrical heat source. The temperature on the heat-generating surface and the HS surfaces are monitored to understand the heat transfer mechanism and cooling performance of the system. Different solid-liquid PCMs (namely paraffin waxes, salt hydrates and milk-fat) are evaluated to compare the material performance. Different heat loads ranging from 4W to 10 W are studied to understand heat generation and dissipation at different power levels representing different IC operating points. An analytical thermodynamics model is developed and iterated using ANSYS-Fluent software to have a better understanding of the cooling performance.

In the proposed set of experiments, a DC power supply is used to generate different heat loads. Hence, different parameters are measured, namely, input voltage, input current, heat generating surface temperatures and HS temperature The

experimental data is recorded using a data acquisition system. The experimental parameters addressed in the measurement setup are:

- Different heat generating power inputs.

- Different PCM materials (which mean different thermal properties such as conduction coefficient, convection coefficient, heat capacity and latent heat of fusion).

- A fixed geometry of HS, fin types, fins spacing and amount of PCM.

1.3 Thesis Outcomes

This work focuses on investigating the thermal performance of a PCM integrated HS system, and evaluating the appropriate optimized HS. Therefore, the main thesis outcomes are:

- The identification of suitable PCMs as heat removal material in electronic packaging.

- An optimized HS design.

- An improved thermal response for electronic packaging to heat load.

- Additional experimental data that can enrich the literature with more insightful knowledge of cooling performance of different types of PCMs under different heat loads.

1.4 Thesis structure

The thesis divided into six chapters includes the introduction of the thesis presented in chapter 1. In chapter 2, a literature review is presented in which recent developments in the field of PCM integrated into HSs are discussed. The chapter

presents the role of HS in cooling systems especially the electronic applications and the effect of integrating of phase change material into HS. The literature cover wide range of work including experimental and numerical studies.

In chapter 3, the experiments and the collected data carried out during thesis work are presented for a HS with PCMs under different design parameters. The schematics of experimental setup for all tested modes of operation are explained. The chapter also presents experiments details and uncertainties in the measured quantities.

In chapter 4, the numerical analysis for a HS with PCMs is reported including mesh independent study and experimental validation. The validated numerical model is used to optimize the integrated PCM heat sink. The numerical parameters and the data used in the CFD software are also presented in this chapter.

In chapter 5, the parametric analysis, the experimental and the numerical results are presented. In this chapter a detailed description of the collected data are discussed.

In chapter 6, the conclusions drawn from this thesis work are presented. Based on the experimental and numerical work different recommendations for the way forward are presented.

All used references are listed in the bibliography section at the end of the thesis.

Finally, Appendix are supplementary material supported the research including figures and tables for further explanation about some mentioned information in the thesis.

Chapter 2: Literature Review

The dramatic growth in the electronics packaging market is driven by the development of compact multi-purpose electronic devices. The extended use of these devices may cause many of them to overheat and, as a result, may lead to a drop in their performance efficiency. Hence the demand for effective electronics thermal management has grown dramatically to meet the strong growth in the electronics market.

In recent years, the thermal management took two approaches; the first one focuses on-chip cooling while the second one focuses on circuit board cooling. The maximum allowable temperatures of most chips range from 85 °C to 120 °C [1]. It is recommended to keep the temperature of chip and other functional electronic components below allowable maximum temperature at all times during normal operation to avoid any malfunction of the electronic devices [2]. The most popular approach used to cool many older electronic devices is the conventional forced convection cooling technique using HSs and fins to increase the rate of heat transfer and decrease the device components' temperature accordingly. Forced convection, using fans, is an enhanced technique applied to improve the heat transfer rate between the heated electronic device and the ambient air. However, these traditional approaches may not be effective and feasible for some newer electronic applications due to many reasons such as manufacturing cost, size, power consumption, system reliability, weight, noise, and aesthetic constraints [3].

2.1 Heat sink development and applications

In most electronic systems, HSs are widely used as heat exchangers to cool a device by dissipating heat from the hot surface into the surrounding medium. Generally, the HS is a metal object brought into contact with a hot surface.

The HS is usually described as a metal structure consisting of one or more flat surfaces that are in good thermal contact with the components to be cooled. An array of fins is the main component in this structure that helps increase the surface contact with the cooler ambient, usually air [4]. For more improvement in cooling, the HS is often used in conjunction with a fan to increase the rate of airflow over the HS. This combination of HS and fan is known as a forced air system that allows a larger temperature gradient by replacing warm air faster than normal convection system [5].

2.1.1 Heat sink principle

HS operate by efficiently transferring thermal energy from a high temperature object (source) to a lower temperature object (sink) with a greater heat transfer capacity. As a result, this rapid thermal energy transferring leads to quick thermal equilibrium condition between the two objects, thus fulfilling the HS's role as a cooling device [6]. The HS efficiency depend on how fast thermal energy transfer from heated element to the HS, and from the HS to ambient. The high thermal conductivity of the HS material combined with its large surface area result in the rapid transfer of thermal energy to the surrounding cooler air. This process cools the HS and other objects that in direct thermal contact with it [7].

2.1.2 Heat sink design

A HS configuration contains an array of fins, the extended surfaces from the HS base used to increase its surface area and improve the heat transfer process. However, this is not always allowable and a larger HS surface area cannot be always achieved due to space limitation in most electronic devices [8]. The fin shape has an impact on the heat transfer rate in that different shapes have different surface area to volume ratio hence a fin shape can be optimized to render maximum heat transfer [9, 10]. The fin's cross-sectional shape can be cylindrical, rectangular, elliptical or square. A variation calculus technique has been used to find out the optimum fin shape used in cooling systems [11]. Various shapes of longitudinal straight fin HSs have been experimentally examined [12]. Different fin configuration have been tested and the Pin fin configuration is reported to achieve higher surface area in a given volume consequently achieving the maximal heat transfer rates. Aluminum finned HSs with two different shapes, namely, the rectangular pin-shaped, and elliptical pins in low air flow environments. It was reported that the aforementioned fin have nearly equal thermal resistances. However elliptical pin occupying much smaller volume [13]. Another configuration addressed is the flared fin HS where fins are not parallel was tested. It was found that thermal performance of the flared HS is the best among the other tested HS configurations [14-15].

Cavities (inverted fins) embedded in a heat source, are defined as the regions formed between adjacent fins [16]. Since 2004, many researchers have been motivated to find the optimal cavities that minimize the peak temperature (hot spot) of heat generating bodies. Different four cavity shapes: rectangular, elliptical, and triangular and a T-shaped cavity penetrating into a conducting wall have been studied [17]. The

authors demonstrated that the rectangular cavity performs better than the elliptical and triangular ones. [18-19].

2.1.3 Heat sink materials

Ideally, HSs are made of good thermal conductors such as silver, gold, copper, or aluminum alloy. Copper and aluminum are among the most-frequently used materials for this purpose within electronic devices [20] . Copper has excellent heat transfer characteristics in terms of its thermal conductivity but it is significantly expensive than aluminum. Aluminum has the significant advantage that it can be easily formed by extrusion, thus making complex cross-sections possible. Aluminum is also much lighter than copper, offering less mechanical stress on delicate electronic components [21]. Composite materials and alloys also are used as HS material such as copper-tungsten pseudo alloy, AlSiC (silicon carbide in aluminum matrix) and Dymalloy (diamond in copper-silver alloy matrix), are also used as HS materials [22].

2.1.4 Heat sink performance

Performance and durability of many industrial components rely on effective heat transfer, i.e., the maximum heat removal in the allowable space and using the least amount of materials [23]. The cooling performance of the HS is mainly function of the HS material, HS geometry, and heat transfer coefficient from HS surfaces [24]. Generally, combined with forced convection the thermal performance of HS is improved by increasing the thermal conductivity of the HS materials, increasing the surface area (usually by adding extended surfaces, such as fins or foam metal) and by increasing the overall area heat transfer coefficient (usually by increase fluid velocity, such as adding fans, pumps, etc.) [25].

2.1.5 Heat sink applications

HSs are mainly used in most of the electronic applications that require cooling for their components and reduced temperature rise during operation. The microprocessor cooling system is one popular example of the HS application which ensures that the microprocessor components do not overheat [15]. Therefore, the HS is used to transfer heat from the device to the surrounding environment. In computers, HS are used to cool the central processing units or graphics processors [26]. Another example of HS applications is the light- emitting diode lamp. The performance and life of such lighting systems are strongly a function of its temperature and in which eventually depends on how efficiently the heat is being dissipated from the HS [27].

2.2 Phase change material implementation in heat sink

2.2.1 Phase change material characteristics

The importance of thermal management and cooling approach for most of the electronic devices is increasingly growing as the new generation of electronic products squeeze more power into very small packages. This demands further improvement in the characteristics of cooling systems used in these devices. Therefore, recently many HSs are constructed of multiple types of material with desirable characteristics such as, phase change materials (PCMs), which have high energy storage capacities due to their latent heat of fusion [28].

PCMs have been used as temperature regulators in different applications [29-30]. PCM-based cooling system can preserve the compactness and light-weight advantages compared to conventional thermal management system [31]. PCM melts and solidifies at a specific temperature and is capable of storing and releasing a large

amount of energy. Thermal energy is absorbed when the material changes from solid to liquid and is released when the liquid solidifies. The cooling process using the PCM can be classified into three phases. In phase 1, heat from the electronic device is absorbed to gradually raise the temperature of the solid material to its melting point. In phase 2, the PCM starts to melt at a constant temperature. During this phase change, heat is absorbed without rise in the temperature. There might be a small volume change during the transition from the solid to liquid state based on thermal expansion characteristic of the PCM. In phase 3, once the solid PCM has fully melted, the temperature of the liquid PCM rises if heat is continually supplied. Although the PCM can absorb a large amount of energy during the phase change process, its cooling effectiveness may be limited to the time duration for the solid material to turn completely to liquid [32]. Therefore, PCMs are recommended to be used in situations where heat dissipation is periodic or suddenly transient [33].

2.2.2 PCM theoretical and experimental studies

Theoretical and experimental studies based on using PCM in electronic cooling have yielded extensive literature on various aspects of the phase-change problems. As early as in 1971, the relationship between PCM and other thermal control techniques was discussed [34]. The authors provides detailed data about, the material properties of PCMs. They addressed the engineering considerations relevant to PCM systems design. In addition, an extensive review of the physical phenomena associated with phase change in various geometries have presented [35].

Another review dealt with classification of PCM and their properties, heat transfer, and applications in energy storage. The review reflects the significant progress made in the field during the last two decades. The selection of PCM material

for implementation in the cooling system was also addressed [36]. The PCM should have a melting temperature below the device's maximum operating temperature, a high latent heat of fusion per unit mass, a high thermal conductivity, a high specific heat and a small volume change during phase change [37].

On the other hand, unfortunately, most of the available PCMs have relatively low thermal diffusivities in both the liquid and solid phases. Thus inserting fins inside the PCM have been subjected in order to improve its heat transfer capabilities due to the high thermal conductivity paths created by the incorporated metal elements. These paths decrease the thermal gradients in the PCM and allow the maintenance of the temperature across it closer to the melting temperature of the PCM [38].

2.2.3 Application of Phase change material

PCMs are generally used in a wide range of applications including solar thermal systems [39], desalination [40], heat recovery [41], buildings [42-43], and refrigeration [44].

In addition, PCM implemented in HS are used in thermal management of electronics [45-46], spacecraft [47-48], smart textiles [49], personal computing, communication equipment, power electronic equipment and portable phones [28].

2.3 Experimental and modeling study related to heat sink

2.3.1 Experimental analysis

Numerous researchers have focused their attention on using extending fins inside PCM. Cooling effect produced by integrating PCM in electronic packaging was studied with a one dimensional heat transfer model for design optimization [50] and

[51]. Experimentally PCM integrated in aluminum foam with conductive fins have been proven to achieve higher cooling compared to natural cooling, aluminum foam only cooling and PCM only cooling [52-53]. An experimental study on PCM stored in finned enclosure for cooling application have been conducted [54]. The effects of various parameters such as power levels, number of fins, fin height and fin thickness on the HS performance were evaluated. It was shown that increasing the number of fins and fin height can improve the overall thermal performance, while increasing the fin thickness yielded a slight effect. The thermal performance of PCM confined between different configurations of inserts have experimentally examine. It was indicated that increasing fin number for the HS with parallel/crossed fins can enhance heat transfer leading to reduced peak temperatures. Moreover, several authors carried out studies on melting process into PCM with partial fins [55].

Researchers have investigated various configurations of HS units and found several potential engineering applications; for example, low temperature storage unit [56], refrigeration system for refrigerated trucks [57], management of vehicle heat [58], cooling of photovoltaic (PV) devices [59] and electronics cooling [60-61].

2.3.2 Numerical analysis

Numerical studies on PCM filling a rectangular enclosure with horizontal fins heated from one side was carried out [62]. It was concluded that the natural convection effects have improved when the PCM thickness within the fins was large. Moreover, the performance of a metallic container enclosing a series of vertical aluminum fins embedded in a PCM (Aristowax) have been have investigated numerically [63]. In their study, they investigated the thermal performance by varying the number of fins, while the total used mass for PCM as well as aluminum were kept constant during the

simulation run. The authors report that a significant improvement in the thermal performance of the system will take a place by increasing the number of fins while also making the temperature distribution across the heat source nearly isothermal. However, results show that a very large number of fins does not lead to any significant additional gain in the thermal performance.

A numerical investigation of model consists of PCM combined with internal fins have conducted [64]. It was found that the maximization of critical times can be achieved when the latent heat thermal management system (LHTMS) geometry is designed such that complete melting of all the PCM is achieved simultaneously when the critical temperature is reached. In the same aspect, PCM melting injected in a finned rectangular enclosure have analyzed. Four different fin shape configurations, namely, straight fin, T-shape fin, Y-shape fin and cross-shape fin were compared to eight straight fins configuration. Through analysis and simulations they demonstrated a marginal improvement in heat transfer [65].

The geometry of a PCM heat sink subjected to a constant heat flux under forced convection to the surroundings at the top have numerically optimized, using a finite-difference model implemented in MATLAB. The optimization is performed with a sole aim of minimization of the critical time needs for the HS to reach the maximum allowed temperature. Through simulation, they found that a small gap between the fin tip and the top of the enclosure should exist. The optimal volumetric PCM percentage obtained in their study was 72.5% for a heat flux of 16 kW/m^2. Another interesting conclusion was that the isotherms of the PCM were nearly parallel to the longitudinal fin [66].

The melting in a heat storage unit with vertical internal aluminum fins have explored numerically [67-68]. Two and three dimensional transient simulations were performed using the Computational Fluid Dynamics (CFD) method. In a detailed parametric investigation, it was demonstrated how the melting process is affected by changes in the geometry of the system and boundary conditions. The analysis was conducted both for constant temperature and constant heat flux boundary conditions at the base of the heat storage device. Consistent results were obtained for both cases. However, it appears that for a constant heat flux at the base, fin efficiency considerations could not be used for generalization.

In a recent study, Optimizing composite HSs by considering internal fins with trapezoidal and parabolic shapes have attempted [69]. Although these shapes did not yield any advantage during melting, studied the rectangular-shaped fins with optimal dimensions. The others concluded that, for these shapes, the time required for total re-solidification was much lower. The research proposed to perform a multi-objective optimization, where a compromise is made with regard to the critical time, in order to achieve a shorter period of re-solidification [64].

An optimization procedure for the design of a Latent Heat Thermal Management System (LHTMS) used for cooling an electronic device with transient and high heat generation have been numerically explored [70]. The subjected system consists of a HS that integrates PCM between its fins. The study aimed to minimize the LHTMS height, without exceeding the maximum allowable temperature of HS. Two dimensional, three-parametric, finite element (FEM) simulations are performed, with systematically varying both the number and thickness of the fins under several LHTMS heights. The optimized results show that optimal PCM percentages are

inversely related to the range of temperatures expected in the PCM, when critical temperature is reached at the interface thus concluding the relation between fin length and the PCM temperature. It was found that as the length of the fins and the interface heat flux are reduced, the temperature range inside the PCM is expected to decrease and thus the optimal volumetric PCM percentages are expected to increase. On the other hand, decreasing the number of fins should increase the temperature range and thus reduce the optimal volumetric PCM percentages.

2.3.3 Analytical researches on heat sink

Extensive research work has been done in the area of electronic packaging cooling using HSs. A suggested analytical approach for characterizing electronic packages was presented [71]. In their study, a steady-state solution of the Laplace equation for general rectangular geometries was applied, where boundary conditions are uniformly specified over specific regions of the package. An analytical and numerical study on the heat transfer characteristics of forced convection across a micro channel HS has presented [72]. This study included two analytical approaches: the porous medium model and the fin approach. Through the result, the effect of turbulent heat transfer within the micro channel was studied and analyzed. The authors suggested a new proposed concept of micro-channel cooling in combination with micro heat pipes, and have estimated the enhancement in heat transfer due to the heat pipes.

On the other hand, a method to correct the thermal resistance of electronics components by adjusting the junction-to-ambient thermal resistance to account for operational conditions have developed [73].

The thermal performance of HSs with Parallel-Plain Fin under a given design constraint of pressure drop was predicted and optimized using an analytical technique and a thermal and hydrodynamic performance analyzers for HSs were developed [74].

Chapter 3: Experimental Setup

In this chapter, a detailed description of the used experimental setup is presented. In addition different configurations of the conducted experiments are given in the subsequent sections. Instrumentation and devices used in the experiment including thermocouples, data acquisition, heat generating source and DC power supply are also shown and described in this chapter.

3.1 Experiment Description

In this study, three different PCMs, four different operational modes and various heat load intensities are investigated. Experimental setups are prepared to suit the different set of experiments conducted in this research in order to provide a better understanding of the performance for different PCM integrated in the metallic HS. The ultimate goal of the conducted experiments is to clearly identify the effect of using PCM for cooling the electronic package and to evaluate the comparative thermal performance of different PCMs.

3.1.1 Test Setup Overview

In this study, the HSs were prepared as metallic containments with array of vertically aligned rectangular fins with optimized inter-fin spacing that are commercially available. The HS is filled with three types of PCMs, namely: a paraffin wax, salt hydrate-calcium chloride and milk-fat, and is subjected to various heat loads at 4W, 6W, 8W and 10W. The heat generating surface temperatures are monitored and plotted against time at each power input for each of the PCMs at different modes of operation. Four modes of operation are experimentally tested in this study. These are:

1) HS under natural convection,

2) HS integrated with PCM under natural convection,

3) HS under forced convection, and

4) HS integrated with PCM under forced ventilation.

3.1.2 Thermo-physical Properties of Used PCMs

PCMs have been characterized by a variety of thermos-physical properties. Generally, PCMs are selected based on higher latent heat of fusion, higher specific heat, controllable temperature stability, and small volume change during phase change [75]. Heat is stored during melting and is released during the freezing period [45]. Over last 40 years, mainly the PCMs that have been studied are hydrated salt, paraffin waxes and fatty acids [76]. The experiments conducted in this study are limited to three commercial PCMs products namely Paraffin wax-RT41, Salt hydrate-calcium chloride hexa-hydrate and Milk-fat.

Salt hydrate-calcium chloride hexa-hydrate is a well-known PCM with high volumetric storage density, relatively higher thermal conductivity, higher latent heat, higher heat of fusion and moderate costs compared to paraffin waxes as shown in (Table 1). However, it has some disadvantages which limit its applications. Salt hydrates consist of salt and water in a discrete mixing ratio which may suffer from phase segregation. Sub-cooling phenomena, lack of thermal stability and corrosion due to its chemical ingredients are other weak spots [76]. Using of extra water was suggested and claimed that this principle would prevent formation of the heavy anhydrous salt. However, it was found that this principle reduce the storage density of the material [77]. Another technique was suggested using some nucleating agent to

minimize sub-cooling such as borax [78]. But it need further work to prevent settling of high density borax [76].

Commercial paraffin waxes are one type of organic PCMs with moderate thermal storage densities and a wide range of melting temperatures. They undergo negligible sub-cooling and are chemically inert and stable with no phase segregation [79]. On the other hand, they have some disadvantages like: low thermal conductivity, low volumetric latent heat storage capacity, relatively large volume change, and flammability [80].

Milk-fat is an attractive candidate as a bio-PCM which is easily obtained from nature. This material is also safe to use since it is chemically nontoxic unlike some PCMs while it has acceptable thermal properties. The thermal properties for each of the aforementioned PCMs are described in Table 1.

The main disadvantage of the PCMs is the relatively low thermal conductivity. The researches have proposed various heat transfer techniques [46]. Some methods to improve PCM conductivity such as: using metallic fillers [81], combined the PCM with the fins [38] and using metal matrices [82-83].

Materials	Salt hydrate-calcium chloride hexa-hydrate	Paraffin wax-RT41	Milk-fat
Thermal conductivity (W/m.K)	0.6 [84]	0.2 [85]	0.29 [86]
Specific heat capacity (kJ/kg.K)	2,000 [84]	2,000 [85]	2,300 [86]
Density (kg/m^3)	1,500 [84]	802 [85]	911 [86]
Viscosity (kg/m.s)	0.00184 [84]	0.003 [85]	0.0450 [86]
Solidus temperature (° C)	27.70 *	37.53 *	9.93 *
Liquids temperature (° C)	32.23*	42.89 *	40.30 *
Latent heat of fusion (kJ/kg)	213.66 *	141.7 *	58.97 *

Table 1: Thermo-physical properties of PCMs

* The values are found experimentally using DSC test.

In this study, the Differential Scanning Calorimetry (DSC) has been used to determine the latent heat of fusion, the liquids and solidus temperatures, the temperature of the material in which it is completely solid, and compare them with the provided material properties. DSC is an analytical technique in which the difference in the amount of heat required to increase the temperature of a sample and a reference material by equal amount is measured as a function of temperature. Both the sample and the reference are maintained at nearly the same temperature throughout the experiment. Figure 1 shows the schematic diagram for the DSC test. The type of DSC machine used in this study is DSC-AT Q200 which is shown in Figure 2.
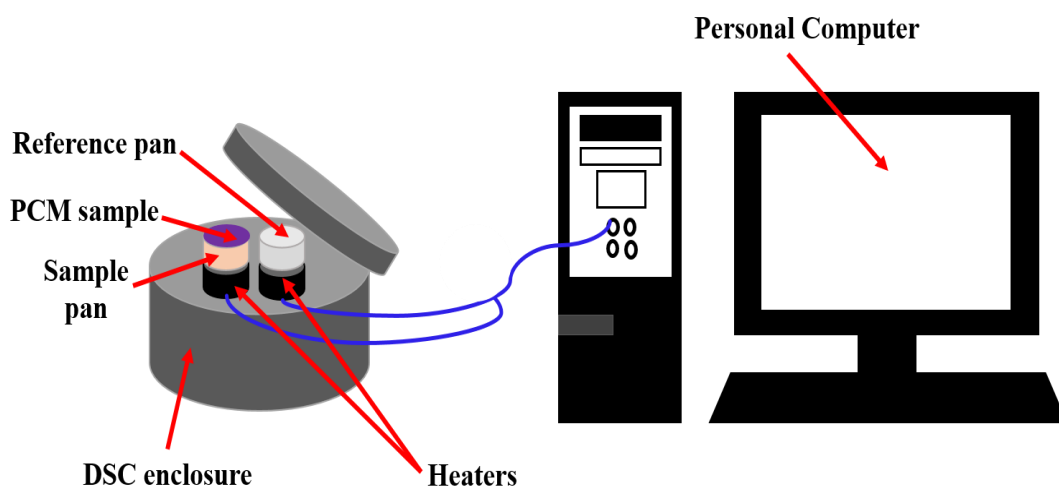
Figure 1: Schematic diagram for the DSC test

Figure 2: DSC setup- DSC-AT Q200

In the DSC test, two pans are used: the sample pan, where the PCM sample is placed and the other one is the reference pan, which is left empty. Each pan is placed on top of an electric heater. The heater supplies heat to both the pans at a specified rate. The computer is used to monitor temperature and regulate heat flow. The DSC thermal analysis in this research is performed with heating and cooling rates of 5 °C/min in the temperature range from 0 to 70 °C. Figures 3, 4 and 5 show the DSC curves for Paraffin, Salt hydrate and Milk-fat respectively.
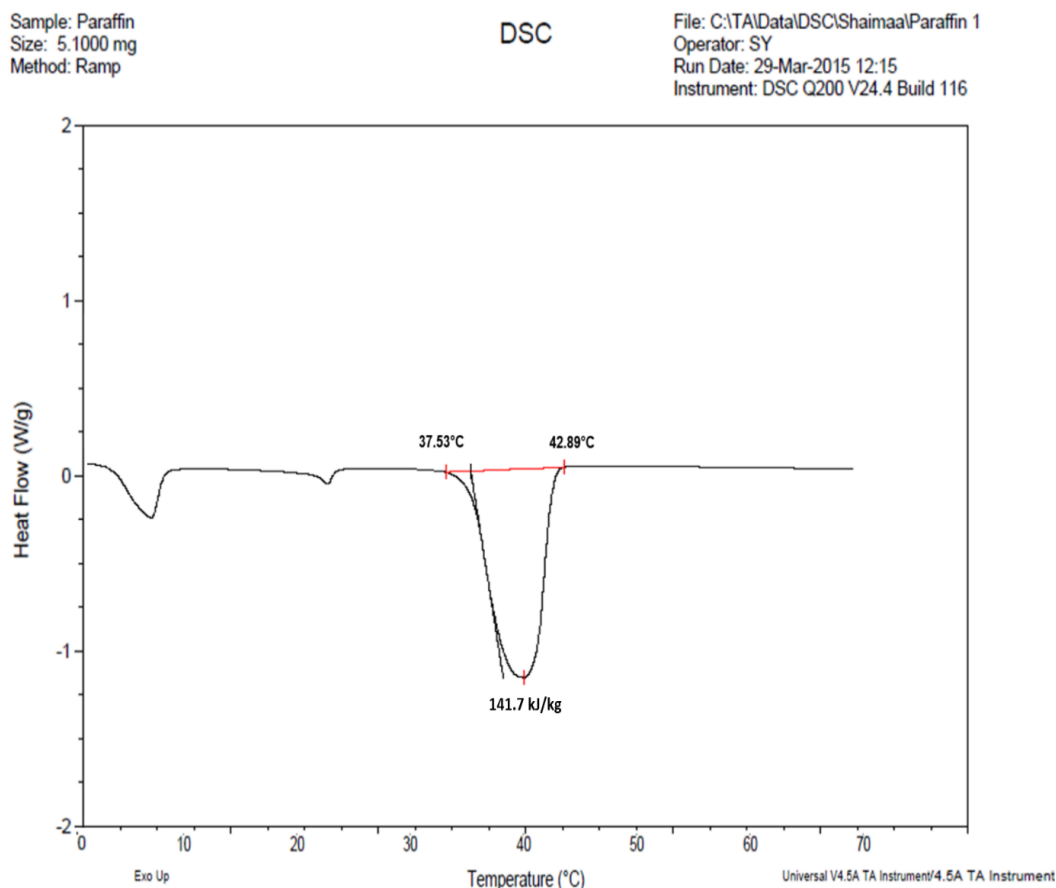
Figure 3: DSC curve for Paraffin

The DSC curves in Figure 3 clearly show the liquids and solidus temperatures for paraffin ($T_1 = 42.89$ °C and $T_s = 37.53$ °C). The latent heat of the solid–liquid phase change has been calculated by numerical integration of the area under the peak of the DSC curve and it was equal to 141.7 kJ/g for Paraffin.

For the salt hydrate material, liquids temperature is equal to $T_1 = 32.23$ °C and the solidus temperature is equal to $T_s = 27.70$ °C. The latent heat of the salt hydrate is calculating and equal to 213.66 kJ/g as found from the DSC curve (shown in Figure 4).
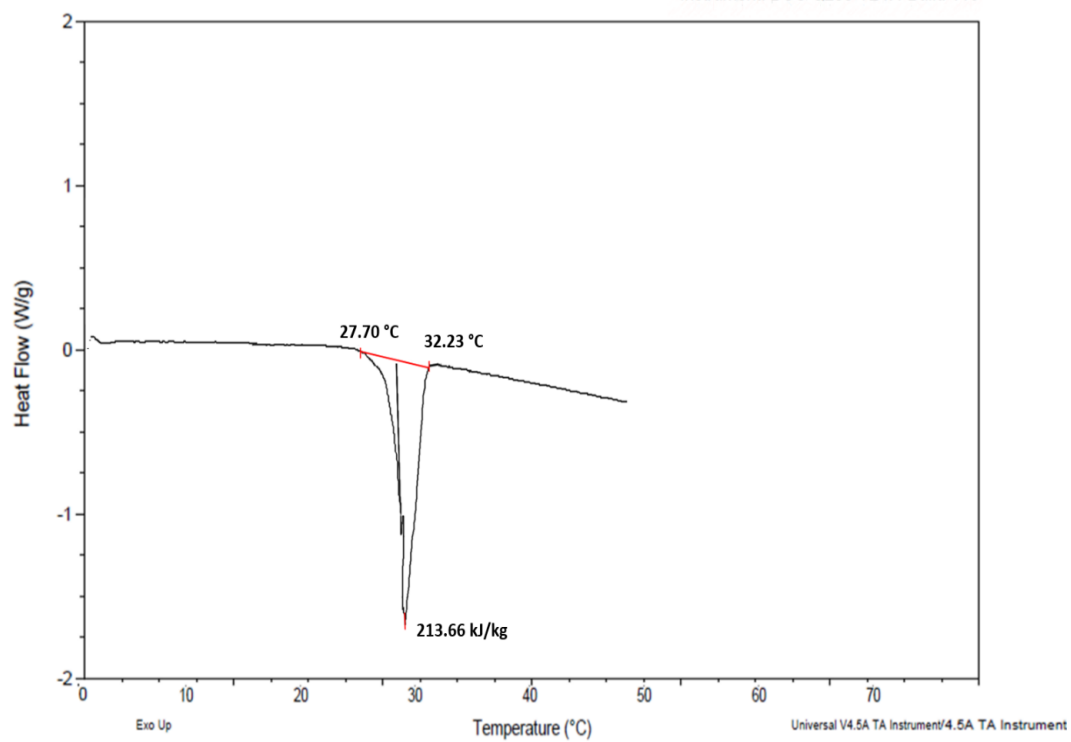
Figure 4: DSC curve for Salt hydrate
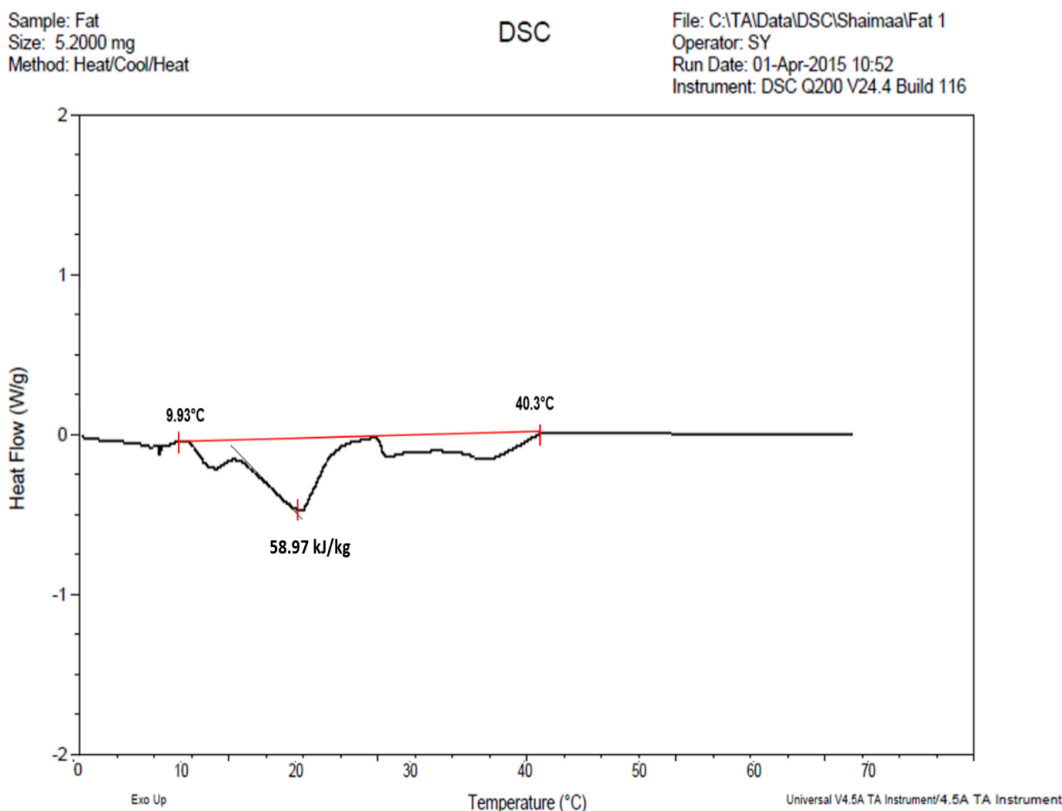
Figure 5: DSC curve for Milk-fat

Figure 5 shows the DSC curve for Milk fat. The melting temperature of the milk-fat was found to be $T_l = 40.3\ °C$ while the crystallization temperature is determined be $T_s = 9.93\ °C$. The large melting range for the milk-fat material is because the material consist of large number of elements and components. Each of these elements has its own melting point and combining the melting points for all elements of milk-fat material explain its large melting range. The numerical integration of the area under the peak of DSC curve of Milk-fat represent the latent heat which is equal to 58.97 kJ/g for milk-fat.

The DSC results show a good agreement with published material properties with acceptable error less the 5%.

The Other mentioned material properties were used from the data sheets provided for each used material [84-86].

3.1.3 Instrumentation

Schematic diagrams of the apparatus for the two experimental setups used in this study are shown in Figure 6 and Figure 7. They consist mainly of a PCM container, a chassis mount resistor (RCHB-10ND with maximum power rating of 10 W and 1% tolerance) as heat generator, a fan for a setup #2 only, a programmable DC power supply, temperature data logger and a personal computer. In addition, the cooling system has been insulated with a polystyrene chamber.
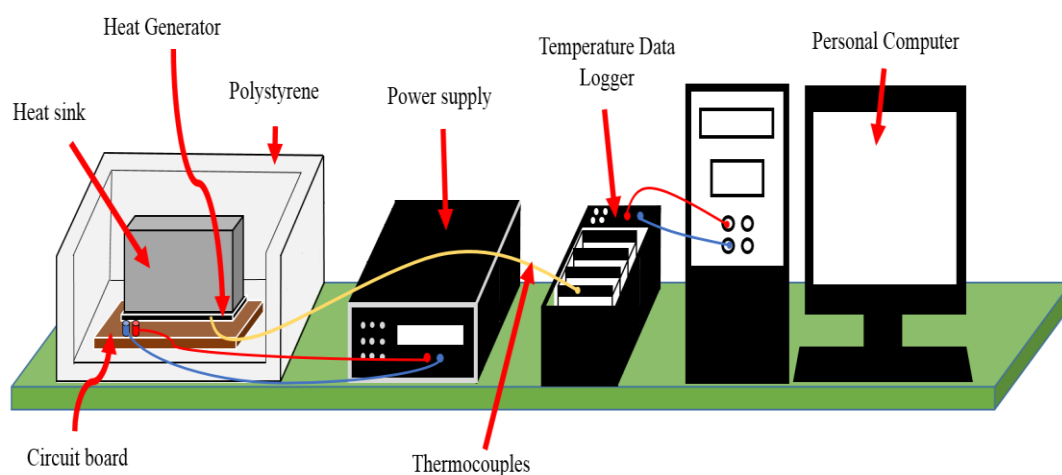
Figure 6: Schematic diagram of the apparatus in experimental setup #1 with No Fan
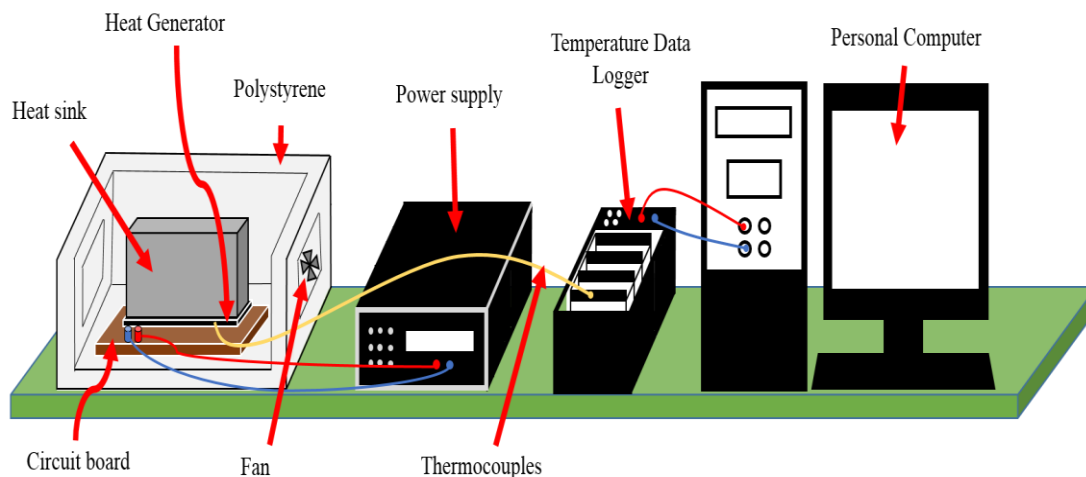
Figure 7: Schematic diagram of the apparatus in experimental setup #2 using Fan

Figure 6 shows the experimental system including the personal computer with exterior connections to the NI–DAQ-Pro data acquisition system to log the temperatures values measured by the calibrated T-type copper-constant on thermocouples. The system shown inside the polystyrene insulated chamber houses a circuit board for heat supply and a HS attached to it. The circuit board provides a heat generating surface on top of the HS to which the thermocouples are attached. Figure 7 shows the same system with one main modification made to the polystyrene insulation chamber in which an air channel ventilated by a fan is installed. The exterior connections of the fan to the AC power source, the circuit board to DC power supply and thermocouples to the NI DAQ Pro data acquisition system are also shown in Figure 7.

An experimental apparatus has been designed and built to accurately measure the instantaneous solid–liquid interface evolution and temperature distribution within the PCM. Figure 8 shows the schematic representation of the HS cooling system.
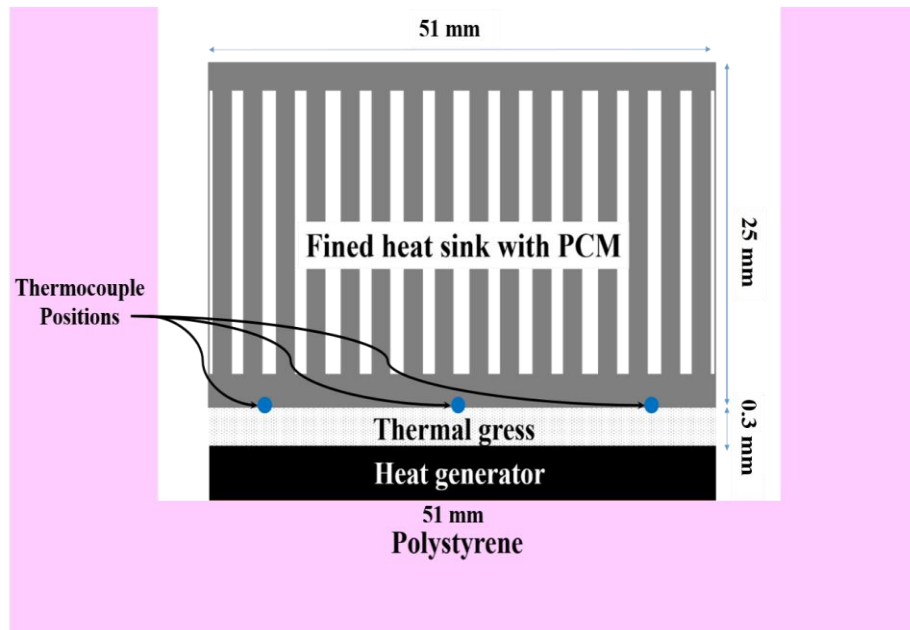
Figure 8: Schematic representation of the heat sink

This system consists of a closed rectangular coated aluminum HS with vertical fins manufactured with dimensions of $51 \times 20 \times 25$ mm^3. The surface between the HS and the heat source is sandwiched with thermal grease to reduce contact thermal resistance.

3.1.3.1 Heat Generator Resistor

Heat Generator Resistor is integrated electronic circuit (IC) compact in a small plate known as a chip. The IC is attached to the HS and is used to generate the heat inputs from the equivalent applied power. Heat Generator Resistor RCHB-10ND is used to generate the heat during the test (shown in Figure 9). This type of IC is designed to be mounted easily onto a HS with catalog maximum applied power rating of 10W and tolerance of ± 1%. The heat generating surface is L= 50.7 mm and w =20.3 mm while heat element diameter D=2.4mm [87].
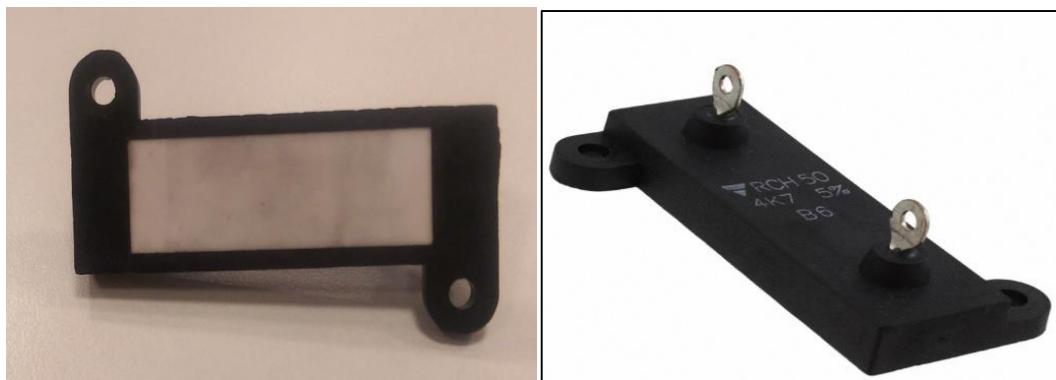
(A)   (B)

Figure 9: Heat Generator Resistor_ RCHB-10ND (A: top side and B: bottom side)

3.1.3.2 Thermal Grease

Tgrease-2500 is used in the experiment as an interface material between the HS base and the heat generator top surface to thoroughly wet out thermal surfaces and create a very low contact thermal resistance of 0.000015 m^2.K/W. It is a silicone-free, non-toxic and environmentally safe thermal grease with a high catalog thermal conductivity of 3.8 W/m.K for use in high performance applications [88]. Thermal grease properties are tabulated in Table 2.

Properties	Description
Color	White
Density	3.42 g/cc
Temperature Range	-55°C to 150°C
Thermal Conductivity	3.8 W/m.K
Thermal Resistance @ 10 psi @ 50 psi	0.023°C-in^2/W (0.15 C-cm^2/W) 0.020°C-in^2/W (0.13 C-cm^2/W)
Volume Resistivity	3.5 x 10^{12} Ohm-cm

Table 2: Properties of Thermal Grease_Tgrease-2500

3.1.3.3 Power supply

A DC Programmable Power Supply _ PPT -3615 is the type of power supply that used in this research (Figure 10).
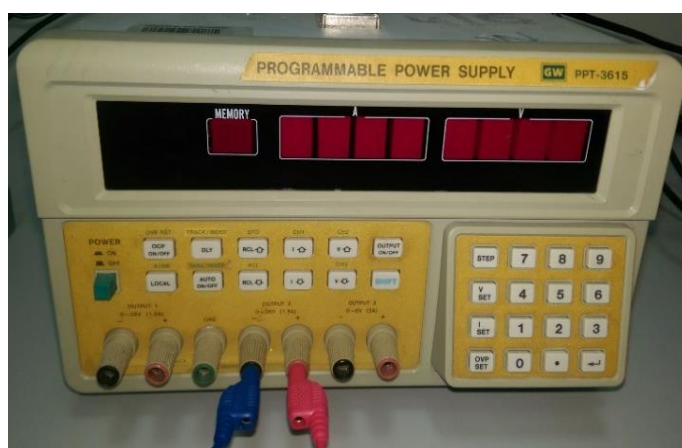
Figure 10: DC Programmable Power Supply _ PPT -3615.

It is powered from an AC mains electricity and then convert it to fixed DC load. DC programmable power supply allow remote control of its operation through a

digital interface to supply a controlled amount of voltage and current which in turn is passed through an electric circuit to generate a heat from the heat source.

3.1.3.4 Forced ventilation system

An axial DC fan with dimensions (length = 40 mm, width = 40mm, thickness = 10mm) is used as forced cooling system in case of forced convection experimental setup to ventilate the HSs. Figure 11 shows the used DC Fan.

Figure 11: DC Fan used for ventilation

It is powered by direct current (DC) electrical flows, operated at 12V and rotating in one direction. The fan produces an airflow rate of 9.9 cubic feet per minute (CFM) and the rotational speed of 8500 RPM revolutions per minute (RPM) [89].

The advantage of DC fans is the noise produced by fan is an audible noise, economical price range and they create less electromagnetic interference that enables them to cool computer systems without disturbing processes with electromagnetic interference.

3.1.3.5 Thermocouples

Thermocouples mainly consist of two dissimilar conductors or semiconductors that contact each other at junction and voltage difference is produced when they expand differently under the same temperature.

The thermocouples with type K probes (Chromel- Alumel) with a small wire diameter of 0.21 and calibrated accuracy of ±0.05 °C were used in this system as a temperature sensor (shown in   Figure 12). The temperature measured in degree °C and the temperature range from -50 °C until to 200 °C.   The thermocouples placed in different locations to measure the transient temperature distribution [90].

Figure 12: Thermocouples type K

3.1.3.6 Data acquisition

Data acquisition is the process of measuring an electrical or physical quantity. DAQ system consists of sensors connected to DAQ modules, DAQ measurement hardware, and a computer with programmable software. Connecting the thermocouples with the DAQ, the data is measured in voltage then converted into temperatures values through a calibrated equation in the DAQ measurement hardware using programmable software.

3.1.3.6.1 DAQ measurement hardware

The type of data acquisition used in these experiments is NI DAQ Pro_ cDAC-9174 for data acquisition slot chassis (shown in Figure 13). The DAQ chassis can carry up-to four module. NI-9213 thermocouple input is the temperature module used in this research. It consists of sixteen channels with 24-bit ADC for up to 0.02 °C measurements sensitivity [91].

It is connected to logging system program with graphic displays and a built-in function system to show and record the measured temperature via thermocouples which connected to different locations in the HS.

Figure 13: NI DAQ Pro_ cDAC-9174 data acquisition

3.1.3.6.2 Data logger software – LabVIEW

Laboratory Virtual Instrument Engineering Workbench (LabVIEW) is a system-design platform with a graphical programming syntax known as visual programming language. LabVIEW used in this research as a data logger program to show and to record the temperature measured by thermocouples through data acquisition system since it includes built-in support for NI hardware platforms such as Compact-DAQ, with a large number of device-specific blocks for such hardware.

LabVIEW mainly consists of block diagram, a front panel and a connector panel. The front panel which is the user interface is built using controls and indicators. Controls are inputs that allow a user to supply information to the program while indicators are outputs that indicate, or display, the results based on the inputs given to the program.

The block diagram is the programmer window and it contains the graphical source code on which the programmer built the program by connecting different function blocks by drawing wires and modify the properties. All of the objects placed on the front panel appear on the block diagram as terminals. Front panel window and block diagrams codes used in this study are shown in Appendix 1.

3.1.4 Calibration

Accuracy is an importing aspect in any experiment to trust an experimental results and draw a conclusion accordingly. Calibration is a procedure used for adjusting the accuracy of a measuring instrument to provide a result within a suitable range of errors. Although the procedure for instrument calibration varies from one device to another, but mainly could be defined as a comparison between measurements – one of known magnitude with one device and another measurement made in as similar way with a second device. In this research, thermocouples are calibrated by measuring known temperatures which is ice melting temperature $T_{ice} = 0$ °C. The values are found closely to the reference temperatures with error range $(0.5 - 1)$ °C. Also, the temperature values found by the used thermocouples are compared with calibrated thermometer and the error was less than 1%.

3.1.5 Experimental Procedures

In this experimental study, the effects of the following parameters are examined:

1) <u>Power level</u>:

Different power input levels were set at 4W, 6 W, 8 W and 10W.

2) <u>Different PCMs</u>: For each power input of mentioned power inputs, three different material were examined.

3) <u>Ventilation system effect</u>: Two ventilations system were used, namely, natural ventilation (without using fan) and forced ventilation system by using fan.

To investigate and analyze the thermal performance of the PCM-integrated package, different experimental operation modes have conducted at different heat inputs namely 4W, 6W, 8W and 10W.

The four models that were studied are:

1) Metallic finned HS subjected to natural ventilation.
2) Metallic finned HS subjected to forced convection ventilation.
3) Metallic finned HS filled with PCM subjected to natural ventilation.
4) Metallic finned HS filled with PCM subjected to forced convection ventilation.

The HS is fabricated from Aluminum sheet with enclosure dimensions: length= 51 mm, width= 21 mm and height= 25 mm. The HS enclosure contains equally spaced array of standard size fins. The number and geometry of the fins with their alignments and the base plate thickness are shown in Figure 14.
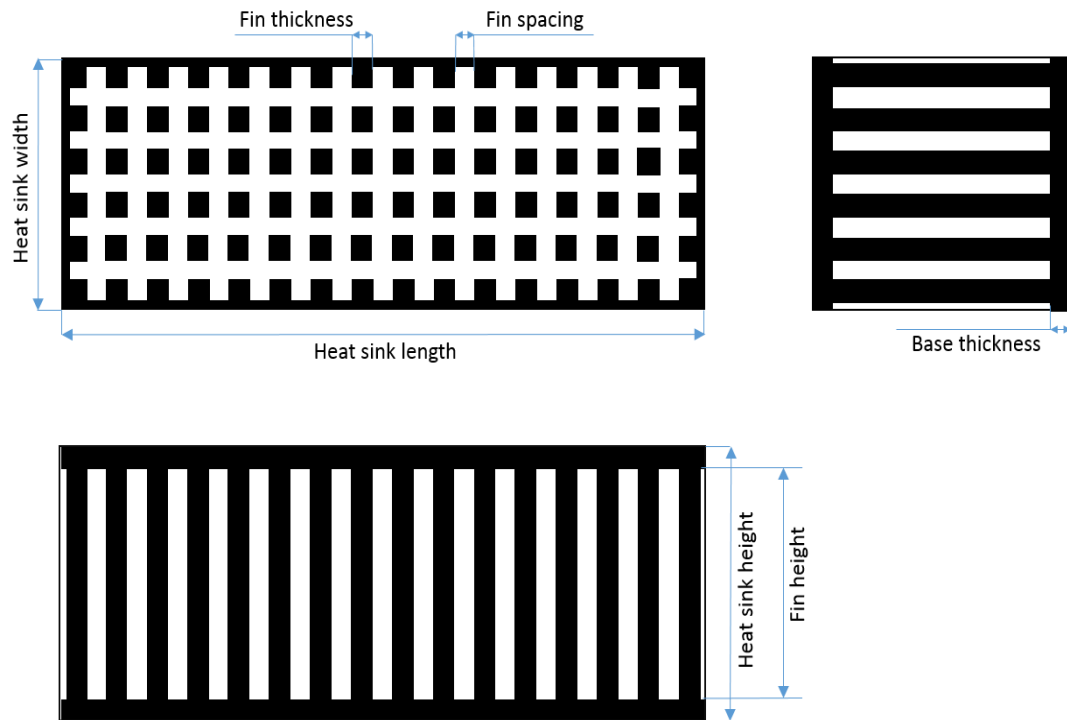
HS height (mm)	HS width (mm)	HS length (mm)	Fin spacing (mm)	Fin thickness (mm)	Fin height (mm)	Base thickness (mm)
25	21	51	1.6	1.6	20	2.5

Figure 14: Detailed design for heat sink

A total of nine thermocouples are used in the experimental part. Three thermocouples placed in the bottom surface of the Hs, five thermocouples are fixed into inner wall of the polystyrene enclosure and one thermocouple is used inside the enclosure to measure the surrounding temperature.

Three grooves have been made in the bottom side of HS and three thermocouples are then placed (soldered) at specified positions on the bottom face of the HS to measure the temperature of the heat sink surface as shown in Figure 15.
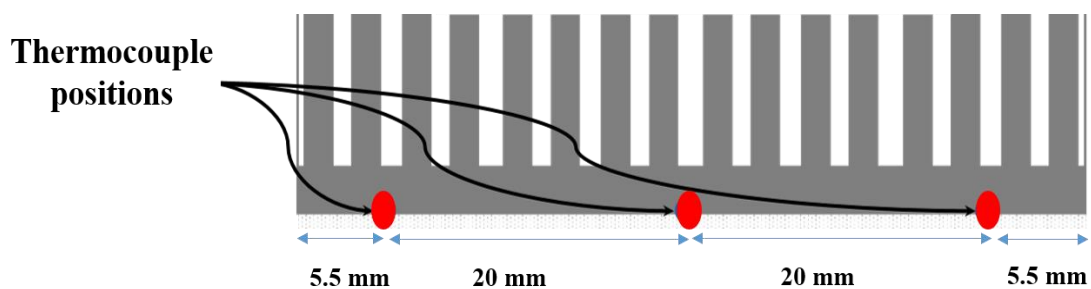
Figure 15: Thermocouples positions

A 0.3-mm thermal grease layer is applied to the HS base as an interface between the HSs and heat source to reduce contact thermal resistance, to increase the mechanical fixture of the structure assembly and to eliminate air gaps or spaces at the interface area. The temperature of Heat sink generated surface is assumed to be equal to the temperature of the bottom side of the heat sink surface.

The HS was subjected to different level of heat power inputs (4W, 6W, 8W and 10W) for both cases of ventilation (natural convection without using fan and forced convection system by fan). The correct voltage for the desired power output has been supplied to the heater from a DC programmable power supply. Table 3 shows the voltage (V) and the current (I) used to produce the desired output power.

Voltage	Current	Power	Heat flux over generated surface		Heat flux over generated element
(V)	(A)	(W)	(W/m^2)	(W/cm^2)	(W/cm^2)
10	0.998	9.980	9784.31	0.98	221.04
9.15	0.876	8.012	7858.24	0.79	176.84
7.9	0.77	6.083	5963.73	0.59	132.63
6.5	0.632	4.002	4027.45	0.40	88.42

Table 3: DC Power

The HS system has been insulated by 3 cm thick EPDM insulator sheets (k = 0.042 W/m K) in order to avoid effect of external ambient temperature through room HVAC system. One thermocouple is placed inside the insulated compartment to measure the ambient temperature. Five thermocouples are placed on each inner face of the polystyrene chamber to measure the surface temperature which will used in the numerical analysis radiation computations.

The experiments were conducted in a particular sequence of heat inputs. First experimental test considers an empty HS without the PCM and will serve as a reference for direct comparison of its thermal performance other experimental tests that integrate three different PCMs into the HS.

Then, the PCM-integrated HS tests, the metallic finned enclosure is filled with three PCM materials, namely, Paraffin wax-RT41, Salt hydrate-calcium chloride hexa-hydrate and Milk-fat. The materials are filled in liquid phase and are allowed to solidify

in the HS by filling the space between the fins. A syringe is utilized to inject the material into the HS through a small hole in the top surface of the HS. The same volumetric amount of each material is used for every run. Glue has been used to seal the filling hole and to ensure that no PCM material leaks during the experiment. All experiments have been initiated by the solid PCM at the same start temperature of 24 °C.

Each experiment is composed of two stages: the heating run which is marked by temperature rise and melting of the PCM followed by a cooling run marked by the heat removal and solidification of the PCM until the PCM returns to its initial temperature.

In the case of forced convection, a Mini-Vane CFM Anemometer-AN340 is used at three different positions (top, middle and bottom) on each of HS sides to measure the air velocity as shown in Figure 16. The average velocities are then used to calculate the convective heat loss coefficient required for the numerical analysis work as a boundary conditions.

Figure 16: Mini-Vane CFM Anemometer-AN340

The experimental data is recorded using the Data Acquisition Unit which is connected to a PC using LabVIEW program. The temperature of each thermocouple fixed at the specified locations is captured at fixed one-second time intervals and is plotted in real-time.

Each experiment is performed three times to assure repeatability and reproducibility of the data. Figures 17-20 show all experimental configurations used in this study.
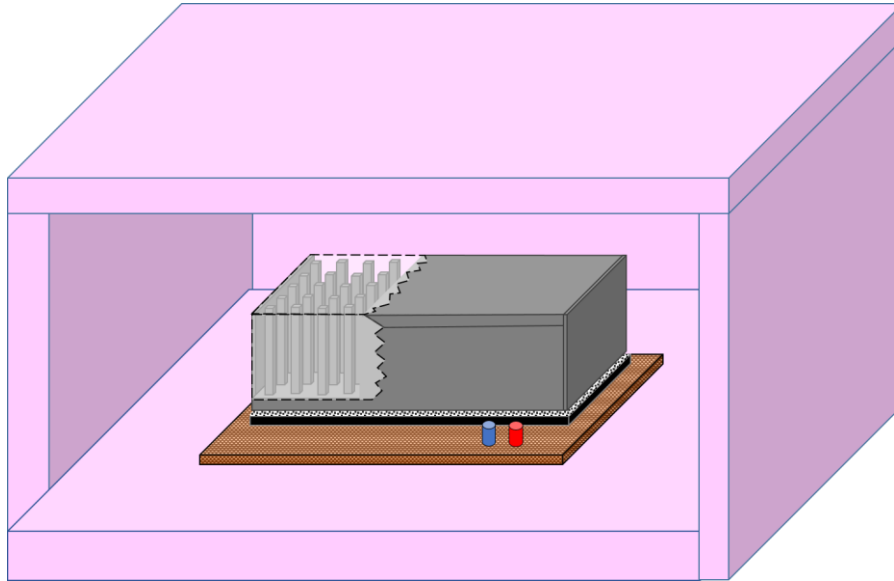
Figure 17: Schematic representation of experimental configuration No.1, for matric finned HS subjected to natural ventilation
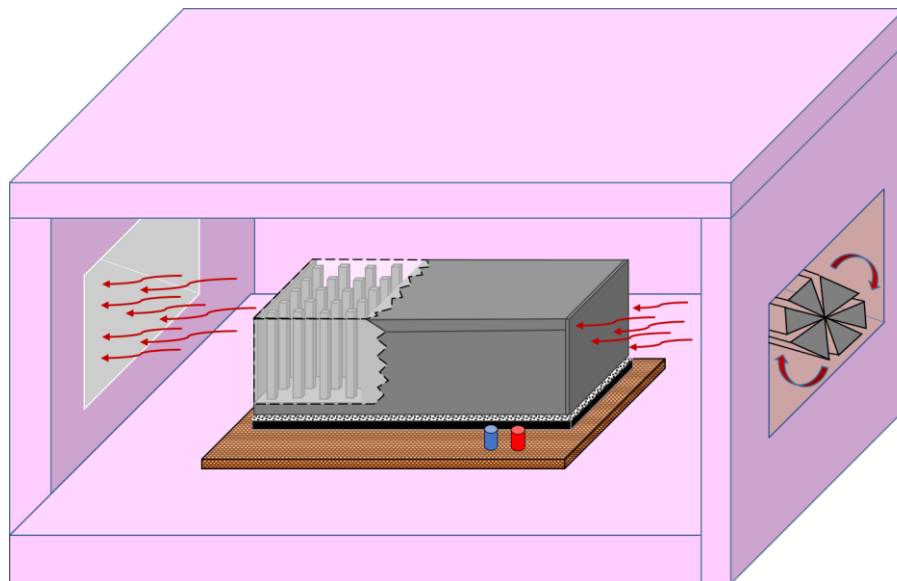
Figure 18: Schematic representation of experimental configuration No.2, for matric finned HS subjected to forced convection ventilation
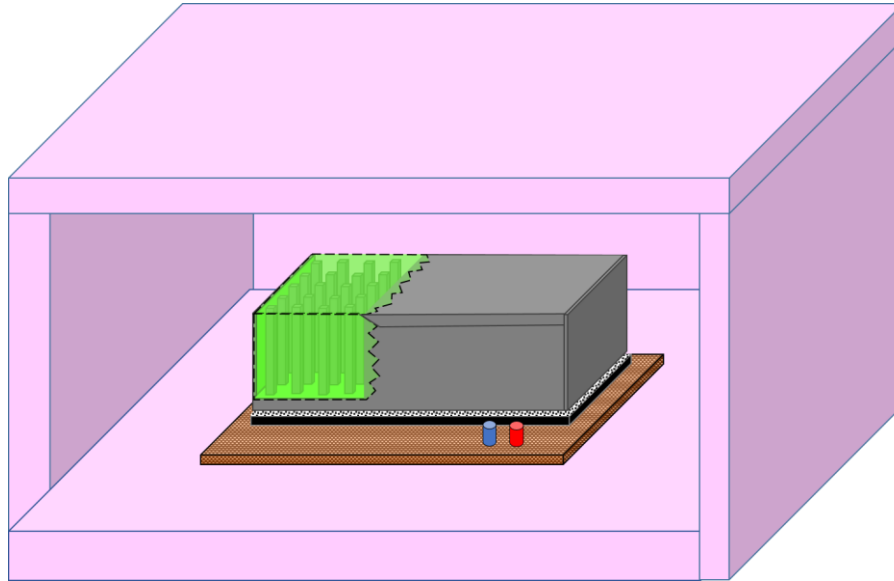
Figure 19: Schematic representation of experimental configuration No.3, for matric finned HS filled with PCM subjected to natural ventilation
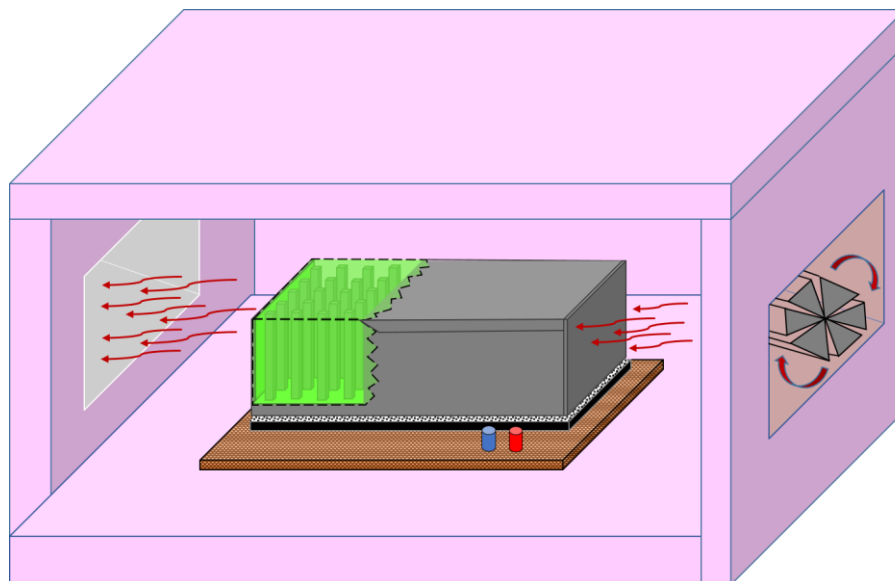
Figure 20: Schematic representation of experimental configuration No.4, for matric finned HS filled with PCM subjected to forced convection ventilation

Two polystyrene partitions are contained inside the sealed and insulated compartment for all four modes of operations to allow the air produced by an external

DC fan to move on a straight central axis of a closed channel and also used in case of natural convection to have same conditions in both ventilation types used in experimental part as shown in Figure 21.
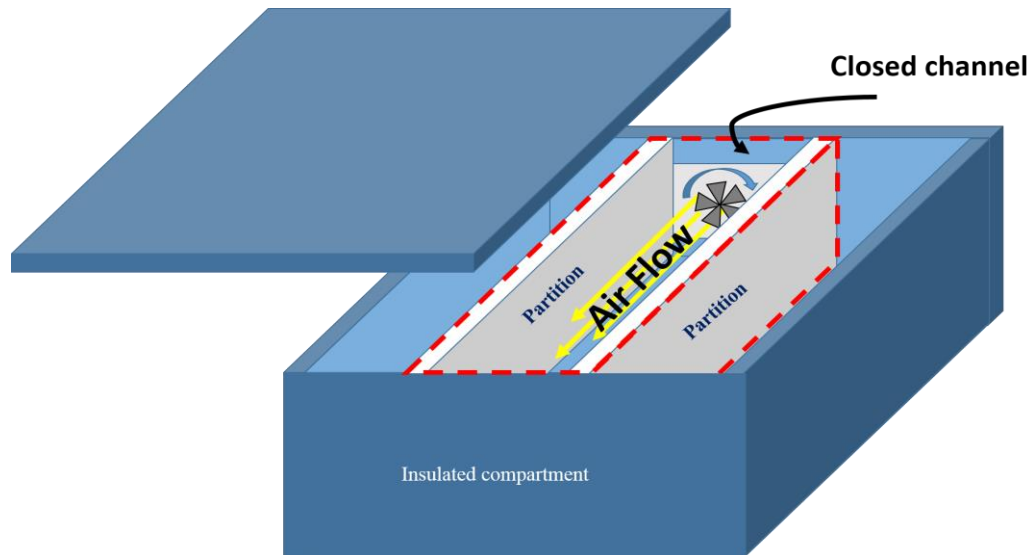
Figure 21: DC fan installed in the closed channel contained insulated compartment

3.2 Uncertainties for Calculated Quantities

The heat rate is calculated using the following equation:

$$\dot{Q} = \dot{m}_{Tol} * c_p * \Delta T \qquad (3-1)$$

The above equation was differentiated in order to calculate the uncertainty heat rate:

$$d\dot{Q} = \frac{\partial \dot{Q}}{\partial \dot{m}_{Tol}} d\dot{m}_{Tol} + \frac{\partial \dot{Q}}{\partial \Delta T} d\Delta T \qquad (3-2)$$

$$d\dot{Q} = c_p * \Delta T * d\dot{m}_{Tol} + \dot{m}_{Tol} * c_p * d\Delta T \qquad (3-3)$$

Where,

$d\Delta T = 0.05 \%$ as mentioned before (section 3.1.3.4)

Then, the uncertainty for heat rate can be calculated as follows:

$$d\dot{Q} = c_p * \Delta T * \dot{dm}_{Tol} + 0.5\,(\dot{m}_{Tol} * c_p\,)$$

Chapter 4: Numerical Analysis

4.1 Introduction

In this study a numerical computational fluid dynamics (CFD) simulation has been employed to better understand the transient heat transfer in a HS that is filled with PCM. The numerical solver codes are well-established and thus provide a good start to more complex heat transfer and fluid flow problems. FLUENT ANSYS (version-15) is a commercial CFD software that is used in this study to model the problem in hand. It is an engineering simulation software which contains the broad physical modeling capabilities needed to model fluid flow, heat transfer, and reactions for industrial applications in order to allow engineers to test systems by simulating fluid flows in a virtual environment.

In this section, numerical computations are performed for the aluminum rectangular finned HS configuration at different power heat inputs to obtain the temperature drop performance over a range of time. The numerical results are validated with the experimental results. The challenges in the numerical model come from that fact that PCM is combined with conjugate heat transfer in two phase in addition to the solid fins.

4.2 Detailed model for the heat sink

The model is producing using ANSYS Fluent (Version-15) for the metallic HS enclosure while the air properties in polystyrene containments surrounding the used HS is used as boundary conditions in the analysis of HS model.

The geometry of the HS is created in ANSYS Design Modeler with the same dimensions as of the experimental part as mentioned in section 3.1.5. Figure 22 shows the HS-CAD geometry in the ANSYS software while Figure 23 shows the detailed sketch for the HS.
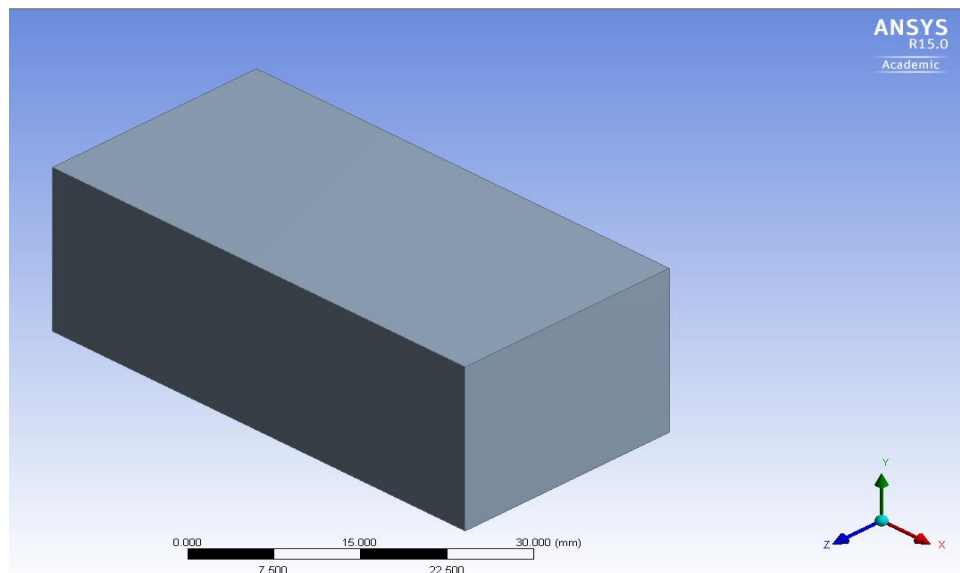
(A)
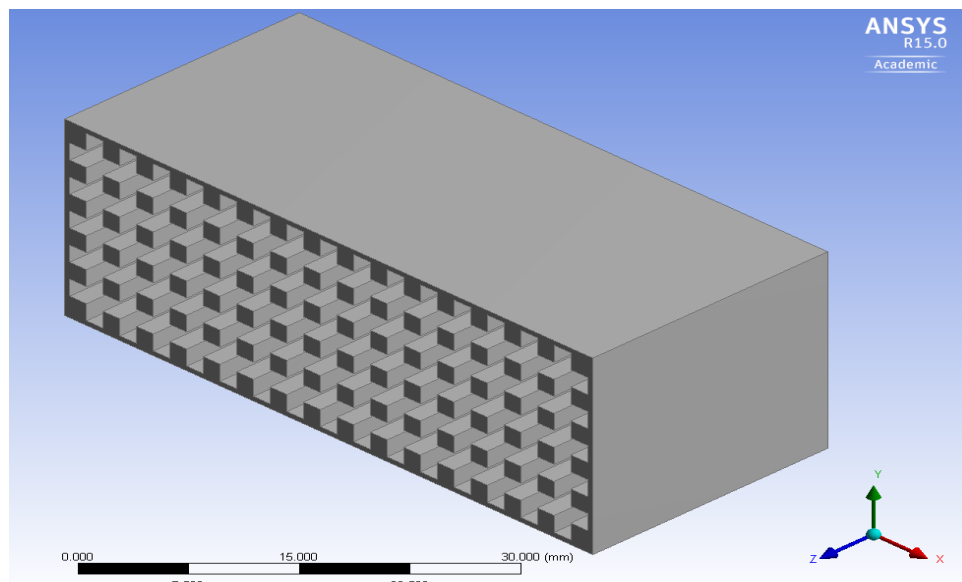
(B)

Figure 22: Heat sink geometry in ANSYS (A), (B) is the cross section area of the HS
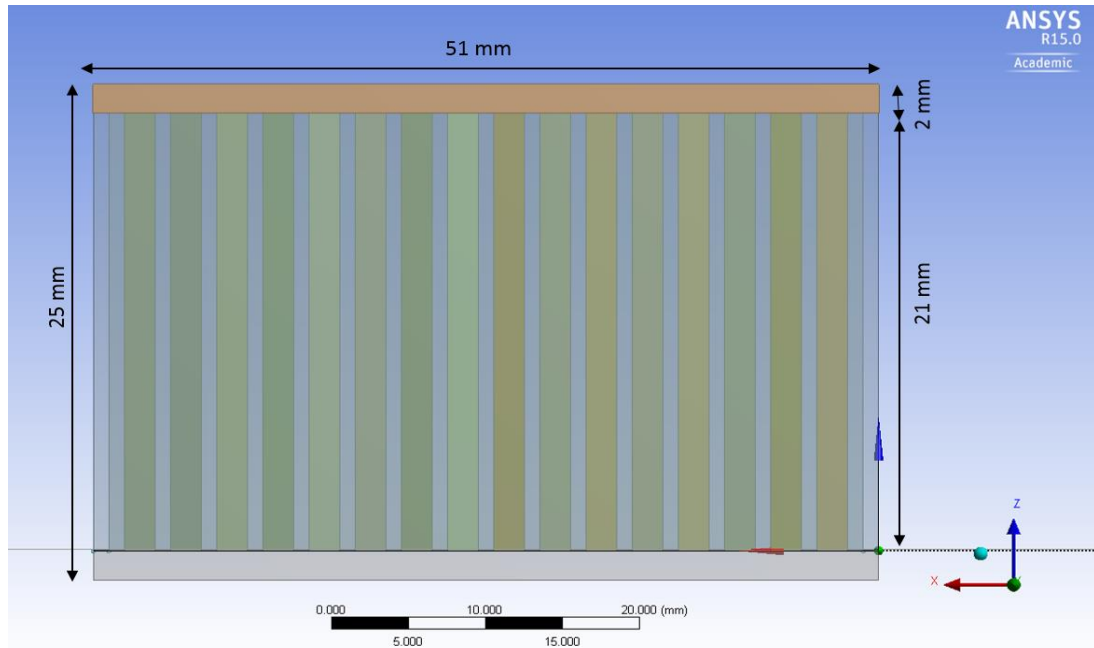
(A)
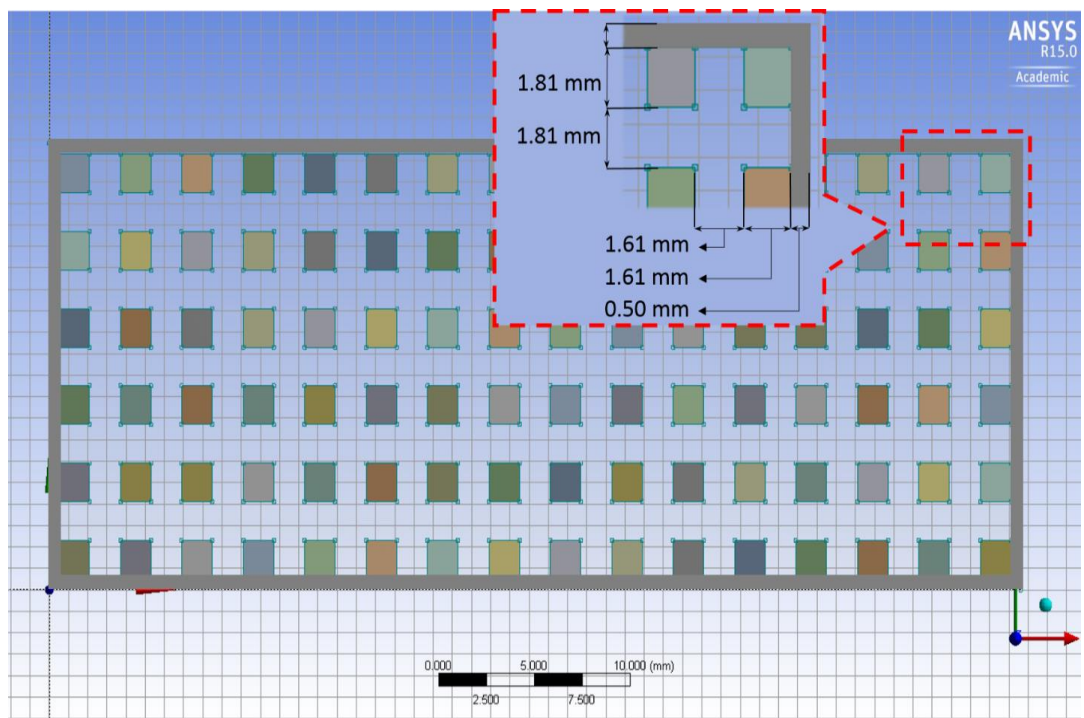
(B)

Figure 23: Size of heat sink, (A) the side-view of heat sink geometry in ANSYS and (B) the top view of the heat sink geometry in ANSYS

After sketching the HS geometry, each face in the geometry is selected and identified with specific name to facilitate boundary condition placement and to simplify post processing. The phase of fin and the HS base is chosen to be solid while the empty spaces surrounding the fins are selected as a fluid (either PCM or Air). Each solid face is coupled with the next layer of liquid face to account for conjugate heat transfer.

4.3 Numerical Setup for the CFD Simulation

After creating the computational mesh for the HS geometry, the numerical setup for CFD analysis is conducted using ANSYS Fluent (version-15). Modeling of phase change processes presents a significant challenge due to the problem complexity and the conjunction of the involved physical phenomena which include (1) volumetric expansion due to the phase change in paraffin wax, (2) convection in the liquid phase, and (3) motion of the solid in the melt due to density differences.

The present work attempts to overcome the limitations and to simulate the HS including the solid fins, solid and liquid PCM or air, while allowing for natural and forced convection, and solid motion in the liquid.

The four experimental modes, defined in chapter 3, are simulated to validate the experimental results conducted for different heat inputs and different PCMs. The numerical analysis uses the same material properties as those used in the experimental setup. The PCM properties are provided in Table 1, section 3.1.2. The HS material is aluminum while air is used as a filling material in case of empty HS. Properties of aluminum and air are mentioned Table 4.

Materials	Air	Aluminum
Thermal conductivity (W m^{-1} K^{-1})	0.0242	202.4
Specific heat capacity (J kg^{-1} K^{-1})	1006.43	871
Density (kg/m^3)	1.225	2719
Viscosity (kg/m.s)	1.7894×10^{-05}	-

Table 4: Thermo-physical properties of air and aluminum [92]

4.3.1 Numerical Model Assumptions

The same surrounding media applied in the experimental setups is produced in ANSYS. Assumptions used in the numerical analysis are:

- Laminar flow

- Uniform wall heat flux

- Constant heat flux

- Incompressible fluid

- Transient time analysis

- Variable thermo-physical properties

4.3.2 Numerical Model Boundary Conditions

For thermal boundary conditions, six boundary wall conditions are applied in the CFD model. Heat flux is applied to the HS bottom wall while the other HS walls are subjected to mixed heat loss mode (conduction and radiation).

4.3.2.1 Input Heat Source

A constant heat flux is applied to the HS bottom wall at different power inputs. The thermal resistance is set to be equal to 0.000015 m².K/W in heat flux face due to usage of the thermal grease in the experimental setups as mentioned in section 3.1.3.2. The heat flux for each power input is calculated using equation (4-1) and tabulated in Table 5.

$$q = \frac{Pwer}{Area} \qquad\qquad (4-1)$$

Power (W)	Equivalent heat flux (W/m²)
10	9784.3137
8	7858.2353
6	5963.7315
4	4027.4509

Table 5: Heat flux for different Power input

4.3.2.2 Heat Loss by Convection

When heat transfer takes place between a solid surface and a fluid system in motion, the process is known as convection heat transfer. The convection coefficient is calculated for the external walls of the HS using the following relations, [93]. The

properties of air at the film temperature and 1-atm (k, Pr, ν and β) were found from

the table of Air Properties in Appendix 2. Where,

$$T_f = \frac{(T_s + T_\infty)}{2} \qquad (4-2)$$

- The <u>Natural Convection</u> coefficient is calculated for the four vertical sides of HS

  by the following equations [93].

$$Re_L = \frac{g\beta(T_s - T_\infty)L^3}{\nu^2} Pr \qquad (4-3)$$

$$Nu = \left\{ 0.825 + \frac{0.387 Ra_L^{1/6}}{\left[1 + (0.492/Pr)^{9/16}\right]^{8/27}} \right\}^2 \qquad (4-4)$$

$$h = \frac{k}{L} Nu \qquad (4-5)$$

- The <u>Natural Convection</u> coefficient is calculated for the horizontal sides (Top-

  Side) of HS by the following equations [93].

$$L_c = \frac{A_S}{P} = \frac{L^2}{4L} = \frac{L}{4} \qquad (4-6)$$

$$Re_L = \frac{g\beta(T_s - T_\infty)L_c^3}{\nu^2} Pr \qquad (4-7)$$

$$Nu = \left\{ 0.825 + \frac{0.387 Ra_L^{1/6}}{\left[1 + (0.492/Pr)^{9/16}\right]^{8/27}} \right\}^2 \qquad (4-8)$$

$$h = \frac{k}{L_c} Nu \qquad (4-9)$$

The heat convection coefficients for each case at different heat inputs for both

the vertical and horizontal sides of HS is calculated and tabulated in Table 6.

Power level		HS integrated with Salt hydrate $(W/m^2 \cdot °C)$	HS integrated with Paraffin $(W/m^2 \cdot °C)$	HS integrated with Milk-fat $(W/m^2 \cdot °C)$	Empty HS $(W/m^2 \cdot °C)$
		Heat convection coefficient			
4 W	Vertical Side	4.93	4.95	4.96	5.14
	Horizontal side	5.49	5.50	5.51	5.66
6 W	Vertical Side	5.25	5.29	5.29	5.34
	Horizontal side	5.79	5.79	5.80	5.87
8 W	Vertical Side	5.56	5.56	5.56	5.58
	Horizontal side	5.89	5.90	5.91	5.96
10 W	Vertical Side	5.76	5.77	5.78	5.83
	Horizontal side	6.02	6.05	6.06	6.21

Table 6: Heat convection coefficient of heat sink under natural convection

- The <u>Forced Convection</u> coefficient was calculated for the four vertical surfaces of HS using the following equations:

$$Re_L = \frac{VL}{\nu} \qquad\qquad (4-10)$$

$$\text{Laminar: } Nu = \frac{hL}{k} = 0.453 \, Re_L^{0.5} \, Pr^{1/3} \qquad Re_L < 5 \times 10^5 \qquad (4-11)$$

$$\text{Turbulent: } Nu = \frac{hL}{k} = 0.0308 \, Re_L^{0.8} \, Pr^{1/3} \qquad 0.6 \leq Pr \leq 60$$

$$5 \times 10^5 \leq Re_L \leq 10^7 \qquad (4-12)$$

$$h = \frac{k}{L} Nu \qquad\qquad (4-13)$$

The air flow velocity over the HS surfaces are measured using Mini-Vane CFM Anemometer device. The velocity has been measured at three different positions for each surface from which the average of the three readings is calculated. Figure 24 shows the HS surfaces and the measured air speed values experimentally.
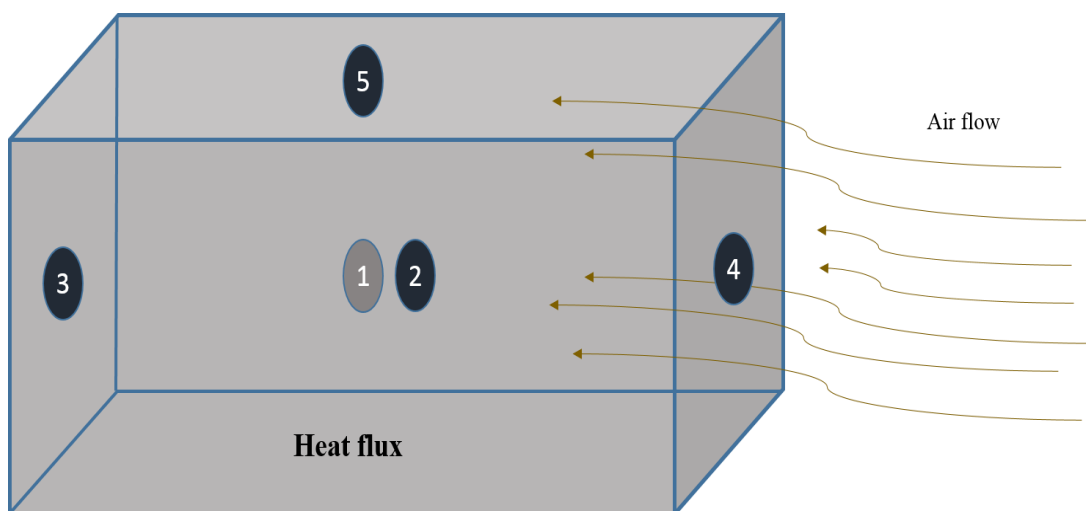
Sides	Air flow (m/s)
Side 1	2.4
Side 2	1.7
Side 3	0.2
Side 4	1.3
Side 5	2

Figure 24: Air flow velocity values for each side (wall) of the heat sink

After measuring the air speed experimentally using Mini-Vane CFM Anemometer, equations (4-10,11,12,13) are used to calculate convection heat loss coefficient for each side of the HS at the different power level (4W, 6W, 8W and 10W) as tabulated in Table 7 according the sides name shown in Figure 24.

Power level		Convection heat loss coefficient $(W/m^2 \cdot {}^\circ C)$
4 W	Side 1	14.07
	Side 2	11.41
	Side 3	5.71
	Side 4	9.89
	Side 5	13.10
6 W	Side 1	14.42
	Side 2	11.76
	Side 3	6.06
	Side 4	10.24
	Side 5	13.39
8 W	Side 1	14.68
	Side 2	12.02
	Side 3	6.32
	Side 4	10.50
	Side 5	13.50
10 W	Side 1	14.89
	Side 2	12.23
	Side 3	6.53
	Side 4	10.71
	Side 5	13.65

Table 7: Heat convection coefficient of heat sink under forced convection

4.3.2.3 Heat Loss by Radiation

The external sides of the HS is exposed to mixed heat transfer modes which are convection and radiation. Radiation, energy transmitted from source through a material medium in form of particles, heat transfer mode takes place in form of electromagnetic waves mainly in the infrared region. The radiation is calculated for the HS top side and other four sides as the following:

$$\dot{Q} = A_1 F_{1\rightarrow2}\sigma(T_1^4 - T_2^4) \qquad (4-14)$$

Where,

A: Heat sink side area (m^2)

$F_{1\rightarrow2}$: View factor (% Determined from Figure 23)

σ : Stefan-Boltzmann constant = 5.670×10^{-8} (W/m$^2 \cdot$ K^4)

The radiation is set in ANSYS software at infinity (far surface) temperature of 42 °C (315 k) for the top wall and 37 °C (310 k) for other sides found from experimentation. The HS is painted black to assure black body emission. The advantage of modeling radiation with ANSYS rather than adding radiation as combined convection coefficient, that it allow the variation of radiation thermal resistance which is more appropriate to reflect real conditions.

4.3.3 Numerical Simulation Procedure

Using ANSYS Fluent (version 15), two-phase conjugate heat transfer is used in simulation analysis. The Energy equation and the momentum equation are activated. The laminar flow is used in the heat sink model. The materials used in the model are

solid "Aluminum" for the HS finned enclosure and the PCMs filled in the HS selected as a fluid "Salt Hydrate, Paraffin and Milk-fat". The melting and solidification option is activated in the Fluent program to simulate behavior of the PCM. The bottom side of the HS is subjected to uniform heat flux calculated according to the Power input over the heat generated area while the other heat sink walls are subjected to mixed heat loss. Each run is set for 1s time step with 20 iteration per time step and with a run time of 4000 iterations (almost 66 minutes), the time needed for the material to complete melting and reach the steady state to allow solution convergence. The temperature is plotted versus time for base wall, top wall and side walls. The liquid fraction is also plotted versus time to show the progress of phase change for each material during each run.

4.4 Numerical Analysis Mesh Independent Study

The meshing for the produced HS geometry is created in the ANSYS meshing application. A mesh convergence means computing the solution on successively finer grids until the solution become independent of mesh size. Mesh independence study has been carried out as per the following steps:

Step 1: In the first simulation, analysis of the initial mesh is conducted and the temperature profile with time for the HS is recorded.

Step 2: Re-meshing the geometry with finer mesh and then resolve the problem with same boundary conditions.

Step 3: Mesh independence is evaluated by monitoring the results of one point with time using both mesh sizes. The process is carried out more than once until the convergence is achieved with an allowable tolerance is less than 2%. The mesh independent solution is achieved when the solution is not changing anymore with

further mesh refinement. Figure 25 shows the transient temperature for different mesh sizes which shows that results keep changing until the mesh element size reaches 0.0005mm. After that, any refinement of the mesh produce no significant changes and the transient temperature becomes independent of mesh size below an element size of 0.0005 mm as shown with mesh size of 0.0001 mm. Hence, to reduce computation time, the mesh with element of 0.0005m is used in this numerical study.
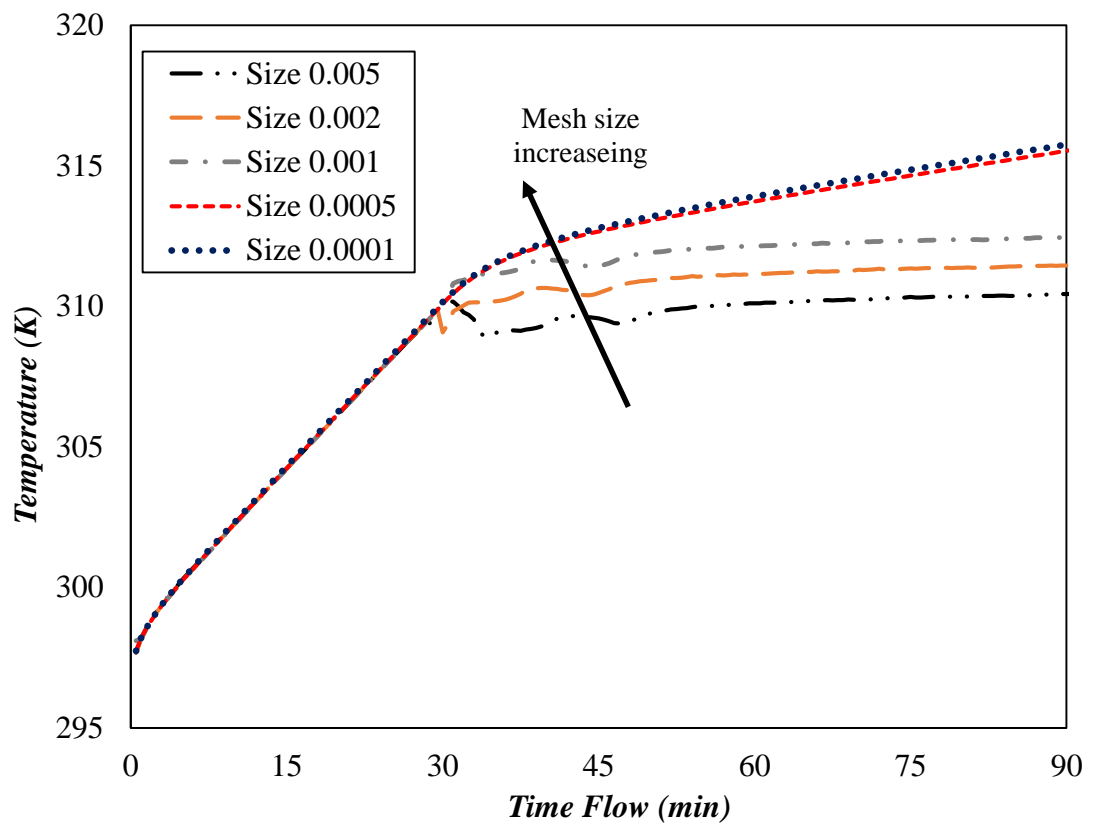
Figure 25: Mesh independent study for heat sink

The produced HS is meshed in ANSYS software. The model is meshed with element size = 0.0005mm in soft scale. Figure 26 shows the meshed HS.
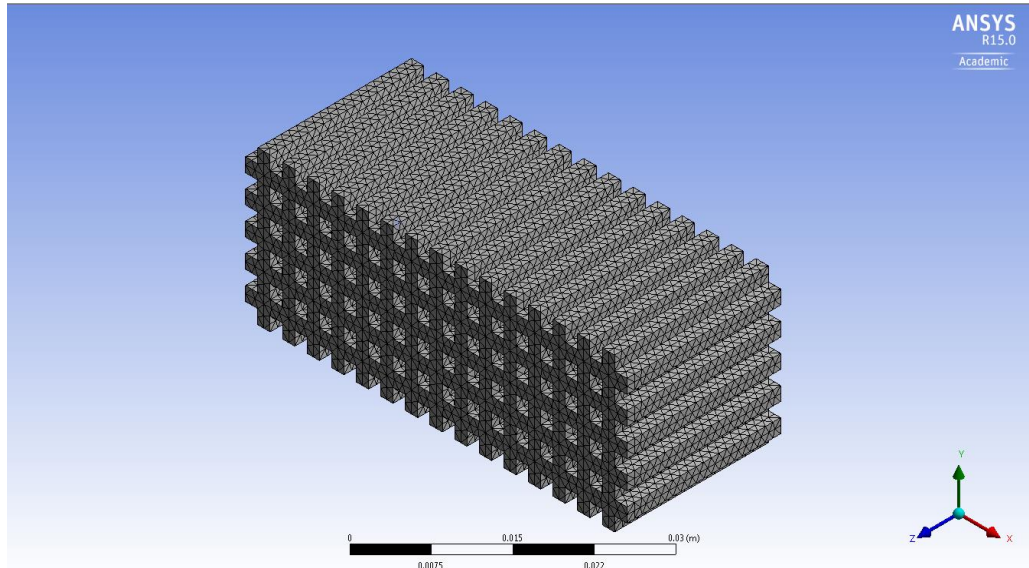
(A)
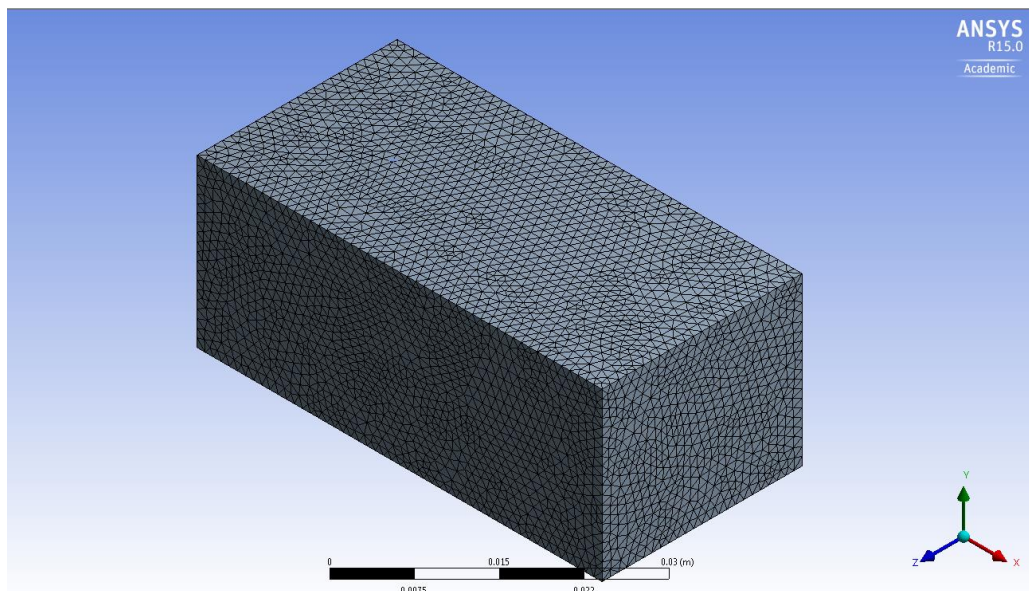
(B)

Figure 26: The computational mesh for the PCM geometry (A), (B) is the
computational mesh for the heat sink geometry in the ANSYS meshing application

Chapter 5: Results and Discussion

5.1 Experimental Results and Discussion

Through the experimental set up explain in chapter 3, various experiments were conducted to find out impact of mode of heat removal, intensity of heat input and inclusion of different PCMs on the thermal management performance of the system address modes. The two most common modes of heat removal namely natural ventilation and fan powered forced ventilation were investigated under heat inputs of 4W, 6W, 8W and 10W for three PCMs, namely paraffin wax-RT41, salt hydrate-calcium chloride hexa-hydrate, and milk-fat. The experimental campaign can be distinguished by four discrete sets of experiments as:

1) Thermal management experiments with metallic finned heat sink under natural ventilation. (WOPCM-Natural convection)

2) Thermal management experiments with metallic finned heat sink under forced ventilation. (WOPCM-Forced convection)

3) Thermal management experiments with metallic finned heat sink filled with PCM under natural ventilation. (WPCM-Natural convection)

4) Thermal management experiments with metallic finned heat sink filled with PCM under to forced ventilation. (WPCM-Forced convection)

All of the above mentioned (1-4) experimental design were investigated at heat inputs of 4W-10W to represent the medium to high heat generation densities common in today's compact electronic packaging with 2W heat input increase in each subsequent experiment. In order to avoid repetition, the results for 6W heat input are

presented in this section as temperatures and melt fraction diagrams to show the impact of PCM on temperature control of electronic and the duration of temperature control.

The experimental results for 4W, 8W and 10W heat inputs are discussed in the this section as potential deviations from 6W in terms of temperature control and time taken for complete PCM melting however the figures are presented in Appendix 2. In this section, at first the effectiveness of different modes of heat removal is compared while the type of PCM is fixed in one set of experiments and secondly the effectiveness of different PCMs for heat removal is compared while the modes of heat removal is kept constant.

5.1.1 Comparison of Different Modes of Heat Removal

In order to compare the thermal management performance of different modes of heat removal, PCM was fixed in each mode of heat removal and it was subject to heat inputs ranging from 4W-10W. The temperatures are measured at three locations on bottom side of HS (Thermocouples locations in section 3.1.5, Figure 15) and the average of the three is plotted against time to represent the uniform heat input on the surface. The results are plotted as the time-temperature graphs for all the four modes of heat removal as one data set for each of the three PCMs investigated at 6W heat through Figure 27 to Figure 29.
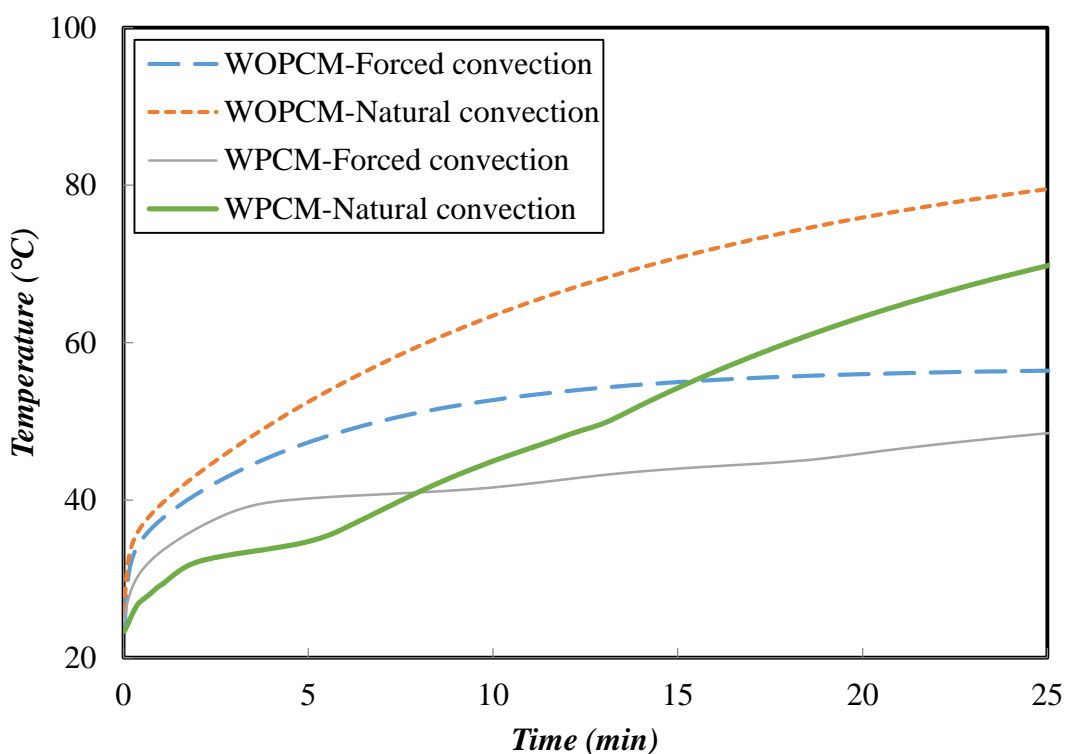
Figure 27: The heat generated variation with time for the four modes of heat removal while using calcium chloride hydrate as PCM under 6 W of heat input

Figure 27 shows the temperature rise of the heat sink surface for the four modes heat removal under power input of 6W (mentioned previously in section 5.1) and with using calcium chloride hydrate as PCM. The results show that the temperature for reference case (WOPCM-Natural convection) as dotted red line exhibits the highest temperature of all the rest of the three modes of heat removal. The gradient of temperature rise was steep in the beginning however kept gradually decreasing until it reached the steady state due to thermal equilibrium with the surrounding. The thermal equilibrium established due to balance in the heat gain from the heating element on heat generator surface and the heat loss by natural convection through the heat sink surfaces (side walls and the top surface). The inclusion of forced ventilation (WOPCM-Forced convection) decreases the gradient of the temperature rise however

follows the similar trend in temperature rise as of natural convection which represents the effect of inclusion of fan on increased heat loss from the heat sink surfaces in achieving thermal equilibrium at a lower temperature. When PCM is added to heat sink under natural convection (represented by the green line in Figure 27) the temperature rise was steep with higher gradient in the beginning for less than a minute which shows the sensible heating of the heat sink and the PCM. At the phase transition temperature (27 °C – 32 °C), the temperature gradient reduced dramatically and the curves showed near isothermal behavior caused by the latent heat absorption by the melting PCM. The temperature remained near isothermal for up to 6 minutes and then started increasing with a larger gradient which shows a shift from latent heating to the sensible heating due to completion of the PCM melting. The gradient again started decreasing to finally reach the steady state to heat balance between the heat gain from heating element and heat loss from the heat sink boundaries.

When adding PCM into the heat sink a time lag in temperature rise is observed due to melting and latent heat absorption. In first 6 min, the heat sink with PCM shows a significant drop in temperature over the other three modes. The graph shows that for first 15 minutes the WPCM-Natural convection) achieved the minimum temperature however it later on raised in temperature and shows a higher temperature than the WOPCM-Forced convection. Using PCM shows a larger heat loss and temperature drop up to 15 °C compared to fan ventilation with no PCM. In both natural ventilation and forced ventilation case, the temperature remains lower with PCM inclusion compared to without PCM at the start, however the PCM under natural convection shows higher temperature than fan ventilation with and without PCM after 15 minutes of exposure which shows that the PCM alone cannot compete with fan alone

ventilation system for larger exposure time mainly due to completion of melting of the PCM followed by sensible heating and heat retention. For comparing different modes of heat removal, two factors are important i.e., 1) the highest near steady state temperature reached short time domain which shows the capability to limit temperature below certain critical operation temperature and 2) the integral of the transient time-temperature curve which shows the net cooling effect produced by each mode. Figure 27 shows that the maximum temperature at the heat generating surface at 6 W is 75 °C without using the PCM under natural convection while using PCM under natural convection reduces it to 62 °C due to PCM cooling effect. Inclusion of forced ventilation without PCM reduces it further down to   50 °C and then inclusion of PCM with forced ventilation brings the temperature down to 42 °C. It shows that combination of the fan powered forced convection and the PCM is the optimum choice for thermal management of the IC packaging in this case. For the larger time exposure (Appendix 3, Figures 53-55), the steady state temperatures under natural ventilation without PCM yields temperatures of 60 °C 85 °C , 110 °C and 125 °C at 4 W, 8 W and 10W power inputs respectively as a reference without using PCM and fan ventilation.

It can be observed that when the fan ventilation is coupled with the PCM, the temperature remains always lower than the rest of the three cases which shows that the combination of the PCM and fan ventilation can be effective even for a larger time exposure, however it may not be an option for continuous operation as PCM needs a non-operation time to get back to solid to be ready for the next duty cycle. It concludes that for a short time transient thermal management, the inclusion of PCM can be a better option than the forced convection thermal management system however, it

cannot operate over a long time operation where the fan powered forced convection mode of heat removal still dominates. The actual operation time for which the PCM based cooling prevails depends on the heat input rates, the nature of the PCM in terms of latent heat of fusion and the amount of PCM determined by size of the heat sink and the PCM density. Although in this research a particular size of heat sink was used, however a future work can investigate different heat sink geometries to allow for more PCM accommodation to allow PCM cooling for longer time.
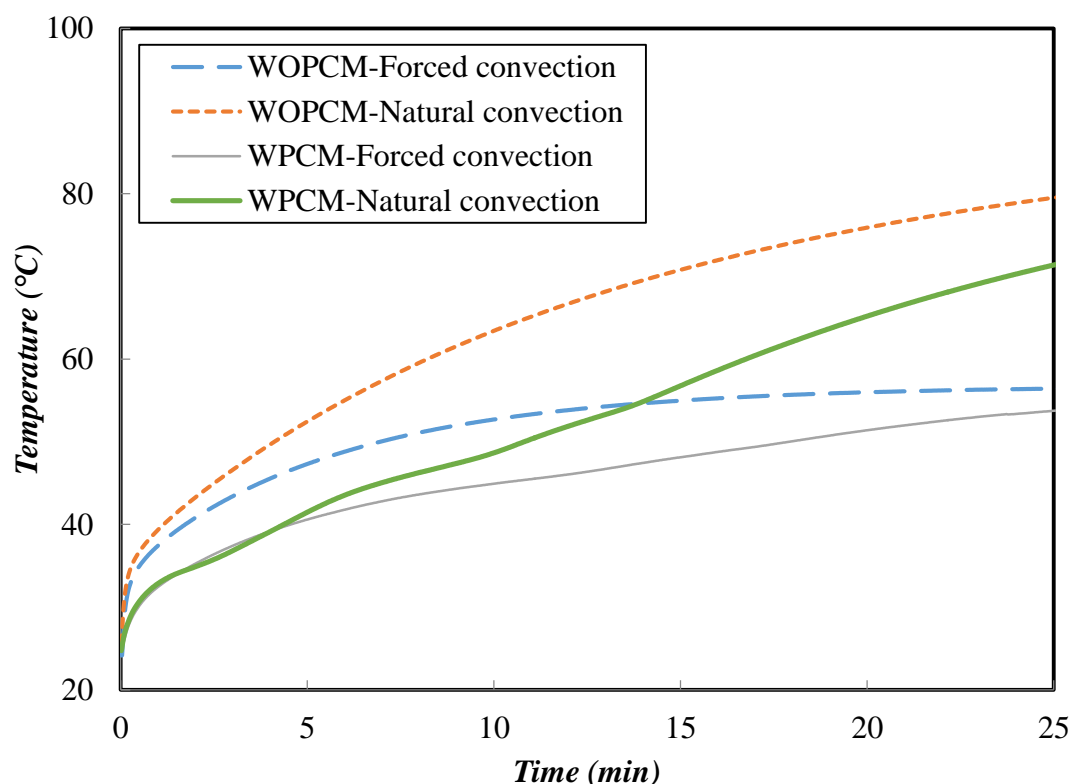
Figure 28: The temperature variation with time for the four operation modes while using paraffin wax as PCM under 6 W of heat input

From Figure 28 shows the similar comparison between four modes of heat removal however in this case the PCM is changed from salt hydrate to paraffin wax keeping the same heat input of 6W. It shows that inclusion of PCM in heat sink reduces the temperature rise of the heat sink. Temperature drops by 9 °C compared with using

fan only while it drop by 12 °C than reference mode (natural convection without PCM). Filling the paraffin in heat sink accompanied with fan cooling shows the best performance in terms of temperature drop in this case too as was observed in the case of using salt hydrate in Figure 27.

The similar behavior is observed when the PCM is changed to milk-fat (Figure 29) however the milk fat shows less temperature drop compared to the salt hydrate and the paraffin wax. The reason being salt hydrating performing better than the paraffin wax and milk fat is due to decreasing order of density, heat of fusion and thermal conductivity between salt hydrate, paraffin wax and milk fat respectively explained in earlier sections.
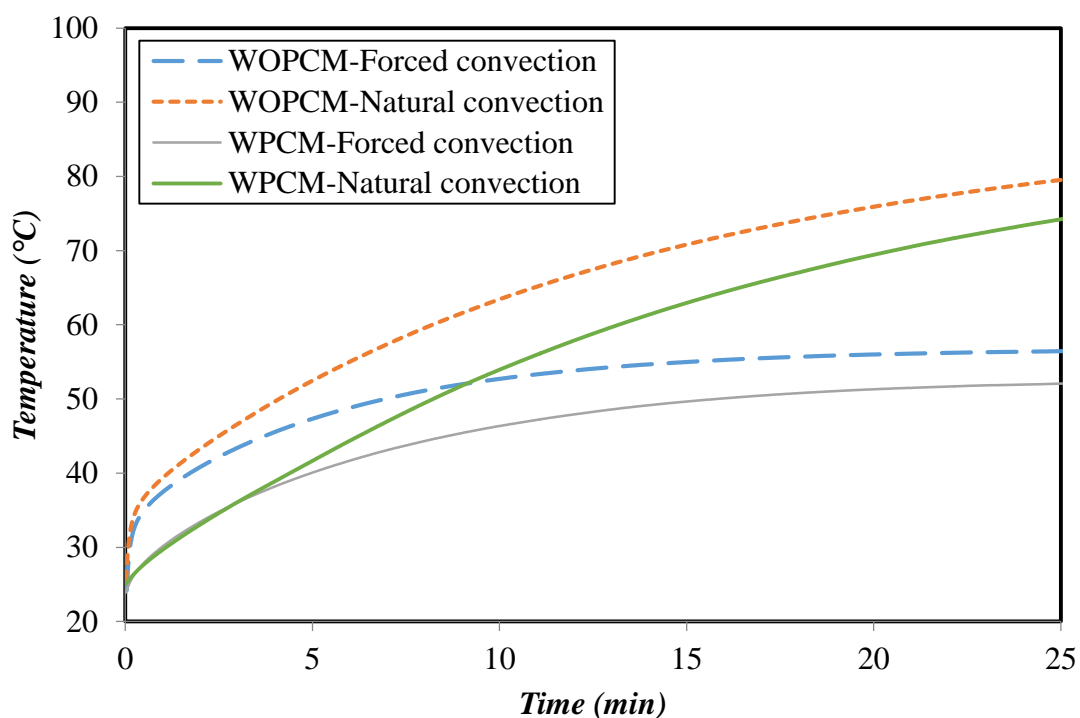
Figure 29: The temperature variation with time for the four operation modes while using Milk-fat as PCM under 6 W of heat input

Summarizing the Figures 27-29, in most cases the highest temperature reached at the end of experiments at the heat generating surface is lower in case of using PCM compared to heat sink without PCM at all power inputs of 4W, 6W , 8W and 10W, with all PCMs and with both the natural and forced convection.

It was noticed through the analysis of the results in case of using external forced ventilation system. When fan is added without PCM, it drops the temperature strongly to very low temperatures compared to natural ventilation in all power inputs from 4W-10W due to increased heat losses from the surfaces of the heat sink to the ambient. This shows that the forced convection is more effective in heat removal from the heat sink compared to natural convection. However, it may be misleading in some cases, as in the studied case the test chamber was not exposed to wind flows as happens in outdoors to mimic the real heat sink enclosure in a packaged device. In some outdoor electronic device exposures, the wind speeds may be much higher than what was in the test chamber and the natural convection may compete with forced convection in high wind speed regions and regimes. So, it needs still further research in testing the effect of natural ventilation and forced ventilation with and without PCM when exposed to outdoor wind speed as to what configuration can be optimum. The future research may eliminate the inclusion of fan in some specific high wind speed locations and can rely only on natural convection with PCM inclusion.

In addition, the impact of using PCM was found. The time lag and temperature drop in case of with PCM compared to without PCM shows the cooling effect of adding PCM under both natural and forced ventilation modes of heat removal. It means inclusion of each of the three types of PCM into heat sinks with natural convection shows higher temperature drop in first 15 min of heating than inclusion of fan (forced

convection) without PCM dominates over PCM only. However, the combination of both the fan ventilation and the PCM always maintain the lower temperature. This leads to conclusion that implementing a PCM in the heat sink will be very useful in thermal management of the electronic device and the application is more suitable under cyclic thermal loading conditions since in all cases the PCM completes melting in certain time and then shows a temperature rise. So, it is recommended to use the HS filled with PCM for short time operation or cyclic operation such as switching operation where PCM can be regenerated to solid during off duty cycle to be ready for the next cycle of heat absorption. It also recommended to use the PCM since it shows the temperature drop compared with the fan system.

For clear understanding of PCM comparative performance in terms temperature drop, the experimental data is presented in time-temperature graphs of heat generating on the bottom side of HS surface comparing all the three PCMs to the reference case (natural convection without PCM). Figure 30 present the results of the PCM heating curve for each power input under natural convection.
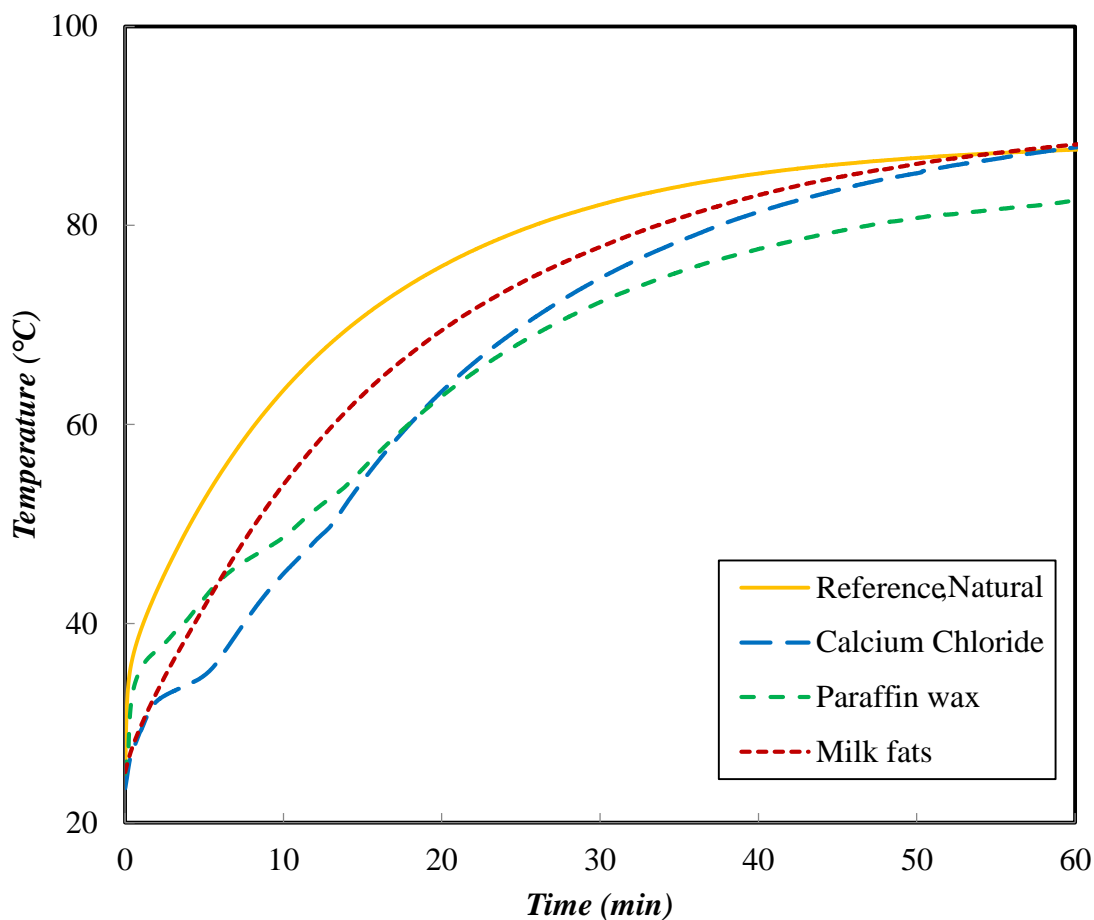
Figure 30: The heating curves for heat sink filled with different PCMs are compared to the reference case heat sink without PCM under 6W heat input and natural convection condition

In case of using natural convection cooling with PCM integrated in heat sink (shown in Figure 30), during the first few minutes of the experiment , milk-fat shows higher cooling effect compared to salt hydrate and Paraffin wax 6W. However, over the whole time duration of the experiment up-to 60 minutes, salt hydrate shows superior cooling performance compared to paraffin wax and milk-fat. The same trend is observed for natural convection cooling with PCM for all the rest of the heat inputs of 4W, 8W and 10W respectively (Appendix 3, Figure 56). This shows that the salt hydrates is more appropriate option when it comes to temperature control over a longer time (60 min under natural convection, 25 min under forced convection).
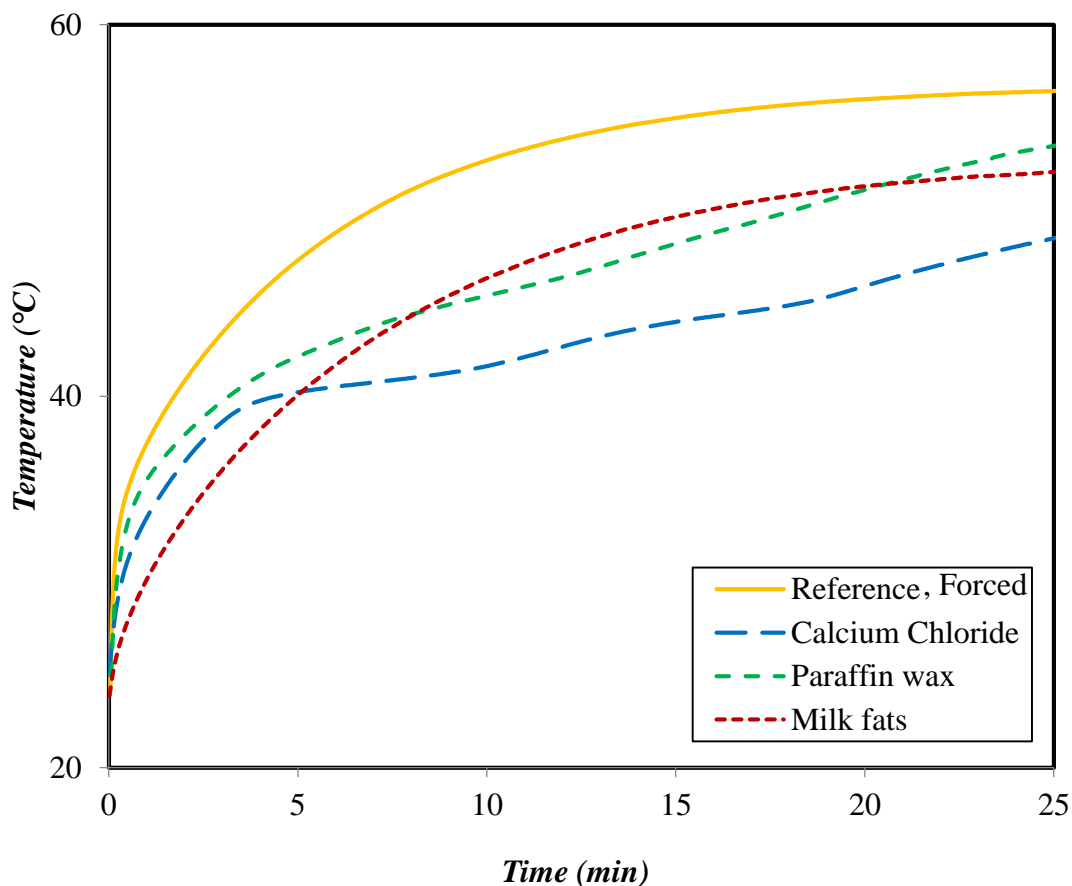
Figure 31: The heating curves for heat sink filled with different PCMs are compared to the reference case heat sink without PCM under 6W heat input and forced convection condition

Applying forced ventilation coupled with PCM during a heating cycle improves the cooling performance for the system compared to natural ventilation with PCM as evident from Figure 31. The milk-fat yields a better temperature drop than paraffin wax and salt hydrate at the start however the salt hydrate performs better both milk fat and paraffin wax as long terms exposure. Similar to what was observed in Figure 30, the milk fat is less effective compared to both paraffin and salt at higher temperatures and longer time exposure mainly due to its lower melting point and early start and completion of melting. The similar trend is observed at the rest of the heat input levels of 4W, 8W and 10W (Appendix 3, Figure 57).

It is also clear that in case of forced convection (Figure 31) that the milk-fat performed the best amongst the PCMs for the first 5 minutes, since milk fat has the lowest melting point of all, it indicates that at the start, the cooling is dominated by the effect of melting temperature of the PCM. Nevertheless, beyond the 5 minutes, the fat-milk capability to absorb heat reduces due to completion of melting caused by its lower heat of fusion, the other two PCMs (mainly calcium chloride which has higher latent heat when compared to the rest of PCM) starts melting forcing temperature to stay lower than the rest of PCM. On the contrary, in natural convection case (Figure 30), the start of experiment is dominated by the conduction heat transfer (as material still is solid) so calcium hydrate dominates the cooling performance since it has the highest thermal conductivity compared to paraffin wax and milk fats.

Concluding Figures 30 and 31 show that the forced convection combined with PCM achieves the lowest possible temperature of all modes of operations however, in addition to increased cooling effect, the coupling of the PCM in electronic packaging with fan has an important safety dimension as well. In case of fan failure with forced ventilation only system, the cooling system may stop and the device operation may be intervened or else the device may over heat and fail. Coupling PCM with fan will always guarantee that in case of fan failure, the PCM can still regulate device temperature and can perform the operation and protect the device from failure for certain time needed for automatic fault diagnostic fixation or a routine device shut down procedure as appropriate. As a conclusion, configuration of forced ventilation combined with PCM maintains the lowest temperature of all four cases for short period of time based on the type of the used PCM. Therefore, a combination of forced

convection through fan and latent heat absorption based cooling through PCM is more effective option for cooling electronic packaging.

It is recommended to use the HS filled with PCM in the cyclic operations such as switching operation or the applications need to have a huge temperature drop at the starting operation. It also recommended to use PCM integrated into a HS to provide a backup passive cooling support especially in case of failure of the fan system during operation as an additional safety cover.

The experimental data for integrated time-temperature difference graphs for all cases using the three PCMs compared with reference case without PCM is summarized in a bar chart to compare the net temperature drop achieved by each PCM (Calcium chloride, Paraffin wax and Milk-fat) over the whole duration of the experiment till steady state in Figure 32.
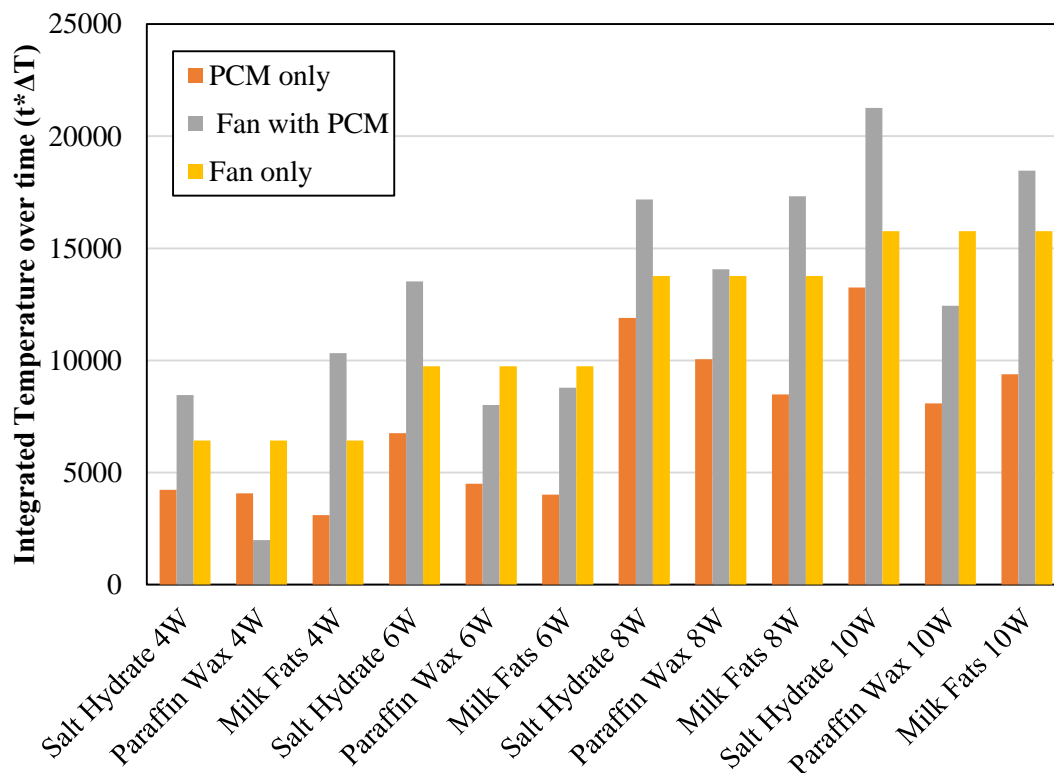
Figure 32: The temperature drop achieved by integrating PCM (Calcium chloride, Paraffin wax and Milk-fat) in the heat sink surface for both ventilation system

From the bar chart results (Figure 32), it is clearly observed that calcium chloride produced highest integral of time-temperature drop which means highest thermal regulation. It provides highest amount of cooling for the whole duration of heating cycle under both natural convection and forced convection regimes for all tested heat inputs.

Paraffin wax achieves better cooling than milk-fat under natural convection for all heat inputs which is understandable as paraffin has higher heat of fusion than milk fats. On the contrary, the milk-fat performs better than paraffin for forced convection, however the proven reason for this contradiction is not well understood and studied and needs further experimentation. Although it needs experimental validation, it seems lower melting point and wider melting range of milk fat (10 °C - 40 °C) combined with

forced ventilation helps remove heat at lower temperatures than the paraffin which melts at higher temperature (37 °C - 43 °C) and allows the heat sink filled with paraffin to raise in temperature at start and limited time of experiment.

5.1.2 Cooling curve performance for different PCMs

The re-solidification or regeneration for each PCM during the non-operation or off-duty cycle is an important factor which determines the cooling performance, choice of the PCM and time lapse between duty cycles of the device for a particular application. Should the PCM take longer time to re-solidify or regenerate, it may be attributed to either the thermos-physical properties of the PCM or the design of the PCM containment, the heat sink in this case. In order to understand the regeneration behavior, the melted PCM in heat sink is subjected to both forced convection and natural convection until complete solidification. The results are plotted for the temperature of the heat generating surface at the heat input of = 6W as shown Figure 33 and Figure 34.
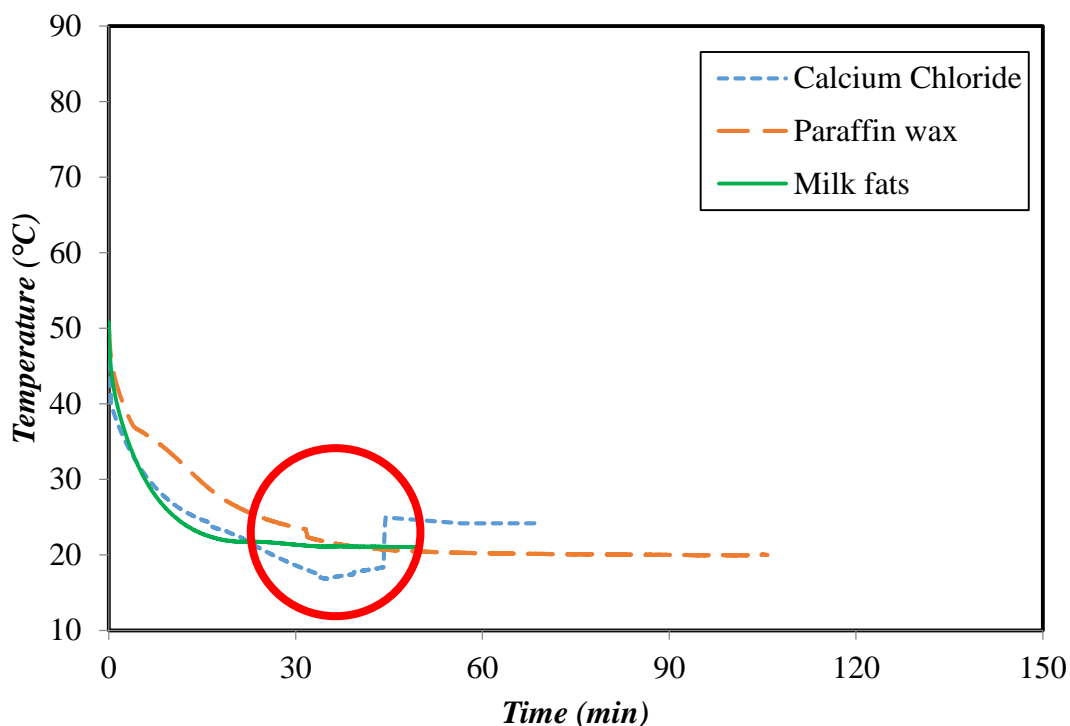
Figure 33: The PCM regeneration previously filled in heat sink for the materials namely, Calcium chloride, Paraffin wax and Milk-fats subjected to heat input= 6W under forced convection

From the Figure 33, in case of forced ventilation, all the PCMs cool down with a similar gradient until the start of the solidification. In case of milk fat, it does not show a clear transition from liquid to solid as expected as the solidification range is quite larger (40 °C - 10 °C) and may not show a clear boundaries of transition in terms of temperature. The paraffin wax shows a drop in temperature gradient between (43 °C - 37°C) which represent the start and end of solidification similar to start and end of melting in the previous sections. The salt hydrate cools below melting range (27 °C - 32 °C) down to about 16 °C in order to crystallize and start solidification and then rises up to the solidification temperature to complete solidification as shown by the red circle. This phenomena is called sub-cooling and is very common in salts which makes it difficult to remove heat from them especially if PCM melting points falls near

ambient temperature as is in this case. The sub cooling is not observed in paraffin wax or milk-fat which mean even if they produce less cooling effect than salt hydrates, they are superior in terms of crystallization and solidification and can re-solidify around ambient temperature for a continuous operation. In other word, during the extraction of the stored heat, salt sub-cools before freezing which drops their regeneration temperature far below the actual solidus temperature. This phenomena does not only happen in forced ventilation but also, happens in natural ventilation cooling system as shown in Figure 34.
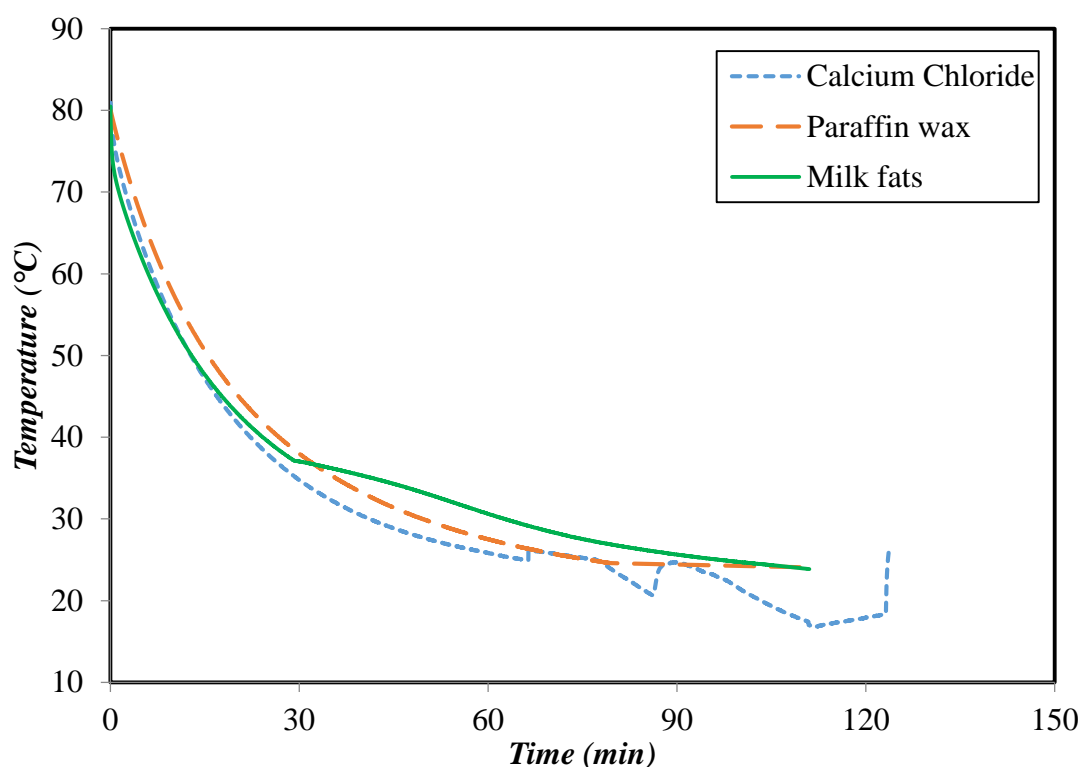
Figure 34: The PCM regeneration previously filled in heat sink for the materials namely, Calcium chloride, Paraffin wax and Milk-fats subjected to heat input 6W under natural convection

From Figure 33 and 34, the regeneration temperatures of salt hydrate-calcium chloride hexa-hydrate falls down to (18-16°C) from solidus temperature of 27 °C. This reduces restricts use of the materials and, in severe conditions, can completely prevent

PCM regeneration to be ready for the next heating cycle. The PCM re-solidification time for all the PCM previously subjected to various heat loads under natural convection and forced convection is summarized in Table 8.

	Calcium chloride hydrate		Paraffin wax		Milk-fat	
	Natural convection (min)	Forced convection (min)	Natural convection (min)	Forced convection (min)	Natural convection (min)	Forced convection (min)
4W	105	45	95	38	80	28
6W	125	50	114	40	83	30
8W	155	50	120	42	85	27
10W	225	53	130	37	87	30

Table 8: The time for solidification for three PCMs filled in heat sink previously subjected to different heat inputs under natural convection and forced convection

5.2 Numerical Results and Discussion

The CFD model for the heat sink integrated with the PCM is numerically established for the system discussed in the experimental section under same material properties and similar conditions. Next subsection discuss numerical validation using experimental results which is followed by numerical optimization of the validated model.

5.2.1 Numerical Validation via Experimental Results

5.2.1.1 Model validation with different heat inputs

In this section, cooling behavior of one PCM is tested at different power inputs. The temperatures of heat generation surface at a range of heat inputs are presented for salt hydrate (calcium chloride hexa) hydrate material numerically and experimentally under the same conditions (as shown in Figure 35, 36, 37 and 38 for power input 4W, 6W, 8W and 10W respectively).

Figure 35: Simulation and Experimental result of temperature for Salt Calcium hydrate at heat power of 4W under natural convection

Figure 35 clearly shows a slight over prediction at the lower temperature regimes for simulated temperature which is possibly because of higher melting onset input to the model. The melting onset is determined from DSC, which may have an error of 2-3 °C. Overall, a good agreement is noticed between the simulation and the

experimental results of the heat sink filled with the salt hydrate at heat load of 4W which shows that the model is reliable to predict PCM performance at lower heat inputs.

Figure 36: Simulation and Experimental result of temperature for Salt Calcium hydrate at heat power of 6W under natural convection

From the numerical results of the PCM (salt hydrate) present in Figure 36, a slight over prediction at lower temperatures and a slight under prediction during melting and medium temperatures is observed in the simulation results compared to experiments however the standard deviation remains under 5% being acceptable. The reason is not clearly understood, but the possibilities are slightly higher melting point and slightly higher heat of fusion being used in numerical simulation achieved through DSC results due to standard device errors. The simulation parameters are achieved from DSC which may contain about 5% error due to very small sample size (3-5 mg) and sensitivity of PCM thermo-physical properties based on sample composition,

heating rate and dehydration. Although, numerical results shows that ideal isothermal melting curve while the experimental curve partially deviates from isothermal, due to the natural convection within melted PCM which is not considered in the model, still the results are in good agreement with deviation less than 5%.
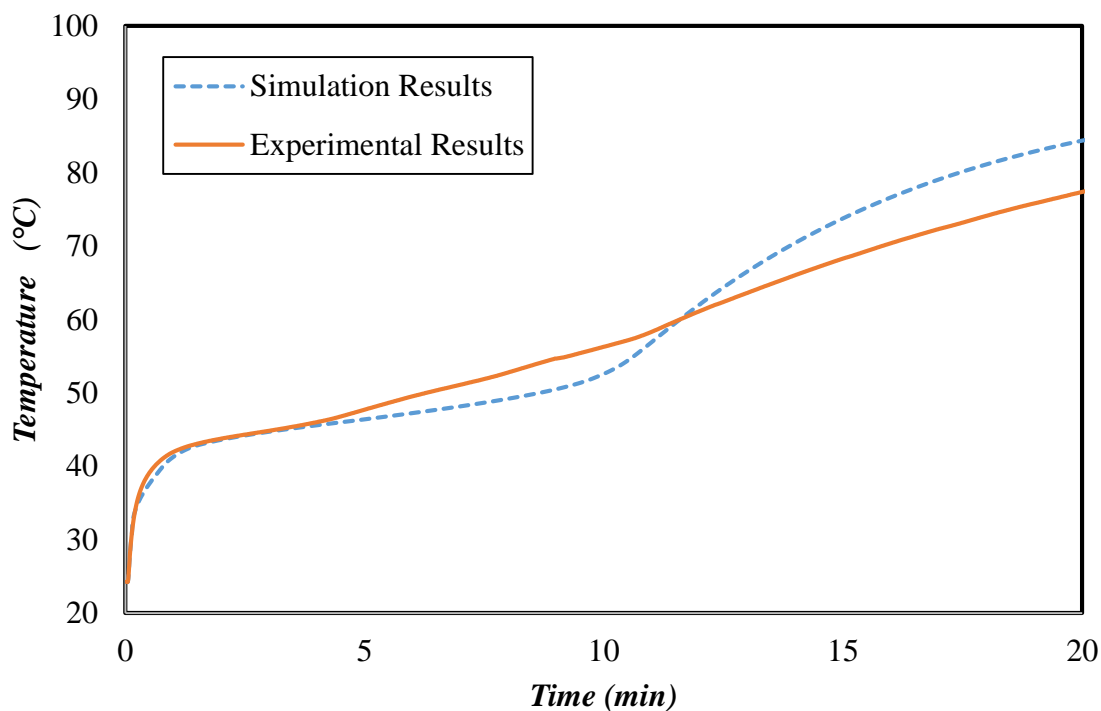
Figure 37: Simulation and Experimental result of temperature for Salt Calcium hydrate at heat power of 8W under natural convection

From Figure 37, the numerical and experimental results of temperature profile for the PCM at 8W under the natural convection show similar results observed at 4 W and 6W with percentage error less than 5%. In both the cases the material starts to melt at the same temperature and completes melting almost at the same temperature and then the temperature which shows that the results are validated and repeatable.
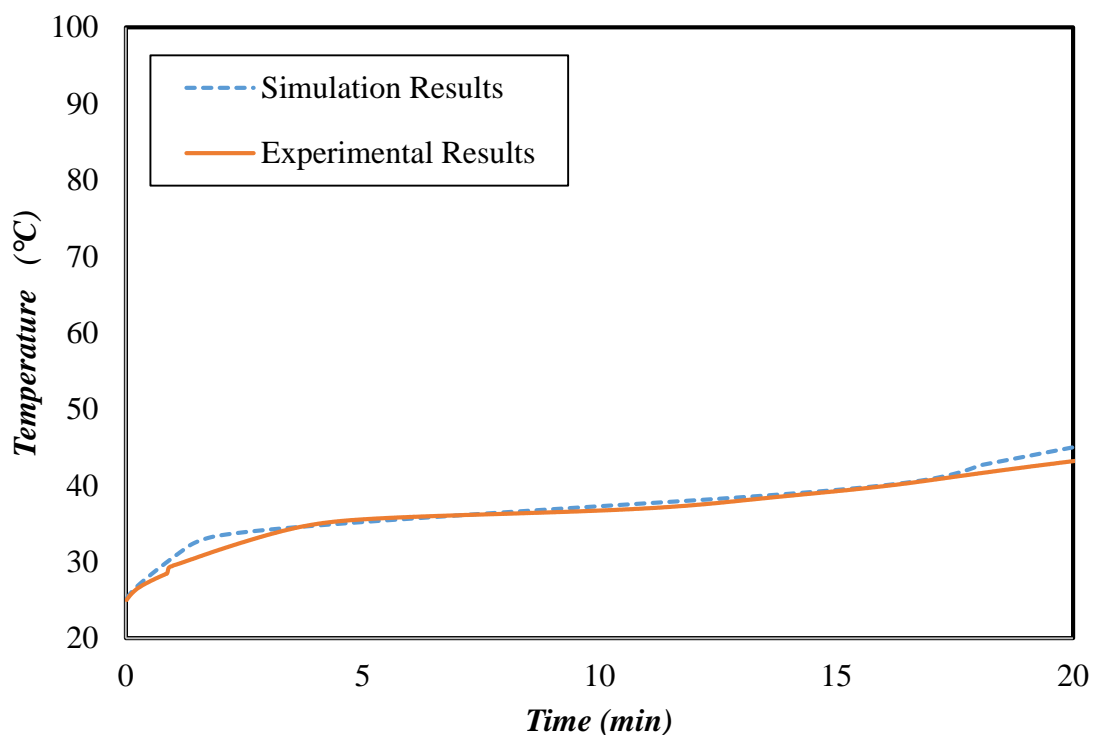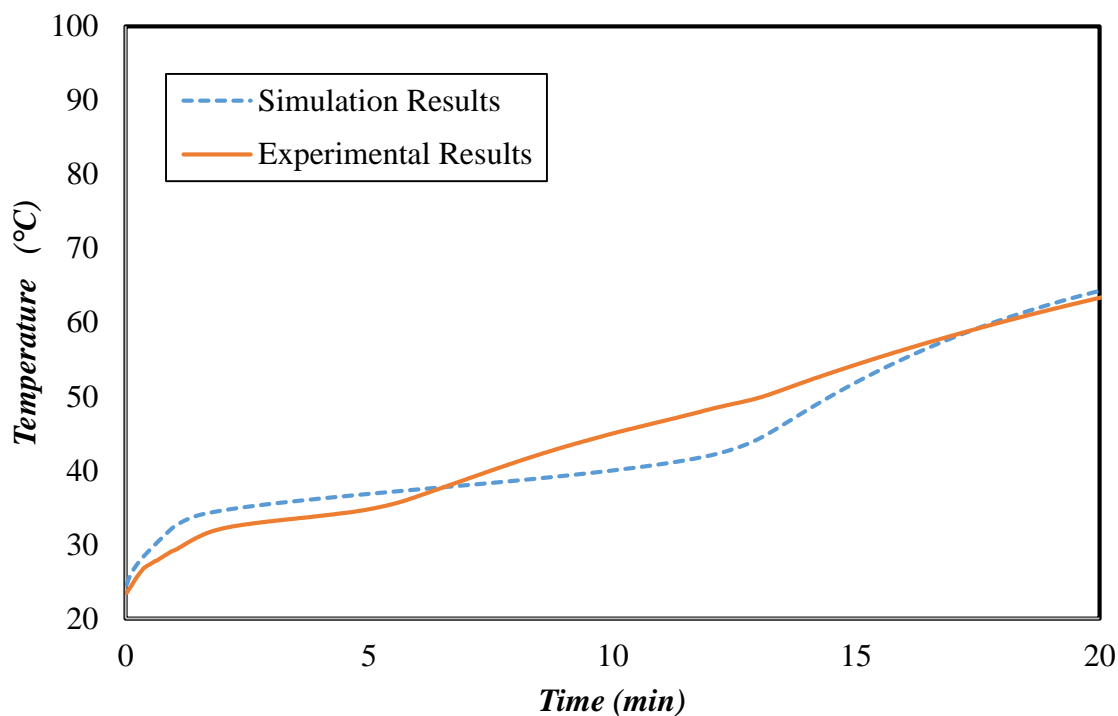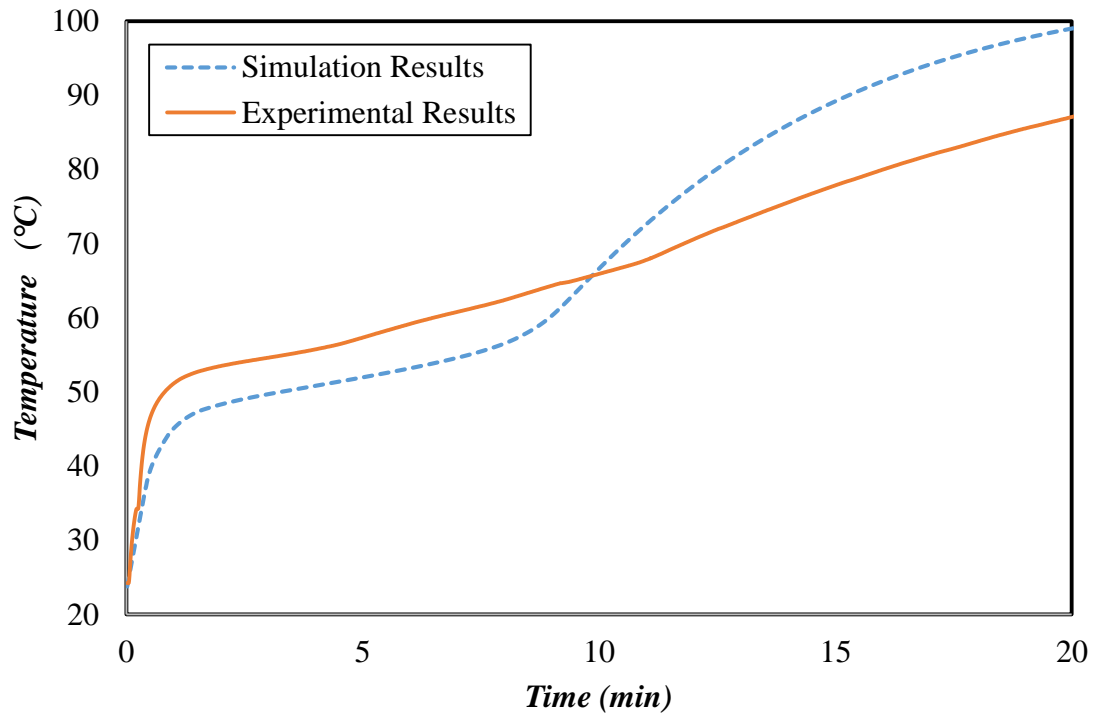
Figure 38: Simulation and Experimental result of temperature for Salt Calcium hydrate at heat power of 10W under natural convection

Figure 38 presents the comparison of experimental and numerical results the heat sink temperature evolution filled with PCM at 10W heat input. The experimental results do indicate a start of melting but do not clearly show a sharp end of melting. The reason can be attributed to the higher heat input which simply damps the temperature gradient at transition boundaries between sensible and latent heat absorption regimes due to faster internal heating of the PCM. The results still shows a reasonable agreement between experiments and simulation, however the deviation is higher than in the previous heat inputs of 4W-8W. However, the general trend of temperature evolution agrees and the deviation still remain less than 5 % in the phase change regimes which is acceptable given than fact that natural convection within melted PCM (which dominates at higher heat inputs) and the DSC standard errors are ignored in the modelling inputs.

From the previous presented data, the experimental results for the PCM at various heat inputs agree with numerical results within acceptable deviation so the simulation model is validated.

From Figure 35- 38, it observed that increasing the heat input while keeping the same amount of PCM will allow the material to melt faster and reduce temperature regulation time. Calcium chloride hexa hydrate takes 18 min to complete melting at 4W while at 10 W it completely melts in only 9 min. The reason is when the material is subjected for the higher heat input with the same PCM amount, the temperature of the enclosure will rapidly increase and that temperature will be absorbed by the PCM and allowing the PCM to melt faster. The time to completely melt against a certain power input will decide the choice of the type of PCM and the amount of PCM based on duration of the duty cycles for a device. However, additional amount of PCM could be added to the enclosure for such application which needs high heat power input and longer time to operate by an appropriate heat sink size.

5.2.1.2 Model validation with different PCMs

As a further supporting study, the analysis is extended to test the different types of PCM. The numerical analysis using ANSYS 3D Fluent model are carried out for the mentioned finned heat sink subjected to the fixed heat input of 6W with different PCMs under the forced convection. Figure 39, 40 and 41 present that simulation results for the different PCMs: Salt Calcium hydrate, Paraffin wax and Milk-Fat, respectively.
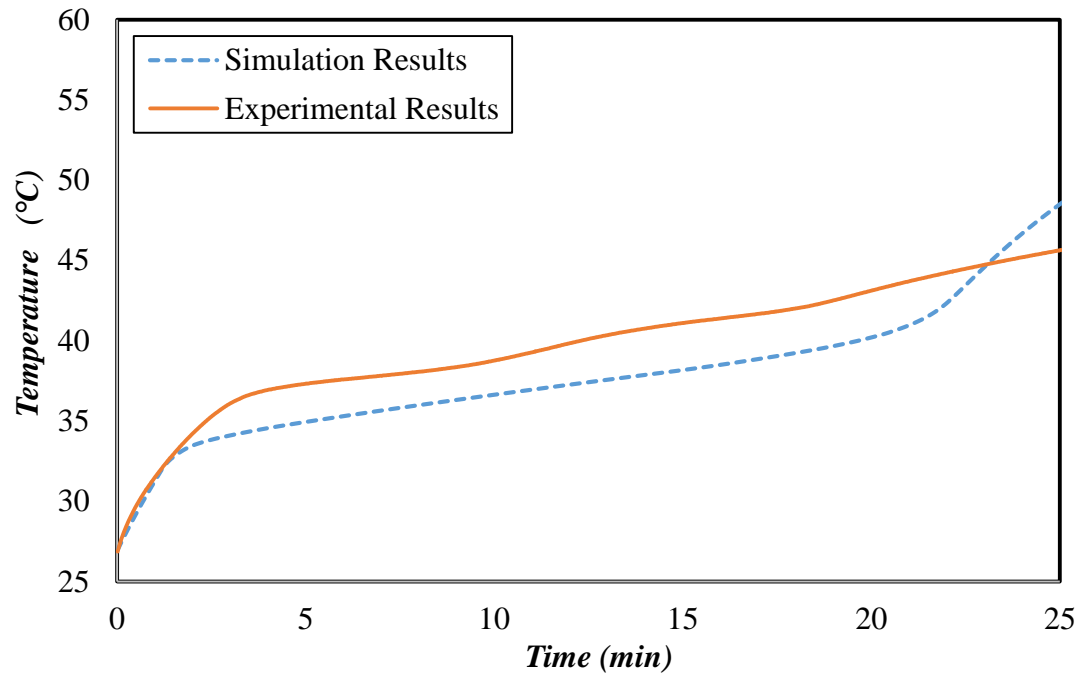
Figure 39: Simulation and Experimental results of heat generated at heat power of 6W under forced convection for Salt Calcium hydrate

From Figure 39, although the numerical prediction of the heat generator surface temperature for salt hydrate is lower than the experiment temperature. However, the material shows a consistent agreement all over the melting regime between both experimental and simulation results.
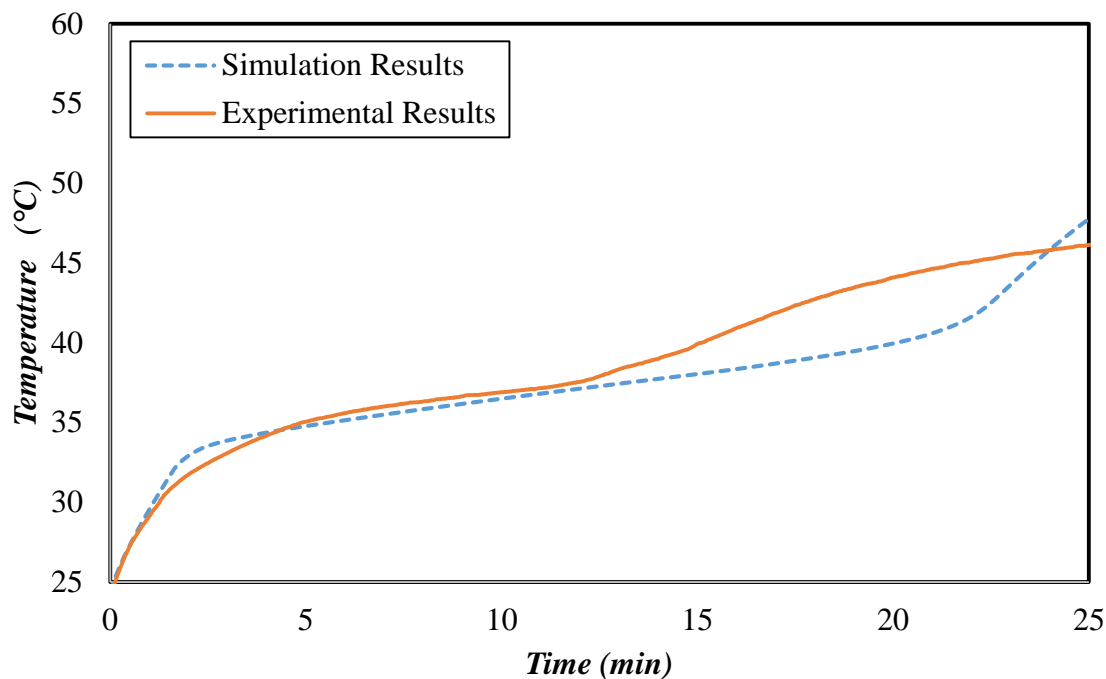
Figure 40: Simulation and Experimental result of heat generated at heat power =6W under forced convection for Paraffin

In Figure 40, the paraffin wax is shows a strong agreement between the numerical and the experimental results at the beginning of the melting process for the material until almost the middle of the melting regime up to 12 minutes. Beyond that the experimental results differ from the numerical results. The reason being that in experimental case, the PCM completes melting and start sensible heating and rise in temperature gradient while in the numerical case the PCM still keeps melting near isothermal. The cause can be either the higher heat of fusion or higher density or both being input to the model due to standard error in the DSC results.
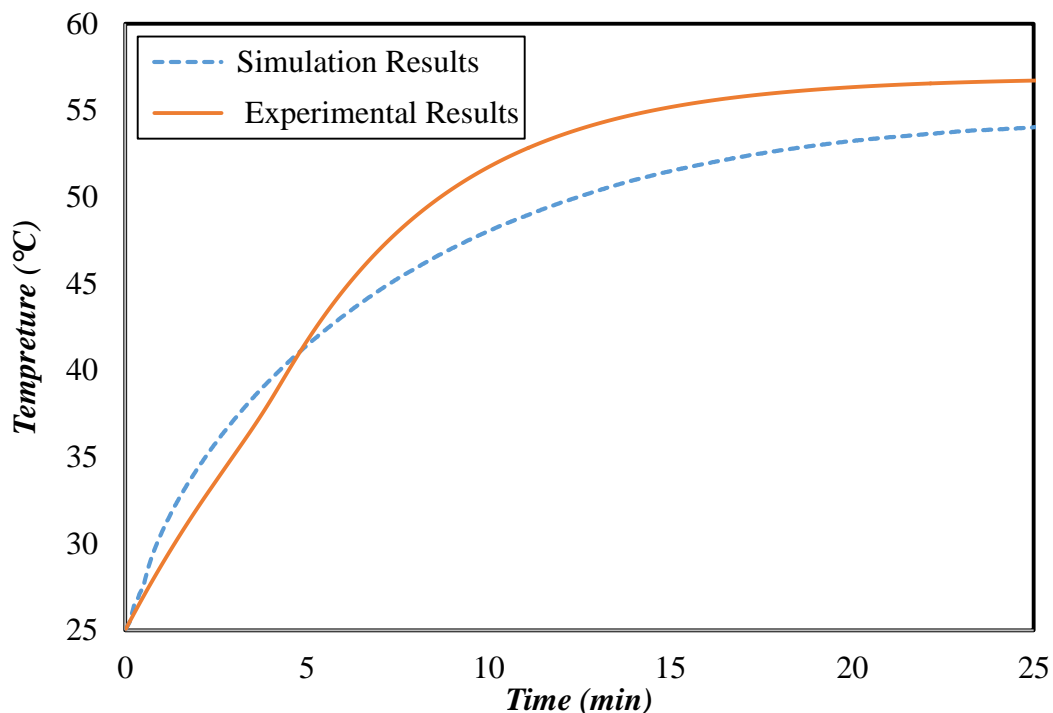
Figure 41: Simulation and Experimental result of heat generated at heat power = 6W under forced convection for Milk-Fat

Figure 41 presents the data for the temperature rise through simulation and experiments for milk fats. The numerical and experimental results of the milk fat material are in good agreement for the subjected heat inputs, however the curve is not consistent over the heating period. In the beginning the numerical temperature is higher up to 5 minutes and after that the experimental result show higher temperature than simulation. That could be explained by the constituents of the fats that consists of more than one components which melt at different temperature (showing more than one start and end of melting) however in numerical simulation with this present model, it is possible to fix only one range of start and end of melting which is put as (10° C – 40° C) which may not represent the true PCM behavior at certain time in time-temperature curve and cause deviation. However, the results in general are within acceptable deviation of under 5 %.

In general, Figure 39, 40 and 41 show that simulation results for all the tested three PCMs are in a good agreement with the experimental results conducted under the same conditions with acceptable error deviation. The numerical results mostly predicted higher temperature drop compared to experimental results however the deviation remained within acceptable range of 5 % given the assumption of ignoring natural convection within PCM and standard errors in source of numerical inputs (DSC).

5.3.2 Numerical Optimization of Heat Sink Geometry

Paraffin wax is used in the optimization analysis as a PCM integrated in the HS. One parameter is testing while the other material properties are kept constant through the analysis.

5.3.2.1 Heat sink height

Increasing the height of heat sink will accordingly increase the size of the heat sink along with fin height (H is in mm) allowing more PCM quantity packed in the heat sink. Figure 42 shows the melt fraction for different heights of heat sinks using volumetric liquid fraction (ratio of volume of liquid PCM to the volume of PCM at any instant) which is a measure of melting progression.
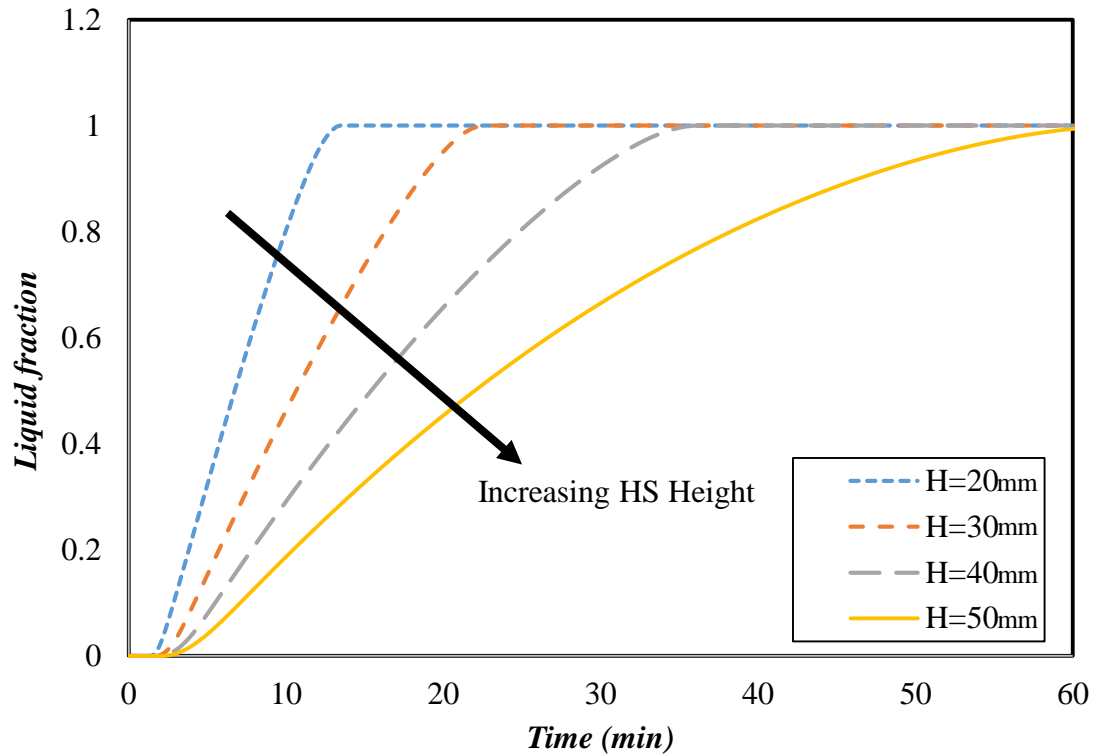
Figure 42: The effect of increasing the heat sink height on the liquid fraction of the PCM (Paraffin) at 6W

From the Figure 42, the time for melting is increasing from 13 min to 65 min as the heat sink height increases from 20 mm to 50 mm, which shows the time for which the heat sink can regulate the temperature of heat generator surface of the device. This is expected due to the increase in the material amount due to larger enclosure volume achieved by increasing heat sink height. The impact of increasing heat sink height (resulting in an increase of the amount of PCM) on the temperature drop of heat generator surface is shown in Figure 43.
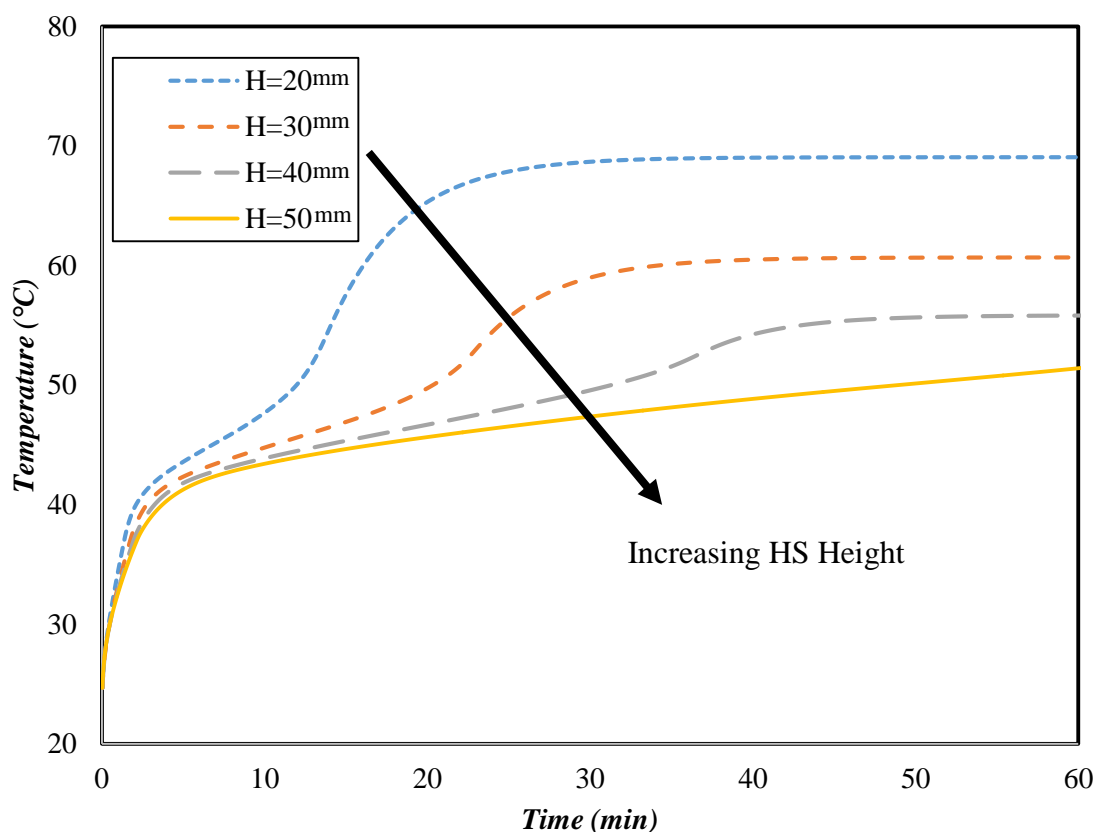
Figure 43: The effect of increasing the heat sink height on the temperature drop of the PCM (Paraffin) at 6W

It is clearly observed that the increasing heat sink height slows the temperature growth and vice versa. It could be explained that this drop in temperature happened because of the latent heat which is added to the system with the additional amount of the PCM. This curve helps to select the height of heat sinks depending on the required time operation of the device and intensity of heat input which depends on operating condition of the electronics component.

5.3.2.2 Fin shape

The effect of using different fin shapes on the temperature drop of the heat sink filled with PCM are evaluated in this section. The shape analysis of the fin will be constrained by keeping the volume of the fin constant. In this analysis the volume of

the fin remain constant however the area per volume changes due to fin shape which is reciprocal to the fin compactness. Table 9 shows the volume and surface area-to-volume ratio for each fin shape. It is clear that the rectangular fin has the highest surface area-to-volume ratio from each fin shape used
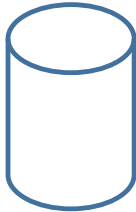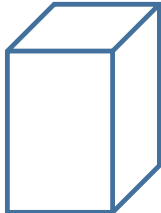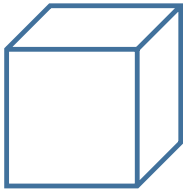
Fin shape	Volume	$\dfrac{\text{Surface area}}{\text{Volume}}$
		1.75
	57.6	2.1
		2.4
		2.34

Table 9: Surface area to volume ration for different fin shape

The heating curve for the PCM at 6W using different Fin shape (Circle, Rectangular, Square and Triangular) is presented in Figure 44.
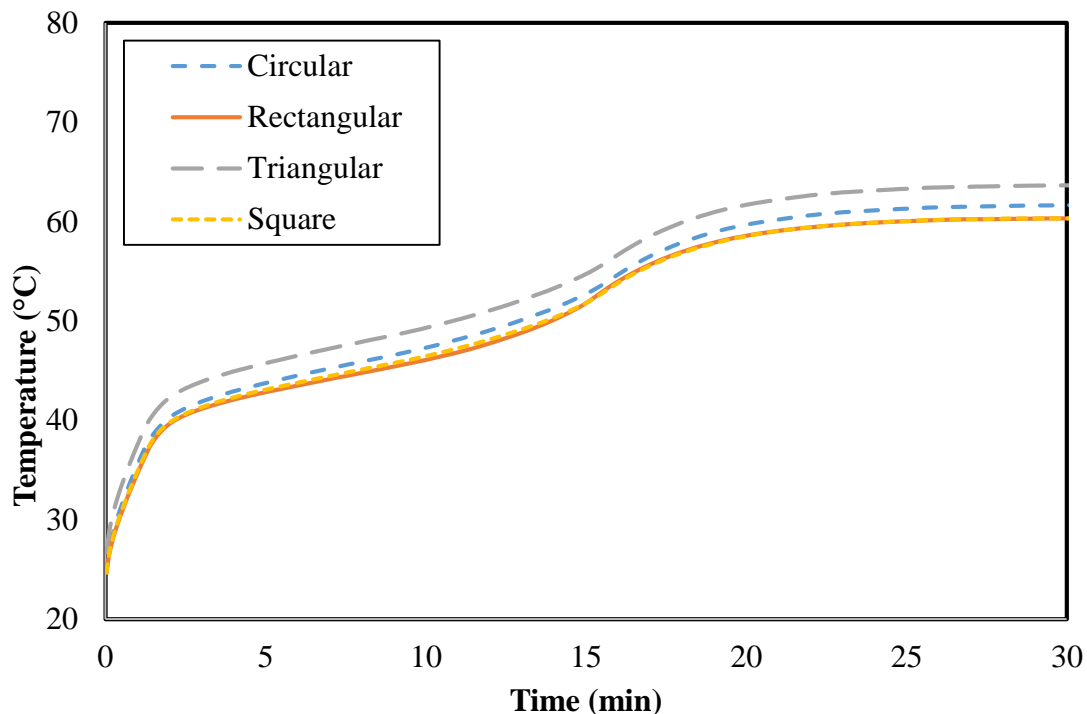
Figure 44: The heating curve for the PCM (Paraffin) at 6W using different Fin shape (Circle, Rectangular, Square and Triangular)

As the surface area of the object increases the heat losses increase. Therefore, from the table it is clearly understandable why rectangular fin shape has better performance in cooling the heat sink because of its larger surface area-to-volume ratio.

5.3.3 Numerical Analysis for Artificial Synthesized PCM

In this section, description and examination of relationship between different parameters of the heat sink and PCM through the numerical simulation model are presented. To understand the effect of different PCM on heat sink and to guide material engineer in synthesizing new PCM material, material properties used in the numerical

model represents paraffin. The numerical model is used to optimize the PCM property and the heat sink geometry under heat load of 6 W. The investigated parameters are:

- Thermal conductivity of the PCM

- Density of the PCM

- Melting point for the pure PCM

- Melting range representative of mixing different PCM

- Amount of PCM

5.3.3.1 Thermal conductivity of PCM

For any material, the higher is the thermal conductivity, the higher would be the heat transfer rate and the lower temperature difference across the material. Depending on the type of PCM, the thermal conductivity dramatically changes from 0.14 W/m °C (for fatty acids) to 0.8 W/m °C for salts hydrates. In Figure 45, a range of thermal conductivity values, are examined while the other material properties are kept constant taken from the thermos-physical properties of paraffin wax as a real material. Figure 45 shows the temperature profile for the paraffin material subjected to heat input of 6W at different thermal conductivity values ranging from 0.1 W/m °C to 0.8 W/m °C representing thermal conductivities of wide range of real PCMs.
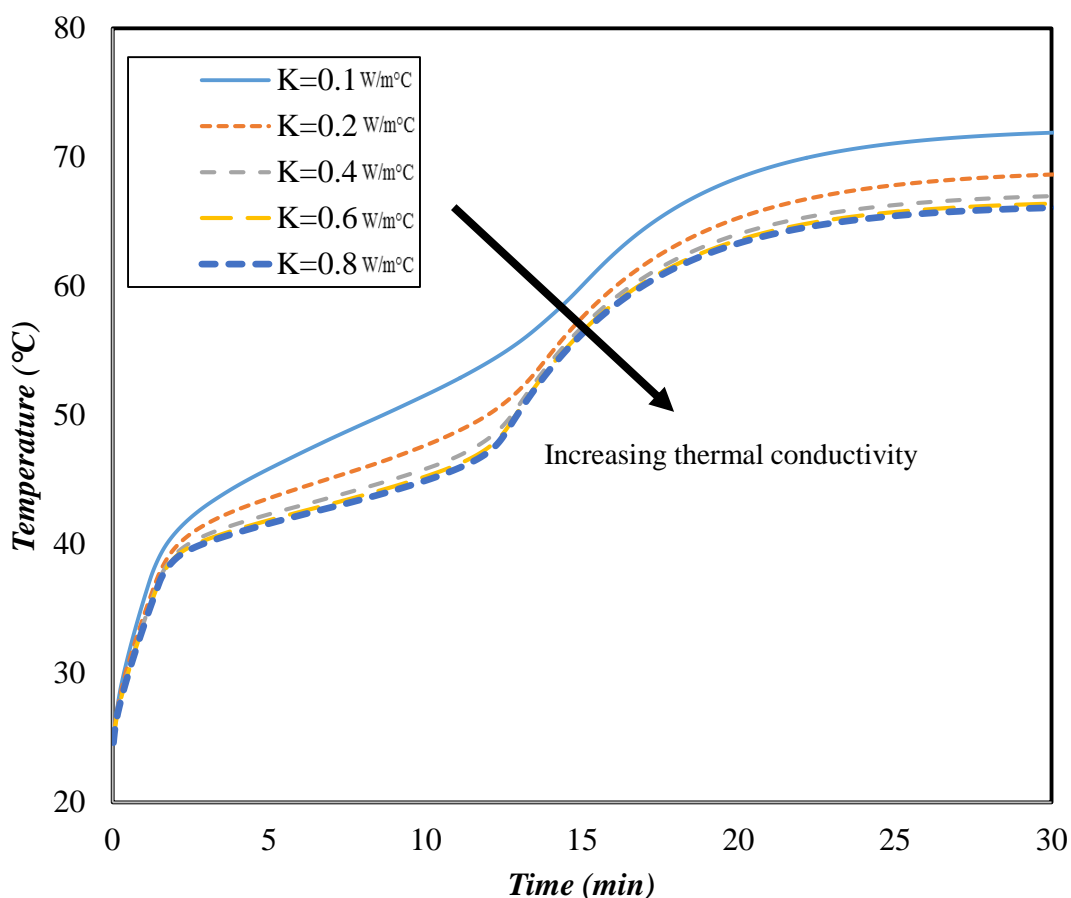
Figure 45: The effect of increasing the thermal conductivity of PCM (Paraffin) at 6W on the temperature drop of heat sink

From the Figure 45 as the value of thermal conductivity increases the drop in temperature increases representing improved cooling performance of the heat sink. Increasing the thermal conductivity of the PCM, will increase the heat transfer rate within PCM and the heat will transports faster from the hot region to an adjacent cooler area (heat sink walls through PCM). Initially the drop in the temperature as thermal conductivity increases from 0.1 to 0.2 is reasonably high (5 °C) however the temperature drop started decreasing and became minimal beyond the thermal conductivity of 0.8 W/m °C. It is conclude for this amount of PCM and specified geometry that the thermal conductivity of 0.8 W/m °C is the maximum impactful conductivity which luckily represent the thermal conductivity of real PCMs (salt hydrate). It means any thermal conductivity enhancers (like nano particles) added into

salt hydrate are least expected to improve the performance of the system showing that the salts naturally possess the optimum conductivities. However since the paraffin waxes used in this study possess less thermal conductivity (0.2 W/m °C), they can be improved by adding nano particles or other thermal conductivity enhancers to moderately increase their thermal conductivities to compete with the salts hydrates.

It has been reported that the thermal conductivity of PCM increased by as much as ten folds, the approach is numerically evaluated while adding the thermal conductivity enhancers into PCM to increase their thermal conductivities beyond the existing ones. Figure 46 shows the impact of using the thermal conductivity enhancers on the cooling performance of the heat sink.
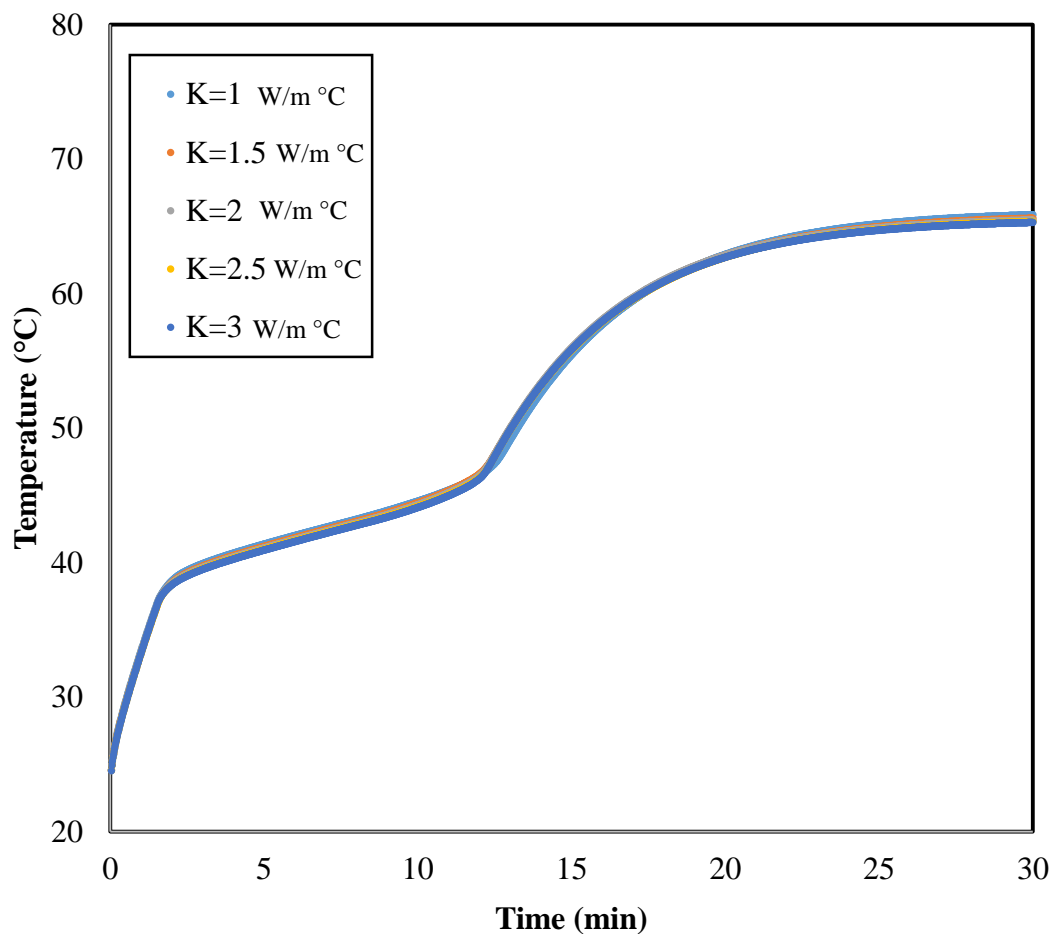
Figure 46: The effect of increasing the thermal conductivity for PCM by using the
enhancement at 6W on the temperature drop of Heat sink

From Figure 46 it can be seen that there is no substantial impact on cooling

performance of the PCM while in thermal conductivity is increased from 1 W/m °C to

5 W/m °C. The reason can be attributed to the present heat sink design which is already

overwhelmed with thermal conductivity enhancing metallic fins and does not have

room for more improvement enhancement. In future the conductivity enhancement can

be studied with various heat sink designs with less number of fins to see the effect of

PCM thermal conductivity enhancement on the heat sink temperature drop.

Figure 45 and 46 conclude that using enhancements for low thermal conductivity material like fatties 0.1 W/m °C will improve the cooling performance and increase the heat loss while using enhancements for high thermal conductivity PCMs like salts will not affect the cooling performance.

5.3.3.2 Density of PCM

The density of the material varies amongst materials and also with temperature and pressure. In this section, the effect of changing the density values (from 802 kg/m^3 to 1700 kg/m^2) on the temperature performance for the PCM by assuming other factors to stay unchanged is investigated subjected to heat input of 6W as shown in Figure 47. The density values range is selected to represent range of existing PCMs obtained from literature.
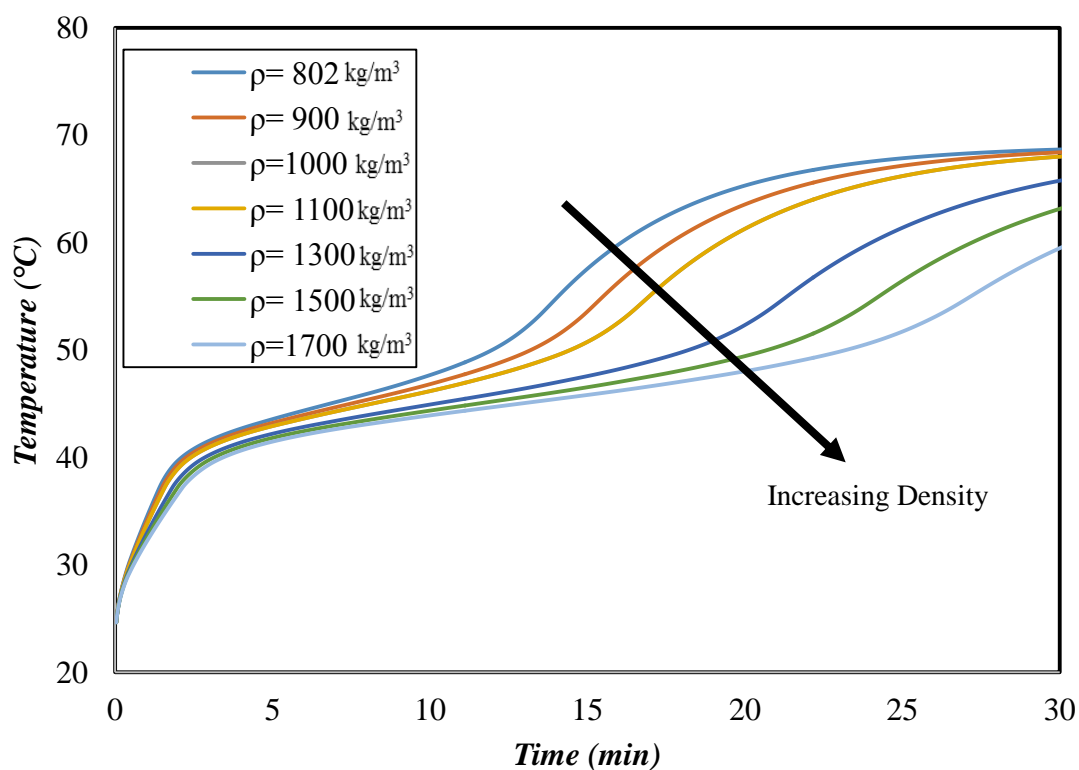
Figure 47: The effect of changing the density of the material on the temperature profile over a time

As the material density increases the temperature of the heat sink decreases especially within the melting region of the material. The drop of temperature is high from (ρ=800 kg/m^3 to ρ=1700 kg/m^3) by more than 20 °C degree. The density of 800 kg/m^3 represents paraffin wax while the density of 1700 kg/m^3 represents salt hydrate. Figure 46 shows that the salt hydrates perform much better than paraffin just due to higher density.

The density will also have an effect on the liquid fraction of the PCM as shown in Figure 48. As the density increases, the time needed for the material to completely melt is increasing which means a higher density PCM can regulate temperature for longer duration of time within the same heat sink size compared to a low density PCM.
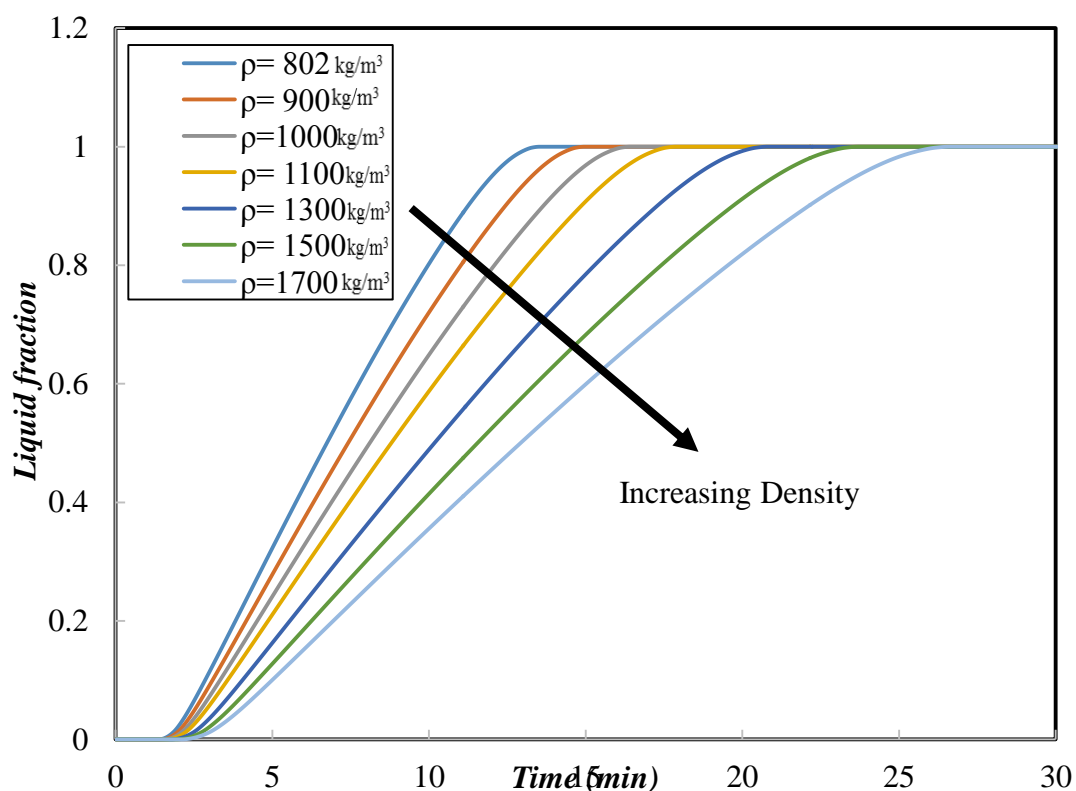
Figure 48: The effect on changing the density of the PCM (Paraffin) on the Solids to Liquid ratio over a time

5.3.3.3 Melting point for the PCM

Changing the melting point for the material will directly affect its cooling performance. A numerical analysis was run for different melting ranges to study that effect. Figure 48 shows how the melting point has effect on the temperature of the heat generating surface for the paraffin wax at heat input of 6W.
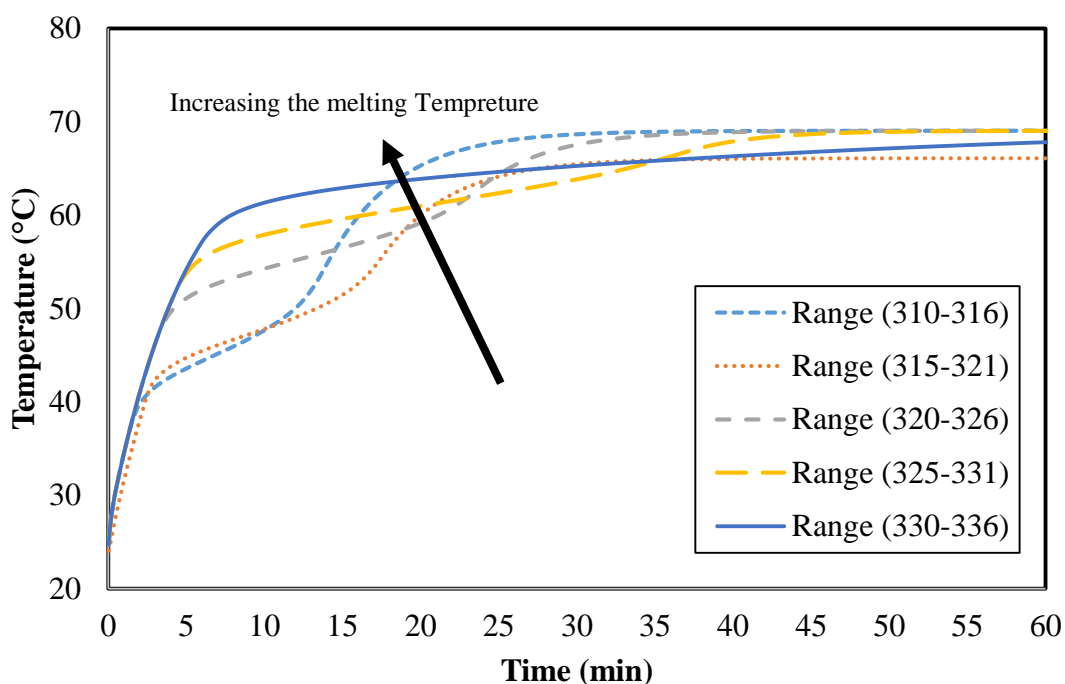
Figure 49: The effect of changing the Melting point range for the PCM (Paraffin) at 6W on the temperature drop of Heat sink

Figure 49 shows, as the melting temperature increases, the temperature drop on the heat generating surface decrease. It shows that the melting point of 37 °C (310 K) and 43 °C (316 K) get similar results and can be used for this type of heat sink and power. Melting temperature ranges of (47 °C (320 K) to 53°C (326 K)) and (52°C (325 K) to 58°C (331 K)) take very long to melt and also result in higher temperature and may not be suitable at the current heat input. So, the optimum PCM selected for our experiments will have melting point from 37°C (310K) to 43°C (316K). It is expected

that the melt fraction of the material will be changed as the melting point change. Figure 50 shows the melting temperature with the melt fraction for the paraffin wax at 6 W.
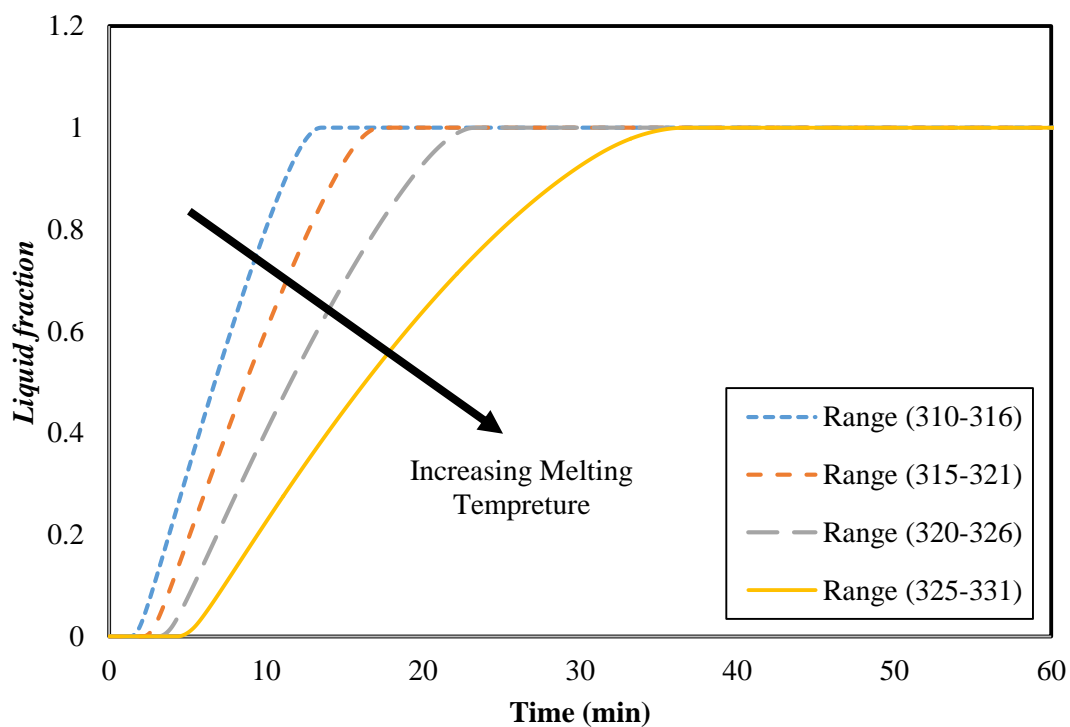
Figure 50: The effect of changing the melting point range for PCM (Paraffin) at 6W on the liquid fraction drop of heat sink

From Figure 50 it is observed that lower melting point PCM completes melting faster and control temperature for shorter time compared to high melting point PCM which is contrary to the cooling achieved where the lower melting point PCM performs better. So, in real design situation, it is a trade-off between the temperature to achieve and the time for temperature regulation which will dictate the optimum PCM for a particular application.

5.3.3.4 Increasing the melting region of the PCM by mixing different materials

Mixing different PCM together will change their melting range which can be important for certain applications. In this section, mixing of PCM is represented by their melting range and numerical analysis is conducted taking rest of the thermo-physical properties of paraffin wax apart from melting range subjected to heat input of 6W.
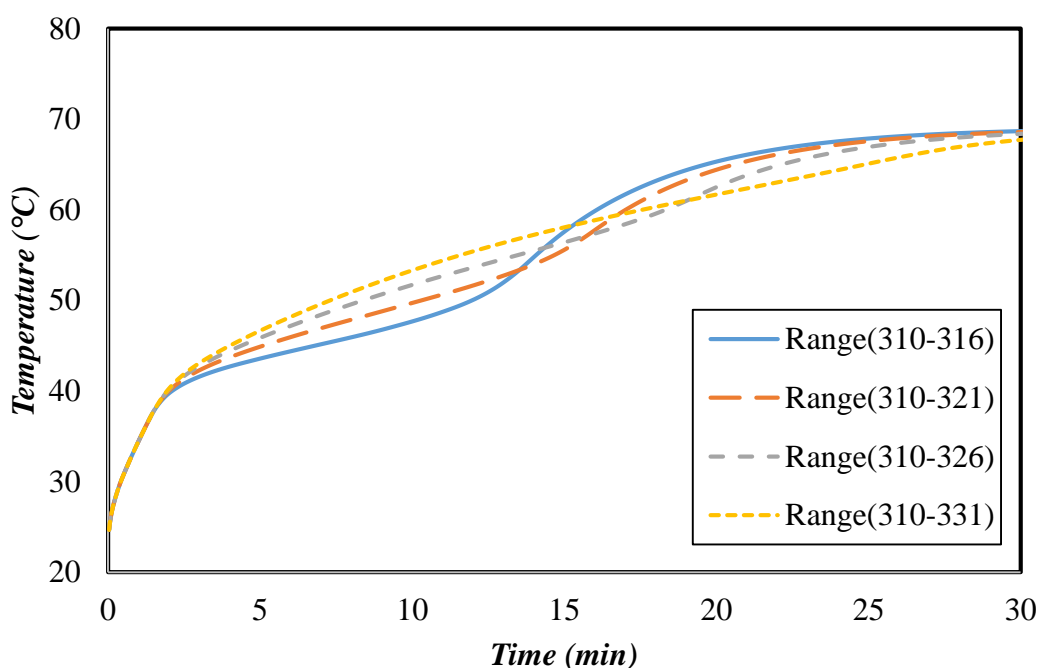
Figure 51: The effect of increasing the melting range for PCM (Paraffin) at 6W on the temperature drop of Heat sink.

Figure 51 shows the effect of increase in melting range on the melting curve and temperature drop of the heat generator surface. It shows that when the melting point is fixed 37 °C (310 K) representing a pure existing PCM the melting curve is sharp which means it can control temperature within the narrow limit. When rang of melting increases to 37 °C – 43 °C (310 K – 316 K) which shows mixture of two materials with different melting points, the melting curve lifts up and less sharp end of

melting is observed which shows it undermines a strict temperature control at a fixed temperature. When the temperature range is further increased to 37°C - 48°C (310K - 321K) and 37°C - 53°C (310K - 326K) which means mixture of more materials with different melting points, the temperature increases and also the sharp end of melting is not observed which shows that for restricted temperature control applications, mixing of materials does not help as it widens the temperature limit which may not be allowable in many devices. Figure 52 shows the effect of increasing the melting range melt fraction of the PCM contained in the heat sink.
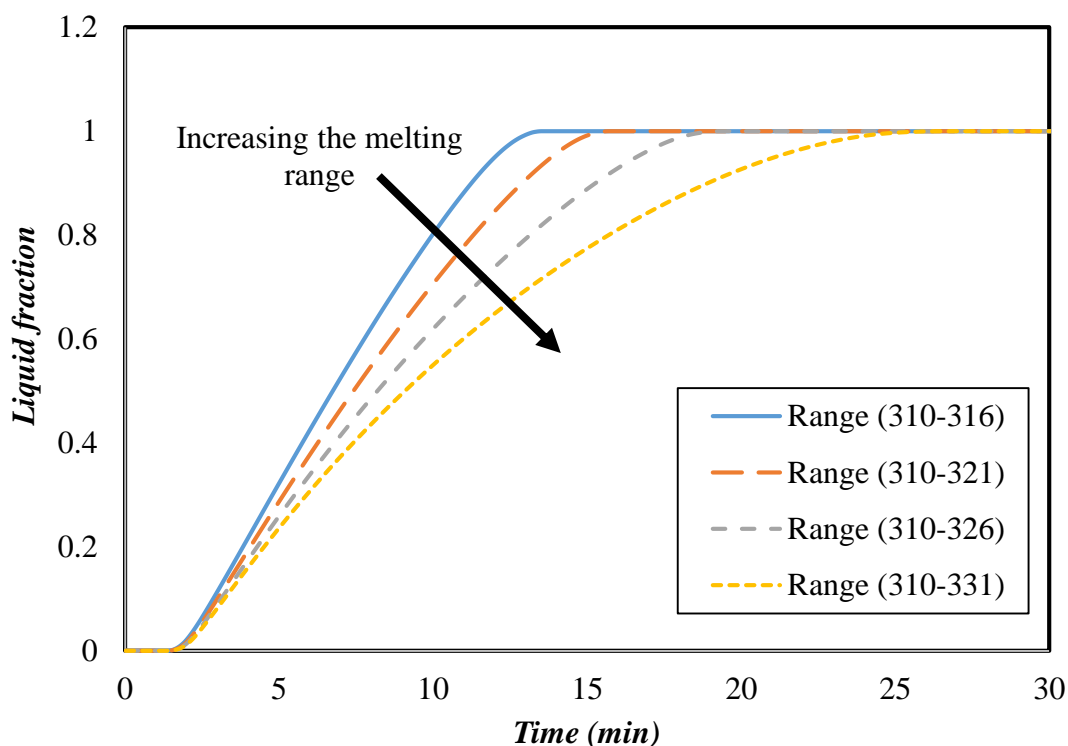
Figure 52: The effect of increasing the melting range for the used PCM (Paraffin) at 6W on the temperature drop of Heat sink

It is observed when melting range increases, the time to complete melting increases which is considered not good for temperature control applications. So, it is recommended that for strict temperature control applications, a PCM with sharp

melting point and narrow melting range should be used and should not be mixed with different melting point materials.

From parametric study, it is observed that a narrow melting point, not mixing of the PCM, good thermal conductivity, higher density, rectangular fin type and a reasonable package size are optimum for the temperature control of electronic devices employing heat sink with PCM.

Chapter 6: Conclusion and Recommendations

6.1 Conclusion

Uncontrolled heat generated by electronic devices does not only decrease the performance, but may ultimately lead to complete system failure. The heat sinks are prepared as metallic containments having fins with fixed inter-fin spacing. The HS is filled with three types of PCMs, namely: a paraffin wax, salt hydrate-calcium chloride and milk-fat, and is subjected to various heat loads at 4W, 6W, 8W and 10W. Four modes of operation are experimentally tested in this study. These are: HS under natural convection, HS integrated with PCM under natural convection, HS under forced convection, and HS integrated with PCM under forced ventilation. In this study, the heat sink filled with PCM is subjected to various heat loads. The heat generating surface and heat sinks surface temperatures are monitored to evaluate the PCM thermal performance.

It found through the results analysis, when adding PCM into the heat sink a time lag in temperature rise is observed due to melting and latent heat absorption. It shows that for first 15 minutes the WPCM-Natural convection) achieved the minimum temperature however it later on raised in temperature and shows a higher temperature than the WOPCM-Forced convection. Using PCM shows a larger heat loss and temperature drop up to 15 °C compared to fan ventilation with no PCM. In both natural ventilation and forced ventilation case, the temperature remains lower with PCM inclusion compared to without PCM at the start, however the PCM under natural convection shows higher temperature than fan ventilation with and without PCM after 15 minutes of exposure which shows that the PCM alone cannot compete with fan

alone ventilation system for larger exposure time mainly due to completion of melting of the PCM followed by sensible heating and heat retention. For the larger time exposure (60 min), the result shows that the maximum temperature at the heat generating surface at 6 W is 75 °C without using the PCM under natural convection while using PCM under natural convection reduces it to 62 °C due to PCM cooling effect.

When fan is added without PCM, it drops the temperature strongly to very low temperatures compared to natural ventilation in all power inputs from 4W-10W due to increased heat losses from the surfaces of the heat sink to the ambient. At the heat generating surface at 6 W, Inclusion of forced ventilation without PCM reduces the temperature down to 50 °C which show that the forced convection thermal management techniques employing heat sinks is effective technique. However, the fan cooling system may fail in certain cases due to involvement of active mechanical components and in worst case damage the device leading to failure. The results present that the effect of in inclusion of PCM with forced ventilation in cooling system, brings the temperature down to 42 °C. Therefore, a heat sink integrated with PCM is found to be an effective cooling system in terms of both higher temperature regulation and increased safety due to passive temperature regulation nature of PCM. Coupling PCM with fan will always guarantee that in case of fan failure, the PCM can still regulate device temperature and can perform the operation and protect the device from failure for certain time needed for automatic fault diagnostic fixation or a routine device shut down procedure as appropriate. As a conclusion, a combination of forced convection through fan and latent heat absorption based cooling through PCM maintains the lowest temperature of all four cases for short period of time based on the type of the

used PCM . This system is the optimum choice for thermal management of the IC packaging in this case. However, it needs still further research in testing the effect of natural ventilation and forced ventilation with and without PCM when exposed to outdoor wind speed as to what configuration can be optimum. The future research may eliminate the inclusion of fan in some specific high wind speed locations and can rely only on natural convection with PCM inclusion.

Comparing the PCMs show that the milk-fat performed the best amongst the PCMs for the first 5 minutes, since milk fat has the lowest melting point of all, it indicates that at the start, the cooling is dominated by the effect of melting temperature of the PCM. Nevertheless, beyond the 5 minutes, the fat-milk capability to absorb heat reduces due to completion of melting caused by its lower heat of fusion, the other two PCMs (mainly calcium chloride which has higher latent heat when compared to the rest of PCM) starts melting forcing temperature to stay lower than the rest of PCM.

It is recommended to use the HS filled with PCM in the cyclic operations such as switching operation or the applications need to have a huge temperature drop at the starting operation. It also recommended to use PCM integrated into a HS to provide a backup passive cooling support especially in case of failure of the fan system during operation as an additional safety cover.

A three dimensional heat transfer CFD numerical model is developed and numerical analysis is performed to compare numerical predictions with the experimental results. A good agreement is obtained between the experimental results and numerical simulations. A fundamental understanding of the conjugate convection–conduction heat transfer in the three-dimensional heat sink is provided.

In general, the result show that simulation results for all the tested three PCMs are in a good agreement with the experimental results conducted under the same conditions with acceptable error deviation. The numerical results mostly predicted higher temperature drop compared to experimental results, however, the deviation remained within acceptable range of 5 % given the assumption of ignoring natural convection within PCM and standard errors in source of numerical inputs

From the parametric study, it is observed that a narrow melting range for the PCM, not mixing of more than one PCM, good thermal conductivity (Higher) and higher density are the optimum thermal properties for effective cooling performance of inclusion PCM into HS. In addition, rectangular fin type and a reasonable package size are also the optimum parameters for the temperature control of electronic devices employing heat sink with PCM.

6.2 Recommendations

Through the current research although it is found that the thermal management of electronic packaging is more effective through combination of the forced ventilation and PCM compared to natural ventilation or forced ventilation without PCM however there are few factors which need to be considered.

1- The proposed thermal management system can limit temperature under designated service temperature for a short time which can only be used to control the transient temperature rise for a specific time. For longer operation time, the PCM acts as a thermal energy retention system and may work against heat dissipation during no operation conditions when the electronic package is cooling down

2- The thermal management systems works very good for a cyclic heat load for certain applications and may not be suitable for a continuous operation

3-The thermal management system needs further investigations in terms of improving the interface heat transfer between heat sink and heat generator surfaces.

4- The thermal management system needs further investigation to improve thermal conductivity of the PCM and the fin surfaces which can be realized through inclusion of appropriate thermal conductivity enhancers such as carbon nanotubes and nanoparticles.

5-The thermal management design needs further rigorous simulation studies in a bid to the design optimization for different heat inputs, heat sink geometries and PCM thermo-physical properties.

Bibliography

1. Kandasamy, R., Wang, X., & Mujumdar, A. (2008). Transient cooling of electronics using phase change material (PCM)-based heat sinks. Applied Thermal Engineering, 28 (8-9), 1047-1057.

2. Leoni, N. & Amon, C.H. (1997). Transient thermal design of wearable computers with embedded electronics using phase change materials. ASME, Natl. Heat Transfer Conf., 7 49–56.

3. Setoh, G., Tan, F., & Fok, S. (2010). Experimental studies on the use of a phase change material for cooling mobile phones. International Communications in Heat and Mass Transfer, 37, 1403-1410.

4. Seri Lee. (1995). How to select a heat sink. Advanced Thermal Engineering, 528-532.

5. Markstein, H. (1995). Optimizing Heat Sink Performance. Electronic Packaging and Production, 35 (10), 38.

6. Tuckerman, D., & Pease, R. (1981). High-performance heat sinking for VLSI. IEEE Electron Device Lett. IEEE Electron Device Letters, 126-129.

7. Bob wolbert, (1997). Designing P.C. Board Heat Sinks. MICREL, 3-189.

8. Gopalakrishnan, T. R., Nair & Aravindh, B., Sri, (2008). Heat sink performance analysis Through Numerical Technique. IEEE Symposium.

9. Hajmohammadi, M., Poozesh, S., Nourazar, S., & Manesh, A. (2013). Optimal architecture of heat generating pieces in a fin. Journal of Mechanical Science and Technology J Mech Sci Technol, 27, 1143-1149.

10. Hajmohammadi, M., Poozesh, S., & Hosseini, R. (2012). Radiation Effect on Constructal Design Analysis of a T-Y-Shaped Assembly of Fins. JTST Journal of Thermal Science and Technology, 7, 677-692.

11. Duffin, R. (1989). A Variational Problem Relating to Cooling Fins. Indiana Univ. Math. J. Indiana University Mathematics Journal, 8, 47-56.

12. Kondo, Y., Matsushima, H., & Komatsu, T. (1993). Experimental study of impingement cooling by heat sinks with thin longitudinal fins for LSI packages. Heat Trans. Jpn. Res. Heat Transfer - Japanese Research, 7, 449-459.

13. Chapman, C., Lee, S., & Schmidt, B. (1994). Thermal performance of an elliptical pin fin heat sink. Proceedings of 1994 IEEE/CHMT 10th Semiconductor Thermal Measurement and Management Symposium (SEMI-THERM).

14. Lasance, C., & Eggink, H. (2001). A method to rank heat sinks in practice: The heat sink performance tester. Semiconductor Thermal Measurement and Management IEEE Twenty First Annual IEEE Symposium, 2005.

15. Forghan, F., Goldthwaite, D. & Ulinski, M.; Metghalch, M. (2001). Experimental and Theoretical Investigation of thermal performance of Heat sinks. ASME.

16. Hajmohammadi, M., Poozesh, S., Campo, A., & Nourazar, S. (2013). Valuable reconsideration in the constructal design of cavities. Energy Conversion and Management, (66), 33-40.

17. Rocha L, Montanari GC, Dos Santos ED & Rocha AD. (2007) Constructal design applied to the study of cavities. Engengeria Termica (Brasil), 6, 41–7.

18. Biserni, C., Rocha, L., & Bejan, A. (2004). Inverted fins: Geometric optimization of the intrusion into a conducting wall. International Journal of Heat and Mass Transfer, 47, 2577-2586.

19. Biserni, C., Rocha, L., Stanescu, G., & Lorenzini, E. (2007). Constructal H-shaped cavities according to Bejan's theory. International Journal of Heat and Mass Transfer, 50, 2132-2138.

20. Geffroy, P., Mathias, J., & Silvain, J. (2010). Heat Sink Material Selection in Electronic Devices by Computational Approach. Advanced Engineering Materials Adv. Eng. Mater, 400-405.

21. Mukesh K., Anil K., & Sandeep K. (2013). OPTIMUM DESIGN AND SELECTION OF HEAT SINK, International Journal of Application or Innovation in Engineering & Management (IJAIEM) 2 (3), 2319 – 4847.

22. Lee, S. (1995). Optimum design and selection of heat sinks. Proceedings of 1995 IEEE/CPMT 11th Semiconductor Thermal Measurement and Management Symposium (SEMI-THERM).

23. Micro-channel Heat Sinks (MCHS). (1988). Springer Reference.

24. Kim, S., Paek, J., & Kang, B. (2003). Thermal performance of aluminum-foam heat sinks by forced air cooling. IEEE Transactions on Components and Packaging Technologies IEEE Trans. Comp. Packag. Technol., 26 (1), 262-267.

25. Tuckerman, D., & Pease, R. (1981). High-performance heat sinking for VLSI. IEEE Electron Device Lett. IEEE Electron Device Letters, 126-129.

26. Shabgard, H., Allen, M., Sharifi, N., Benn, S., Faghri, A., & Bergman, T. (2015). Heat pipe heat exchangers and heat sinks: Opportunities, challenges, applications, analysis, and state of the art. International Journal of Heat and Mass Transfer, 89, 138-158.

27. Azar, K. & Tavassol, B. (2009). Led lighting: A case study in thermal management. Thermal E-magazine .

28. Nayak, K., Saha, S., Srinivasan, K., & Dutta, P. (2006). A numerical model for heat sinks with phase change materials and thermal conductivity enhancers. International Journal of Heat and Mass Transfer, 49, 1833-1844.

29. Lu, T. (2000). Thermal management of high power electronics with phase change cooling. International Journal of Heat and Mass Transfer, 43, 2245-2256.

30. Sabbah, R., Kizilel, R., Selman, J., & Al-Hallaj, S. (2008). Active (air-cooled) vs. passive (phase change material) thermal management of high power lithium-ion packs: Limitation of temperature rise and uniformity of temperature distribution. Journal of Power Sources, 182, 630-638.

31. Sabbah, R., Kizilel, R., Selman, J., & Al-Hallaj, S. (2008). Active (air-cooled) vs. passive (phase change material) thermal management of high power lithium-ion packs: Limitation of temperature rise and uniformity of temperature distribution. Journal of Power Sources, 182, 630-638.

32. Tan, F., & Tso, C. (2004). Cooling of mobile electronic devices using phase change materials. Applied Thermal Engineering, 24, 159-169.

33. Abhat, A. (1976). Experimental investigation and analysis of a honeycomb-packed phase change material device. 11th Thermophysics Conference, 19.

34. Hale, D., & Hoover, M. (1971). Phase change materials handbook. Huntsville, Ala. Lockheed: Missiles and Space Company.

35. Fukusako, S., & Yamada, M. (1999). Melting heat transfer inside ducts and over external bodies. Experimental Thermal and Fluid Science, 19, 93-117.

36. Zalba, B., Marín, J., Cabeza, L., & Mehling, H. (2003). Review on thermal energy storage with phase change: Materials, heat transfer analysis and applications. Applied Thermal Engineering, 23, 251-283.

37. Kamkari, B., Shokouhmand, H., & Bruno, F. (2014). Experimental investigation of the effect of inclination angle on convection-driven melting of phase change material in a rectangular enclosure.International Journal of Heat and Mass Transfer, 72, 186-200.

38. C. Bauer & R. Wirtz. (2000). Thermal characteristics of a compact, passive thermal energy storage device, ASME IMECE, Orlando, USA.

39. Muthusivagami, R., Velraj, R., & Sethumadhavan, R. (2010). Solar cookers with and without thermal storage—A review. Renewable and Sustainable Energy Reviews, 14, 691-701.

40. Arunkumar, T., Denkenberger, D., Ahsan, A., & Jayaprakash, R. (2013). The augmentation of distillate yield by using concentrator coupled solar still with phase change material. Desalination, 314, 189-192.

41. Gu, Z., Liu, H., & Li, Y. (2004). Thermal energy recovery of air conditioning system—heat recovery system calculation and phase change materials development. Applied Thermal Engineering, 24, 2511-2526.

42. Stritih, U., & Butala, V. (2010). Experimental investigation of energy saving in buildings with PCM cold storage. International Journal of Refrigeration, 33, 1676-1683.

43. Tay, N., Belusko, M., & Bruno, F. (2015). Designing a PCM storage system using the effectiveness-number of transfer units method in low energy cooling of buildings. Energy and Buildings, 50, 234-242.

44. Liu, M., Saman, W., & Bruno, F. (2012). Development of a novel refrigeration system for refrigerated trucks incorporating phase change material. Applied Energy, 92, 336-342.

45. Fok, S., Shen, W., & Tan, F. (2010). Cooling of portable hand-held electronic devices using phase change materials in finned heat sinks. International Journal of Thermal Sciences, 49, 109-117.

46. Kandasamy, R., Wang, X., & Mujumdar, A. (2007). Application of phase change materials in thermal management of electronics. Applied Thermal Engineering, 27, 2822-2832.

47. Kim, T., Hyun, B., Lee, J., & Rhee, J. (2012). Numerical study of the spacecraft thermal control hardware combining solid–liquid phase change material and a heat pipe. Aerospace Science and Technology, 27, 10-16.

48. Swanson, T., & Birur, G. (2003). NASA thermal control technologies for robotic spacecraft. Applied Thermal Engineering, 23, 1055-1065.

49. Mondal, S. (2008). Phase change materials for smart textiles – An overview. Applied Thermal Engineering, 28, 1536-1550.

50. Khateeb, S., Amiruddin, S., Farid, M., Selman, J., & Al-Hallaj, S. (2004). Thermal management of Li-ion battery with phase change material for electric scooters: Experimental validation. Journal of Power Sources, 149, 345-353.
51. Khateeb, S., Farid, M., Selman, J., & Al-Hallaj, S. (2004). Design and simulation of a lithium-ion battery with a phase change material thermal management system for an electric scooter. Journal of Power Sources, 128, 292-307.

52. Tan, F., & Fok, S. (2007). Thermal Management of Mobile Phone using Phase Change Material. 2007 9th Electronics Packaging Technology Conference.

53. Kandasamy, R., Wang, X., & Mujumdar, A. (2006). Application of phase change materials in thermal management of electronics. Applied Thermal Engineering, 27, 2822-2832.

54. Hosseinizadeh, S., Tan, F., & Moosania, S. (2011). Experimental and numerical studies on performance of PCM-based heat sink with different configurations of internal fins. Applied Thermal Engineering, 31, 3827-3838.

55. Mahmoud, S., Tang, A., Toh, C., Al-Dadah, R., & Soo, S. (2013). Experimental investigation of inserts configurations and PCM type on the thermal performance of PCM based heat sinks. Applied Energy, 112, 1349-1356.

56. Oró, E., Miró, L., Farid, M., & Cabeza, L. (2012). Thermal analysis of a low temperature storage unit using phase change materials without refrigeration system. International Journal of Refrigeration, 35 (6), 1709-1714.

57. Liu, M., Saman, W., & Bruno, F. (2012). Development of a novel refrigeration system for refrigerated trucks incorporating phase change material. Applied Energy, 92, 336-342.

58. Jankowski, N., & Mccluskey, F. (2014). A review of phase change materials for vehicle component thermal buffering. Applied Energy, 113, 1525-1561.

59. Hasan, A., Mccormack, S., Huang, M., & Norton, B. (2014). Characterization of phase change materials for thermal control of photovoltaics using Differential Scanning Calorimetry and Temperature History Method. Energy Conversion and Management, 81, 322-329.

60. Lu, T. (2000). Thermal management of high power electronics with phase change cooling. International Journal of Heat and Mass Transfer, 43 (13), 2245-2256.

61. Krishnan, S., Garimella, S., & Kang, S. (2003). A novel hybrid heat sink using phase change materials for transient thermal management of electronics. The Ninth Intersociety Conference on Thermal and Thermo-mechanical Phenomena in Electronic Systems (IEEE Cat. No.04CH37543).

62. Lacroix, M., & Benmadda, M. (1997). Numerical Simulation of Natural Convection-Dominated Melting and Solidification from a Finned Vertical Wall. Numerical Heat Transfer, Part A: Applications, 31, 71-86.

63. Shanmugasundaram, V., Brown, J., Yerkes, K., Shanmugasundaram, V., Brown, J., & Yerkes, K. (1997). Thermal management of high heat-flux sources using phase change materials - A design optimization procedure. 32nd Thermophysics Conference, 97, 2451-2463.

64. Akhilesh, R., Narasimhan, A., & Balaji, C. (2005). Method to improve geometry for heat transfer enhancement in PCM composite heat sinks. International Journal of Heat and Mass Transfer, 48 (13), 2759-2770.

65. Hajmohammadi, M., Poozesh, S., & Hosseini, R. (2012). Radiation Effect on Constructal Design Analysis of a T-Y-Shaped Assembly of Fins. JTST Journal of Thermal Science and Technology, 7 (4), 677-692.

66. Leland, J., & Recktenwald, G. (2003). Optimization of a phase change heat sink for extreme environments. Ninteenth Annual IEEE Semiconductor Thermal Measurement and Management Symposium, 351-356.

67. Shatikian, V., Ziskind, G., & Letan, R. (2005). Numerical investigation of a PCM-based heat sink with internal fins. International Journal of Heat and Mass Transfer, 48 (17), 3689-3706.

68. Shatikian, V., Ziskind, G., & Letan, R. (2008). Numerical investigation of a PCM-based heat sink with internal fins: Constant heat flux. International Journal of Heat and Mass Transfer, 51, 1488-1493.

69. Balaji, C., Mungara, P., & Sharma, P. (2011). Optimization of size and shape of composite heat sinks with phase change materials. Heat and Mass Transfer Heat Mass Transfer, 47 (5), 597-608.

70. Levin, P., Shitzer, A., & Hetsroni, G. (2013). Numerical optimization of a PCM-based heat sink with internal fins. International Journal of Heat and Mass Transfer, 61, 638-645.

71. Steinke, M., & Kandlikar, S. (2004). Single-Phase Liquid Friction Factors in Microchannels. ASME 3rd International Conference on Microchannels and Minichannels, Parts A and B, 56.

72. Peng, X., & Peterson, G. (1995). The effect of thermofluid and geometrical parameters on convection of liquids through rectangular microchannels. International Journal of Heat and Mass Transfer, 38 (4), 755-758.

73. Wu, H., & Cheng, P. (2003). An experimental study of convective heat transfer in silicon microchannels with different surface conditions. International Journal of Heat and Mass Transfer, 2547-2556.

74. Steinke, M., & Kandlikar, S. (2006). Single-Phase Liquid Friction Factors in Microchannels. ASME 3rd International Conference on Microchannels and Minichannels, Parts A and B, 45.

75. Sharma, A., Tyagi, V., Chen, C., & Buddhi, D. (2009). Review on thermal energy storage with phase change materials and applications. Renewable and Sustainable Energy Reviews, 13, 318-345.

76. Khudhair, A., & Farid, M. (2004). A review on energy conservation in building applications with thermal storage by latent heat using phase change materials. Energy Conversion and Management, 45 (9), 263-275.

77. Biswas, D. (1977). Thermal energy storage using sodium sulfate decahydrate and water. Solar Energy, 19, 99-100.

78. M Telkes. (1952). Nucleation of super saturated inorganic salt solution Indust. Eng. Chem., 44, 1308.

79. Farid, M., & Kanzawa, A. (1989). Thermal Performance of a Heat Storage Module Using PCM's With Different Melting Temperatures: Mathematical Modeling. Journal of Solar Energy Engineering J. Sol. Energy Eng., 111, 152-152.

80. Farid, M., & Mohamed, A. (1987). Effect Of Natural Convection On The Process Of Melting And Solidification Of Paraffin Wax. Chemical Engineering Communications, 57, 297-316.

81. Hasnain, S. (1987). Review on sustainable thermal energy storage technologies, Part II: Cool thermal storage. Energy Conversion and Management, 57, 1139-1153.

82. H. Mehling, S. Hiebler, S. Ziegler (1999). Latent heat storage using a PCM-graphite composite material: advantages and potential applications, In: Proceedings of the 4th Workshop of IEA ECES IA Annex 10, Bendiktbeuern, Germany.

83. M. Kamimoto, Y. Abe, K. Kanari, S. Swata, T. Tani, T. Ozawa. (1986). Heat Transfer in Latent Heat Thermal Storage Units Using Pentarythritol Slurry, Thermal Energy Storage World Congress of Chemical Engineering, Tokyo, Japan .

84. RT-42 Data sheet (Paraffin wax), Retrieved August 6, 2015, from http://www.rubitherm.eu/index.php/produkte/rt-42.

85. SP-29 Data sheet (Salt Hydrate hexahedra), Retrieved August 27, 2015, from http://www.rubitherm.eu/index.php/produkte/SP-29.

86. Fearon, A. BUTTER: Properties and Analysis. Food Chemistry, 498-545.

87. RCHB-10-ND (Heat Generator), Retrieved January 12, 2015, from http://www.vishay.com.

88. Tgrease-2500 (Thermal Grease), Retrieved September 25, 2015, from http://www.lairdtech.com/thermal.
    259-1547-ND (Fan 40 x 10 mm), Retrieved September 27, 2015, from http://www.sunon.com.

89. TP-29 (Thermocouple), Retrieved June 2, 2015, from http://www.bkprecision.com.

90. NI-9213 (Thermocouples DAQ), Retrieved August 14, 2015, from http://www.sine.ni.com/nips/cds/view/p/lang/en

91. ANSYS fluent software- Material and chemical processing, Retrieved September 25, 2015, from http://www.ansys.com/products/Simulation&Technology/ANSYSmaterial.

92. Cengel, Y. (2007). Heat and mass transfer: A practical approach (3rd ed.). Boston: McGraw-Hill

Appendix 1

LABVIEW Software Program

1- Block Diagram

The working window where the program is prepared. Ready used DAQ Assistance icon is connected to array of thermocouple indicators. Then, the system is connect to Excel program to record the table and farther analysis.
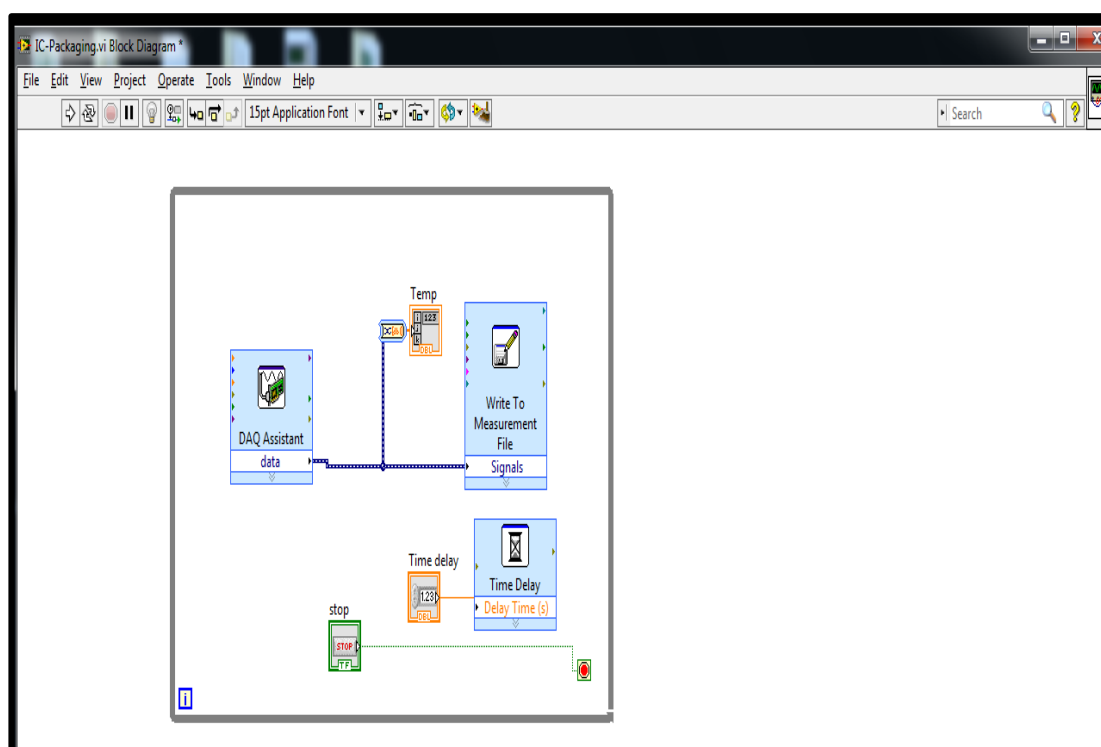
2- Front Panel

The user window where the user can monitor and control the program. The temperatures are measured in Celsius
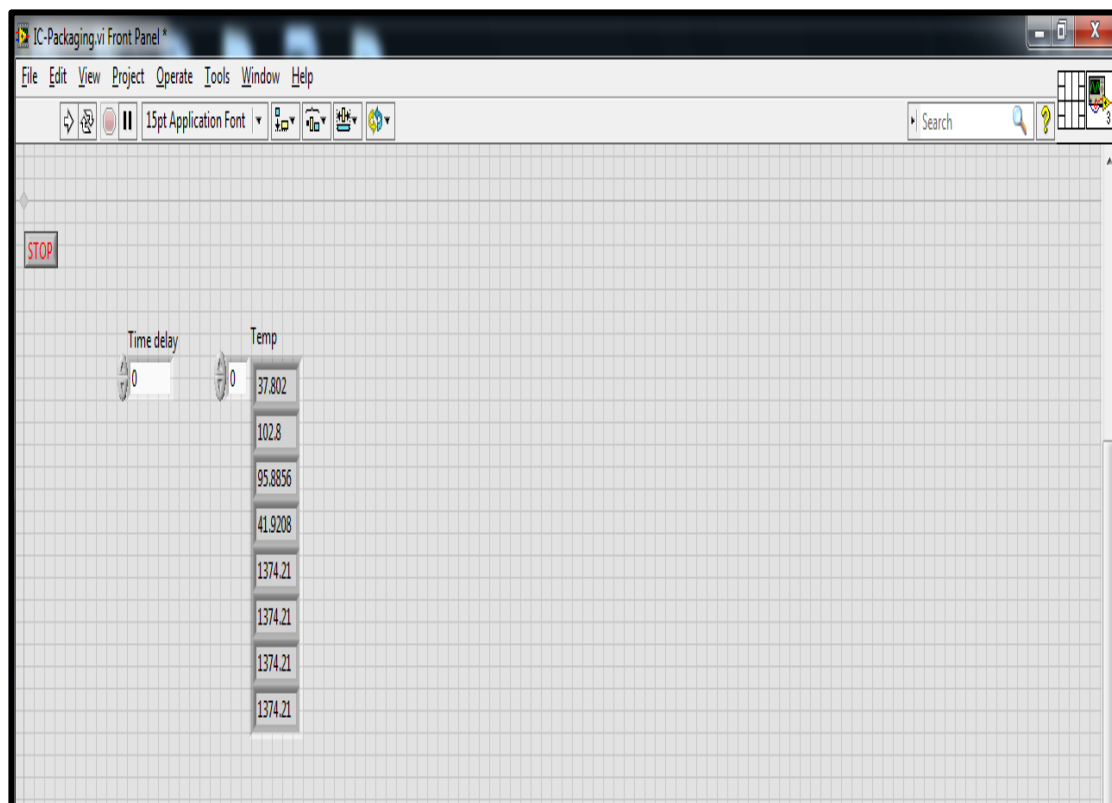
Appendix 2

Table of Air

Temperature			Density	Volumetric thermal expansivity	Heat Capacity	Conductivity	Dynamic Viscosity	Kinematic viscosity	Prandtl
T			ρ	β	C_p	k	μ	v	Pr
[C]	[F]	[K]	$\left[\dfrac{Kg}{m^3}\right]$	$\left[\dfrac{1}{K}\right]10^{-3}$	$\left[\dfrac{J}{Kg \cdot K}\right]$	$\left[\dfrac{W}{m \cdot K}\right]$	$\dfrac{[Pa \cdot s]}{10^6}$	$\dfrac{[m^2/s]}{10^6}$	
0	32	273	1,293	3,664	1003,9	0,02417	17,17	13,28	0,713
5	41	278	1,269	3,598	1004,3	0,02445	17,35	13,67	0,713
10	50	283	1,242	3,533	1004,6	0,02480	17,58	14,16	0,712
15	59	288	1,222	3,470	1004,9	0,02512	17,79	14,56	0,712
20	68	293	1,202	3,412	1005,2	0,02544	18,00	14,98	0,711
25	77	298	1,183	3,354	1005,4	0,02577	18,22	15,40	0,711
30	86	303	1,164	3,298	1005,7	0,02614	18,46	15,86	0,710
35	95	308	1,147	3,244	1006,0	0,02650	18,70	16,30	0,710
40	104	313	1,129	3,193	1006,3	0,02684	18,92	16,76	0,709
45	113	318	1,111	3,142	1006,6	0,02726	19,19	17,27	0,709
50	122	323	1,093	3,094	1006,9	0,02761	19,42	17,77	0,708
55	131	328	1,079	3,048	1007,3	0,02801	19,68	18,24	0,708
60	140	333	1,061	3,003	1007,7	0,02837	19,91	18,77	0,707
65	149	338	1,047	2,957	1008,0	0,02876	20,16	19,26	0,707
70	158	343	1,030	2,914	1008,4	0,02912	20,39	19,80	0,706
75	167	348	1,013	2,875	1008,8	0,02945	20,60	20,34	0,706
80	176	353	1,001	2,834	1009,3	0,02979	20,82	20,80	0,705
85	185	358	0,986	2,795	1009,8	0,03012	21,02	21,32	0,705
90	194	363	0,972	2,755	1010,3	0,03045	21,23	21,84	0,704
95	203	368	0,959	2,718	1010,7	0,03073	21,41	22,33	0,704
100	212	373	0,947	2,683	1011,2	0,03101	21,58	22,79	0,704

Appendix 3

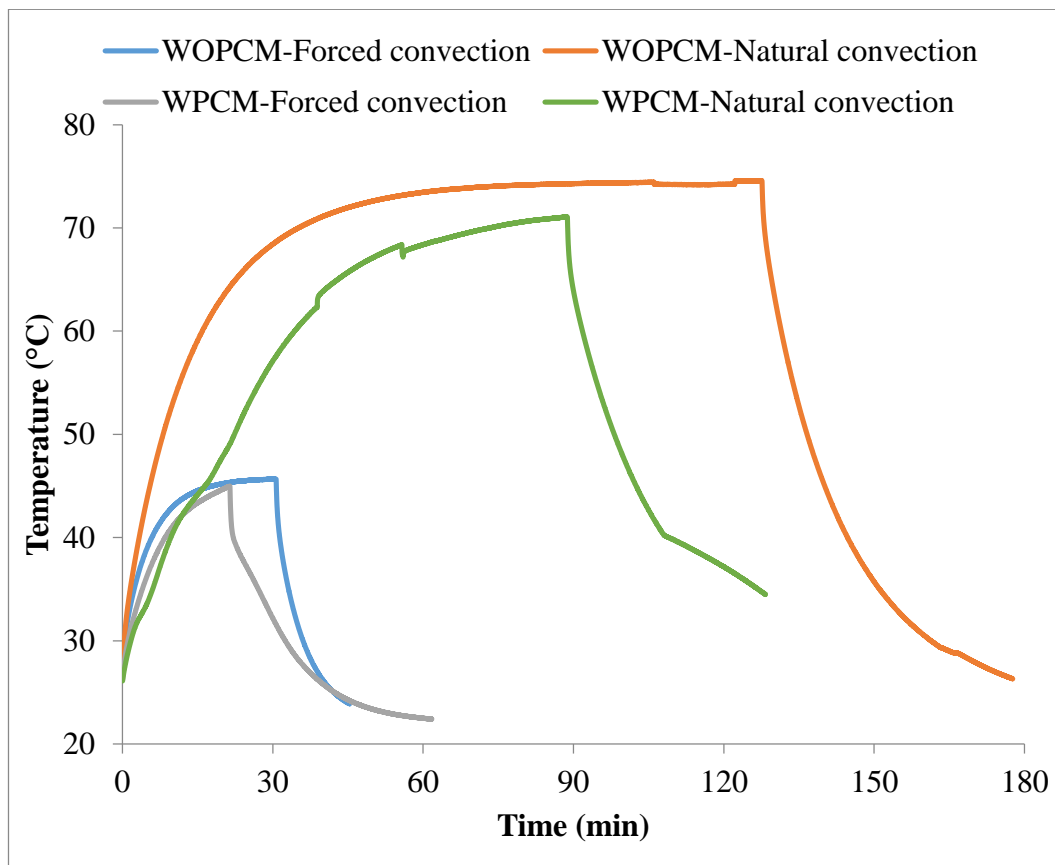**1- The Temperature Evaluation For Heat Sink, For power input = 4 W**

Figure 53: The temperature evaluation for heat sink filled with paraffin wax compared to the reference case heat sink without PCM subjected to heat input 4W under natural convection and forced convection
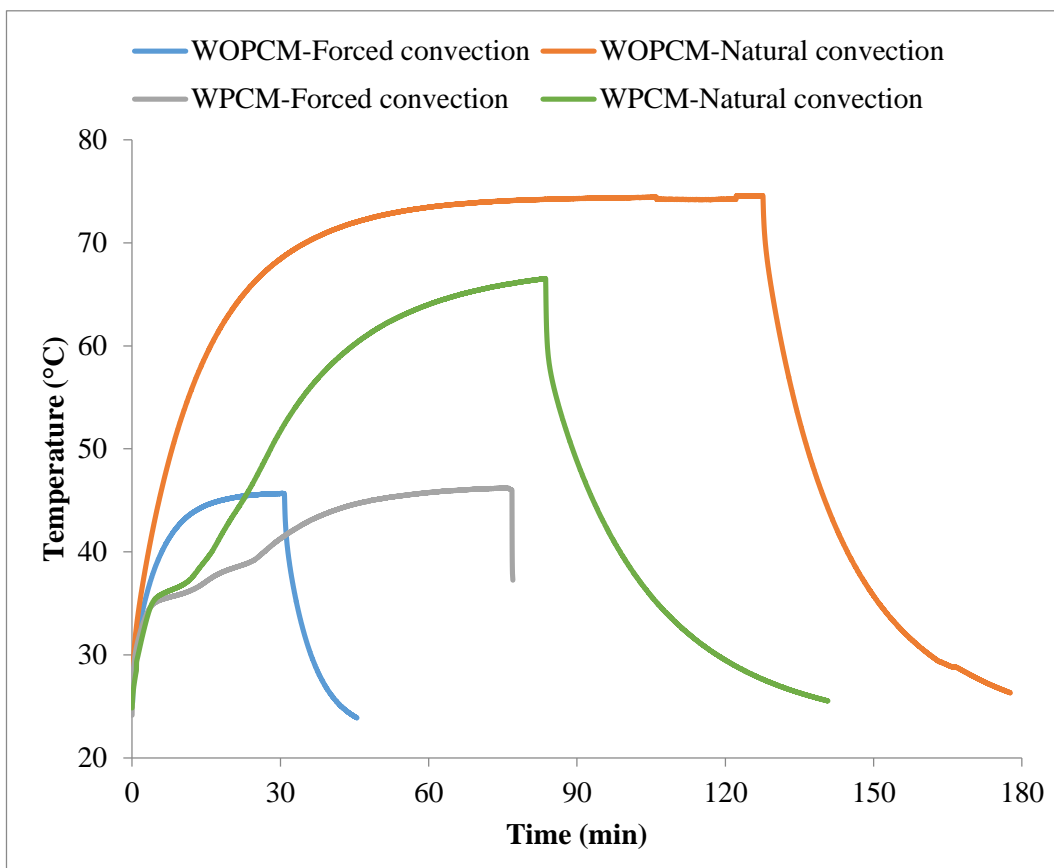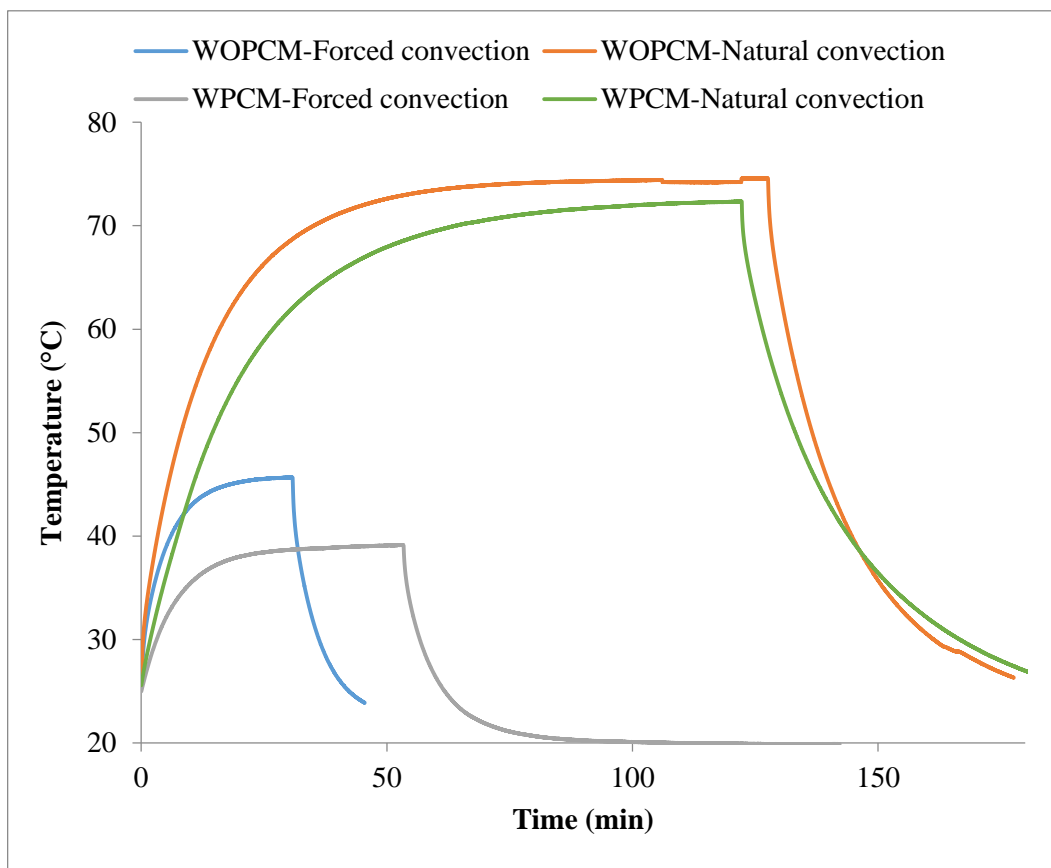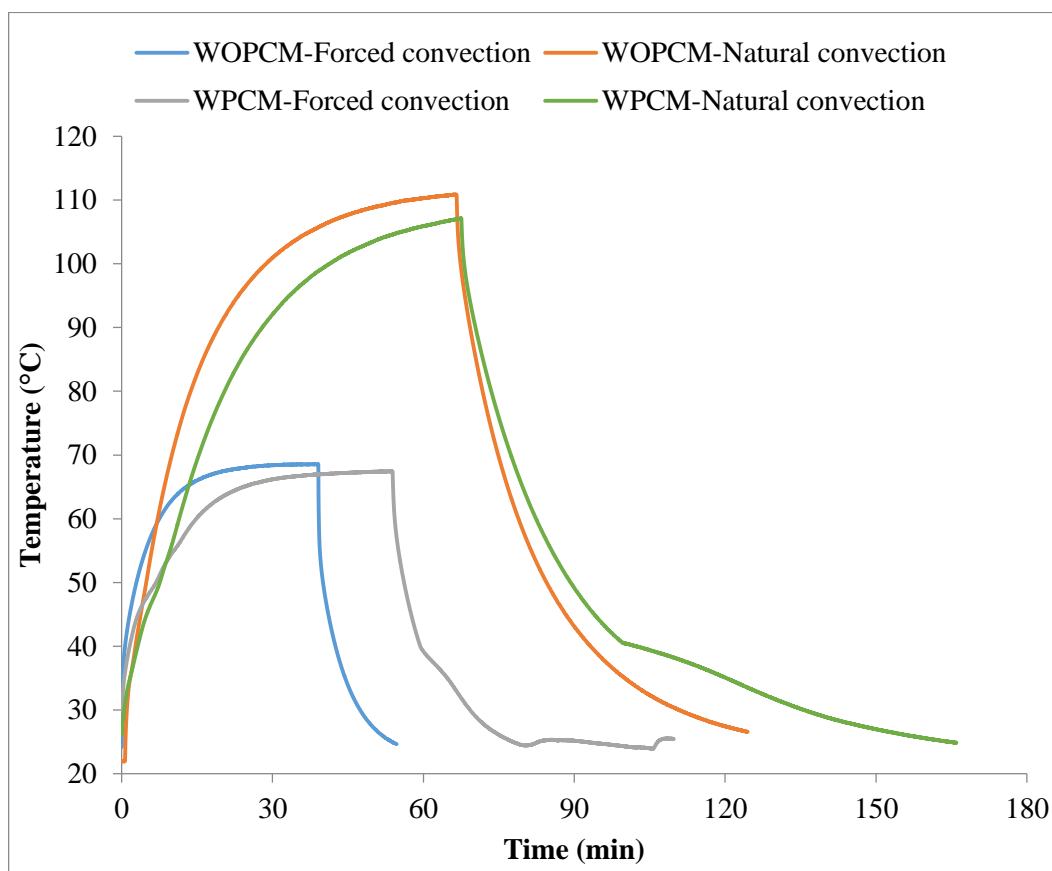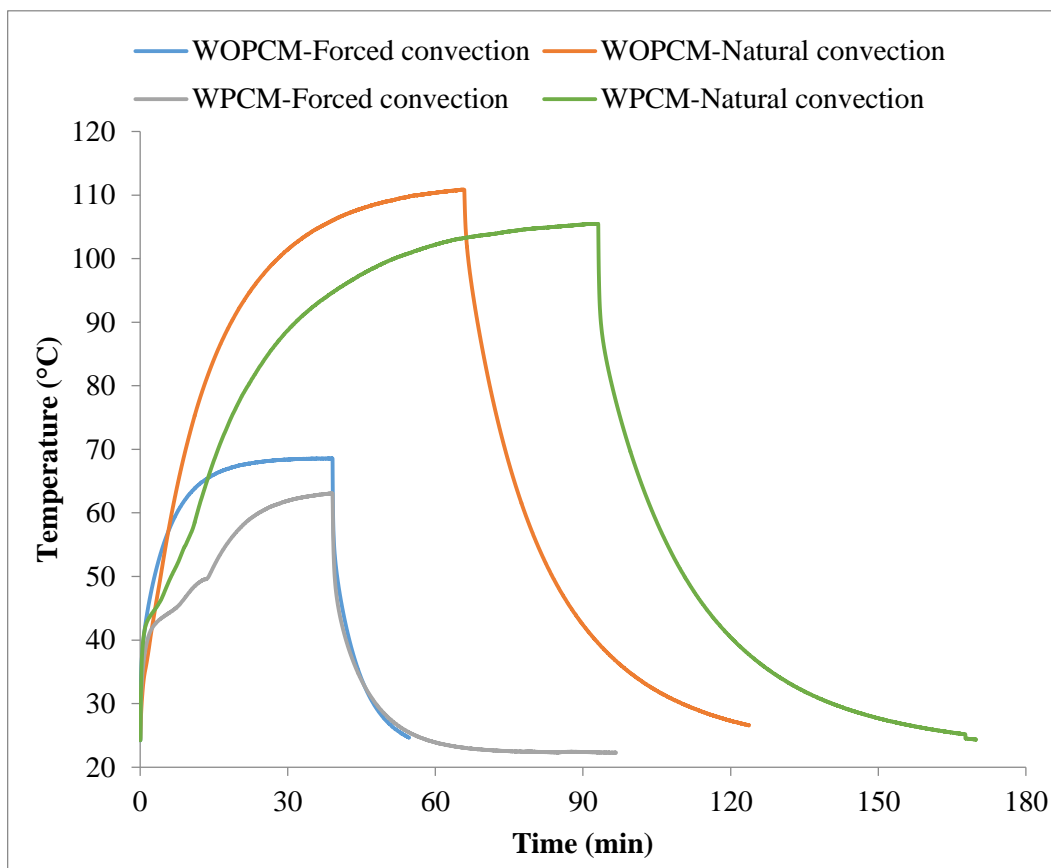
Figure 54: The temperature evaluation for heat sink filled with Calcium chloride hydrate compared to the reference case heat sink without PCM subjected to heat input 4W under natural convection and forced convection
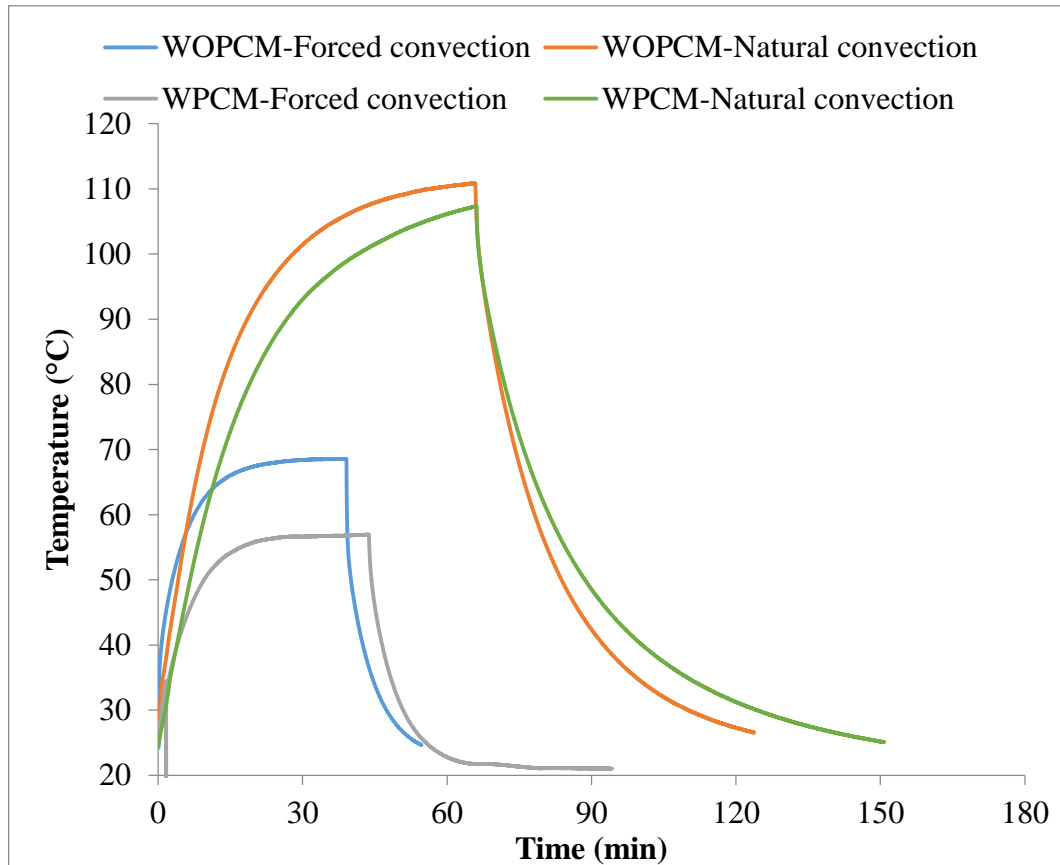
Figure 55: The temperature evaluation for heat sink filled with Milk-fat compared to the reference case heat sink without PCM subjected to heat input 4W under natural convection and forced convection

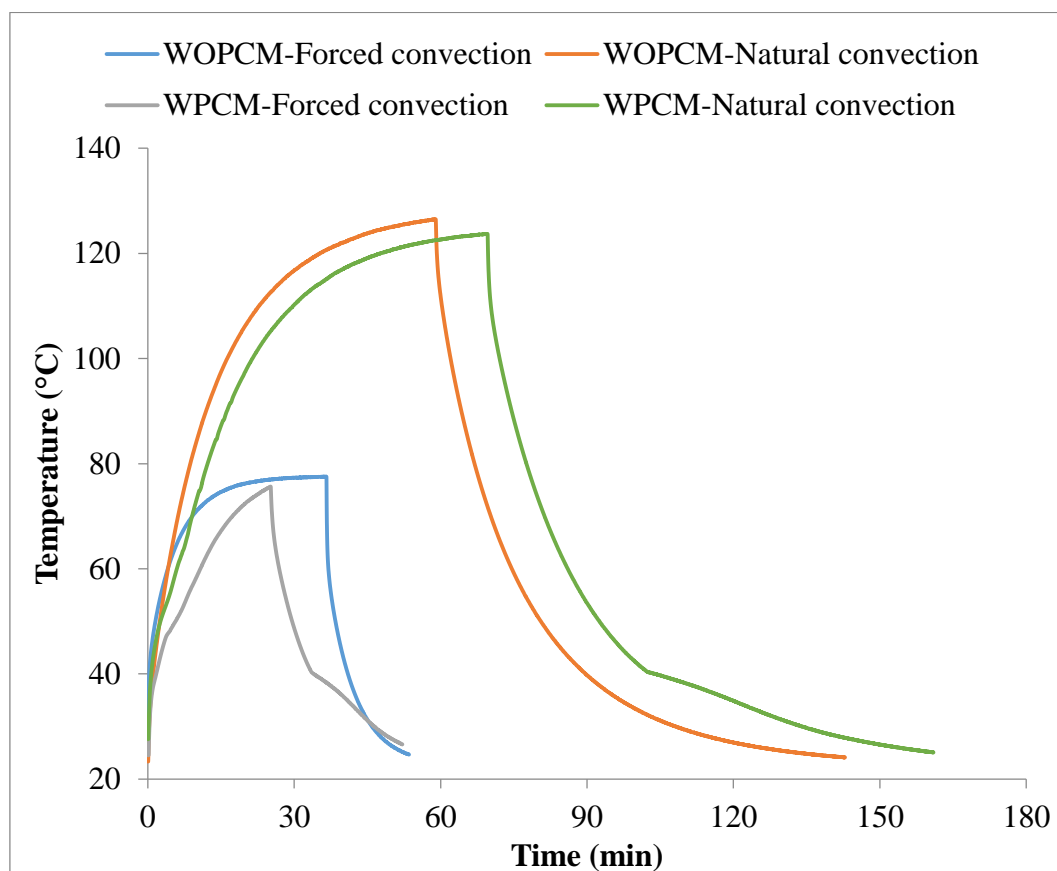**2- The Temperature Evaluation For Heat Sink, For power input = 8 W**

Figure 56: The temperature evaluation for heat sink filled with paraffin wax compared to the reference case heat sink without PCM subjected to heat input 8W under natural convection and forced convection
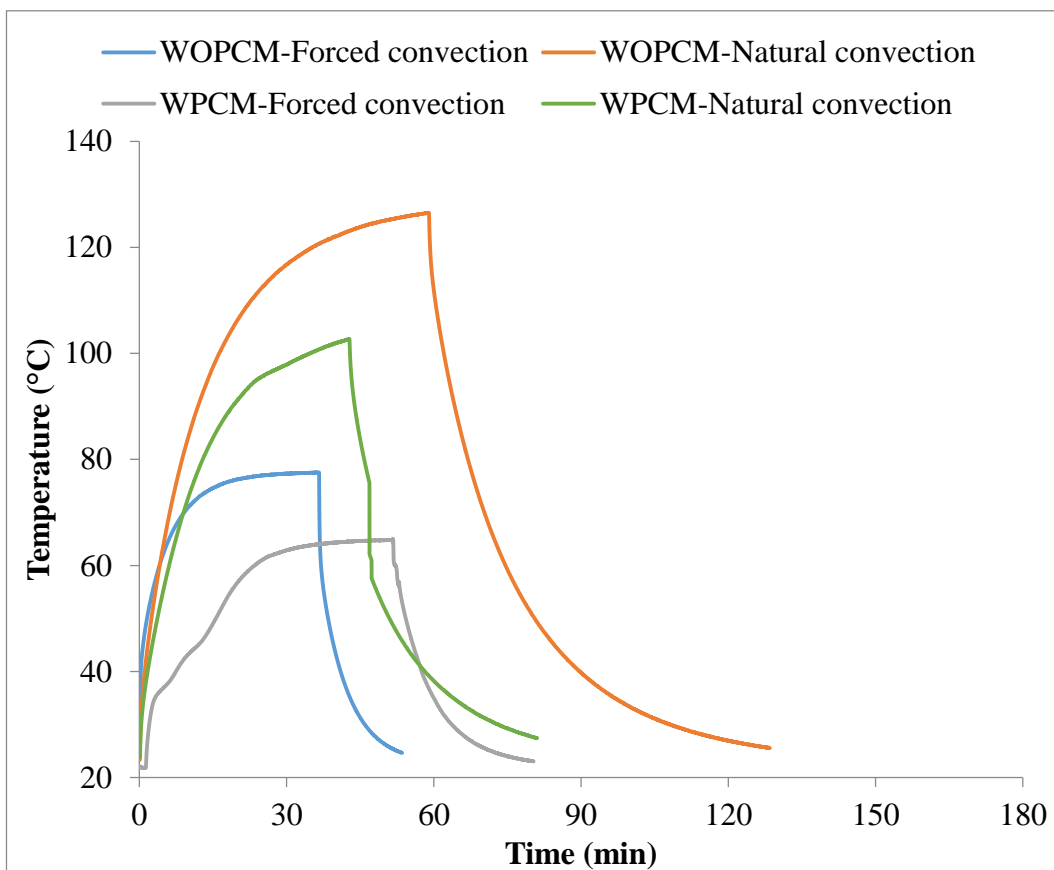
Figure 57: The temperature evaluation for heat sink filled with Calcium chloride hydrate compared to the reference case heat sink without PCM subjected to heat input 8W under natural convection and forced convection
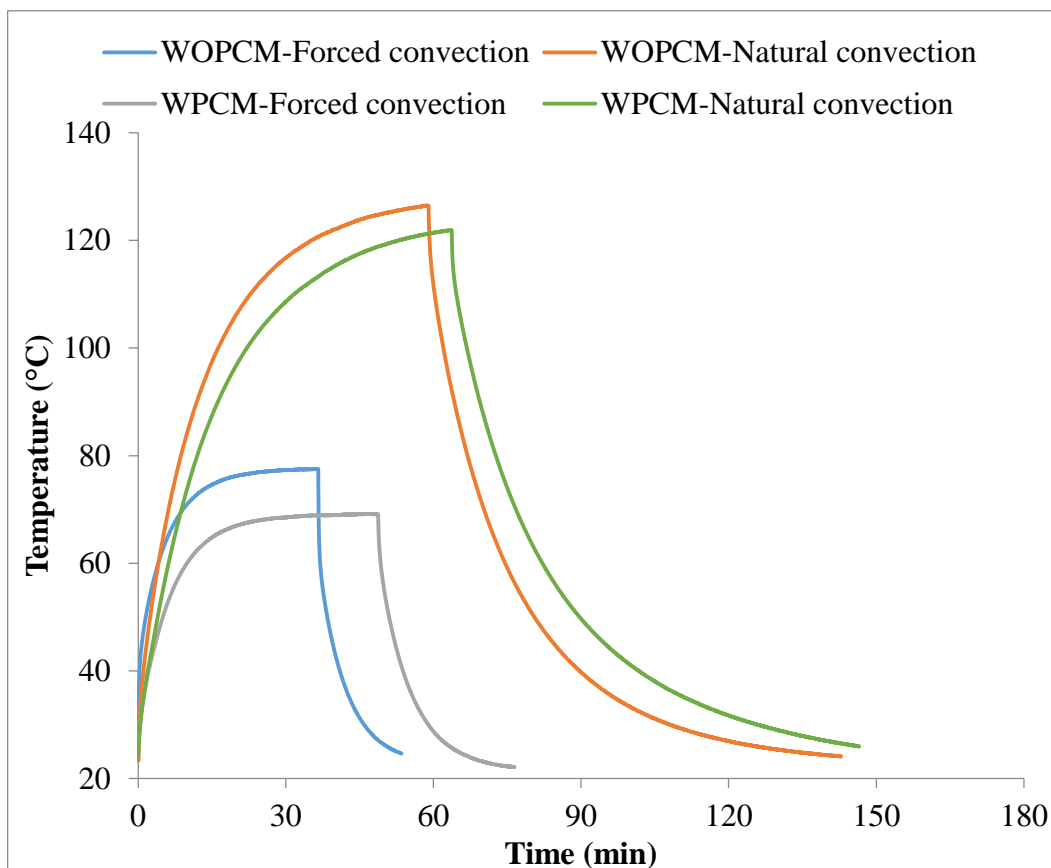
Figure 58: The temperature evaluation for heat sink filled with Milk-fat compared to the reference case heat sink without PCM subjected to heat input 8W under natural convection and forced convection.

3-   The Temperature Evaluation For Heat Sink, For power input = 10 W

Figure 59: The temperature evaluation for heat sink filled with paraffin wax compared to the reference case heat sink without PCM subjected to heat input 10W under natural convection and forced convection

Figure 60: The temperature evaluation for heat sink filled with Calcium chloride hydrate compared to the reference case heat sink without PCM subjected to heat input 10W under natural convection and forced convection.

Figure 61: The temperature evaluation for heat sink filled with Milk-fat compared to the reference case heat sink without PCM subjected to heat input 10W under natural convection and forced convection

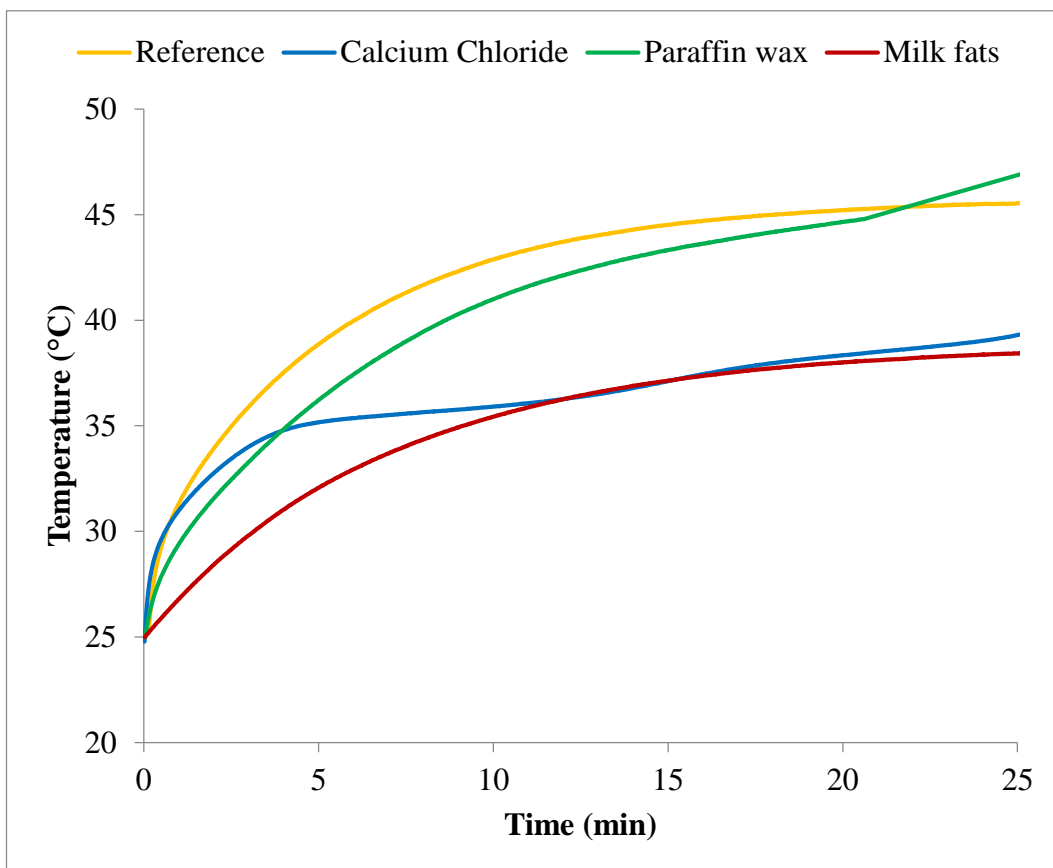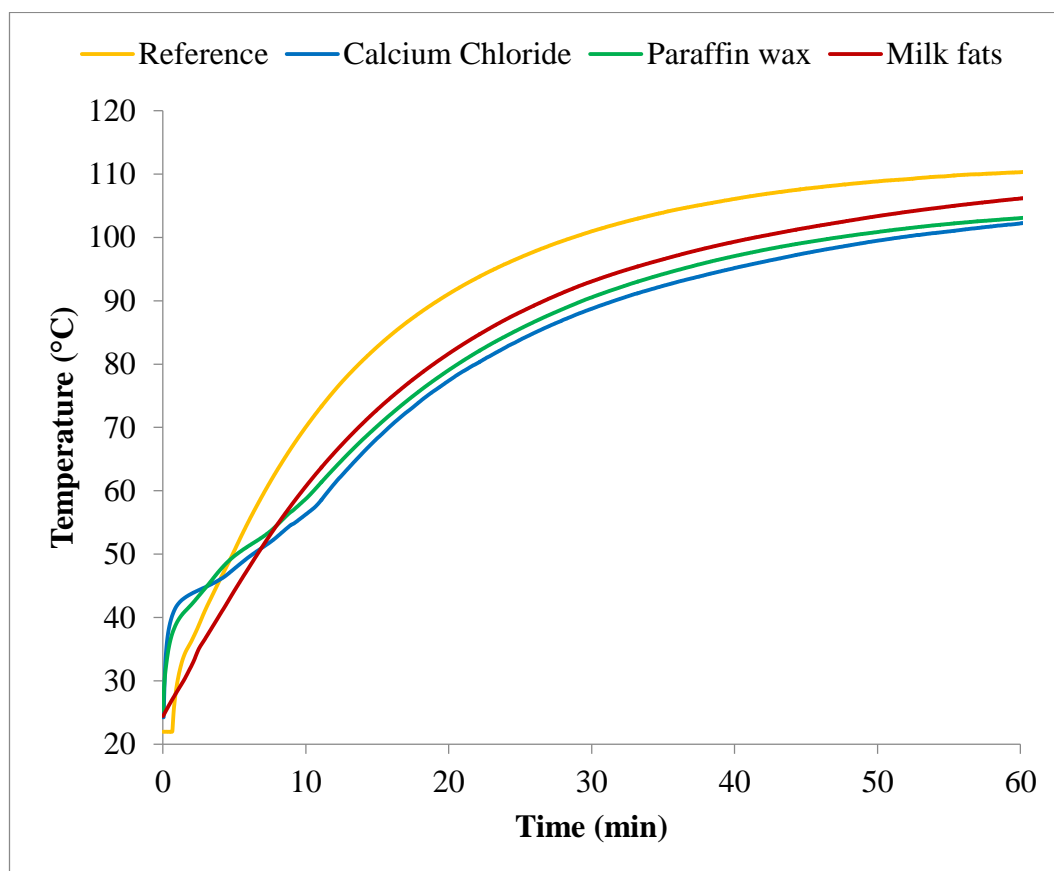**4-   The heating curves for heat sink filled with PCMs, For power input =4W**
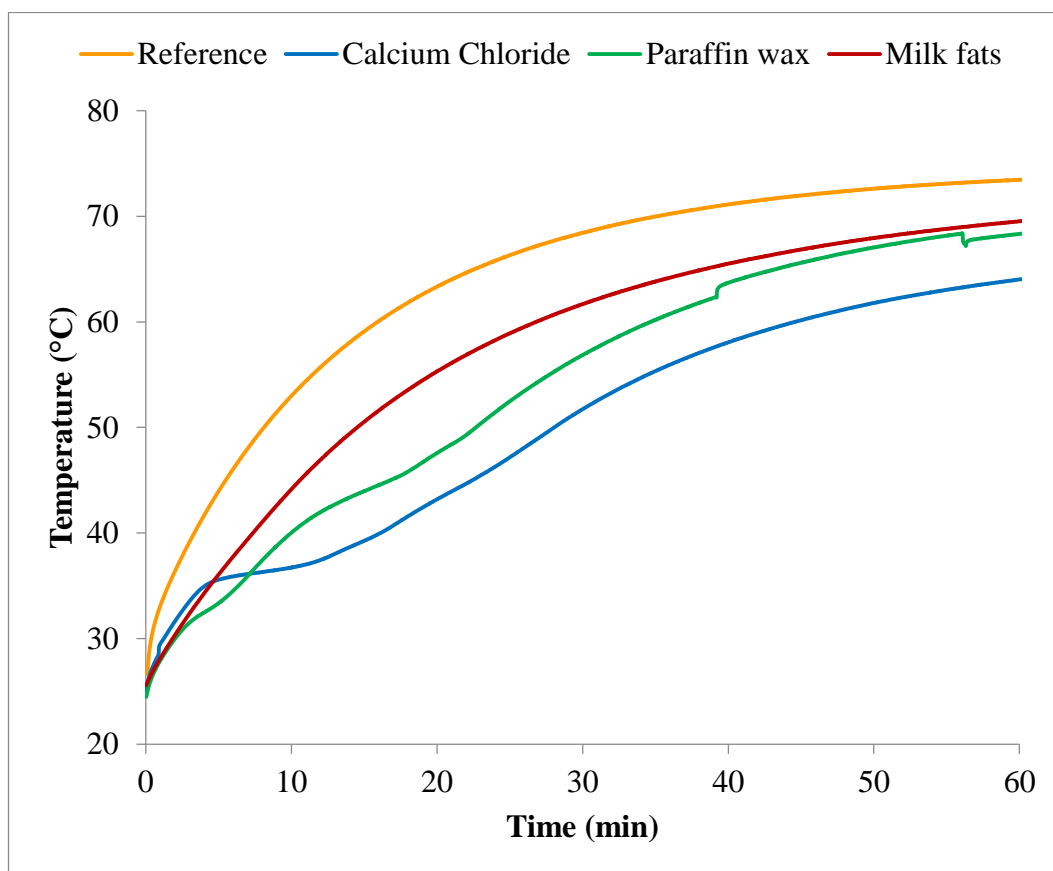
Figure 62: The heating curves for heat sink filled with three PCMs, namely Salt hydrate, Paraffin wax and Milk fats compared to the reference case heat sink without PCM subjected to heat input 4W under natural convection

Figure 63: The heating curves for heat sink filled with three PCMs, namely Salt hydrate, Paraffin wax and Milk fats compared to the reference case heat sink without PCM subjected to heat input 4W under forced convection

5- The heating curves for heat sink filled with PCMs, for Power input =8 W

Figure 64: The heating curves for heat sink filled with three PCMs, namely Salt hydrate, Paraffin wax and Milk-fat compared to the reference case heat sink without PCM subjected to heat input 8W under natural convection
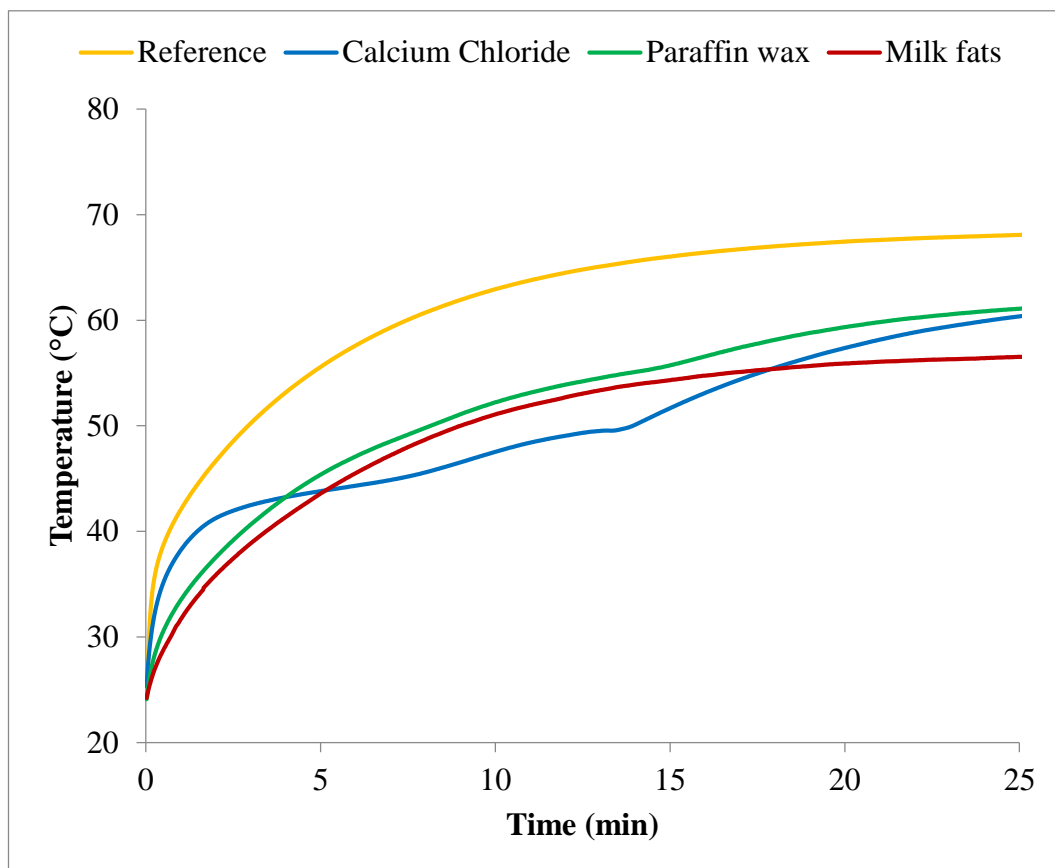
Figure 65: The heating curves for heat sink filled with three PCMs, namely Salt hydrate, Paraffin wax and Milk-fat compared to the reference case heat sink without PCM subjected to heat input 8W under forced convection
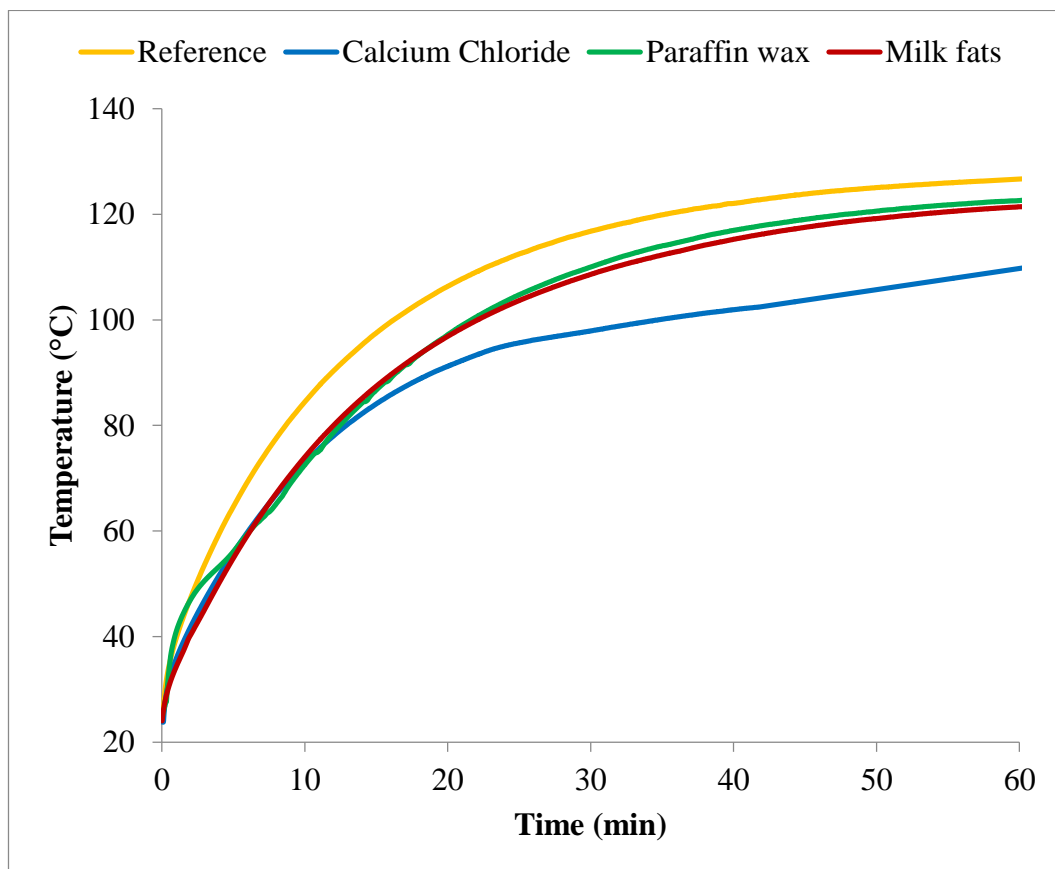
6- The heating curves for heat sink filled with PCMs, For power input =10 W

Figure 66: The heating curves for heat sink filled with three PCMs, namely Salt hydrate, Paraffin wax and Milk-fat compared to the reference case heat sink without PCM subjected to heat input 10W under natural convection
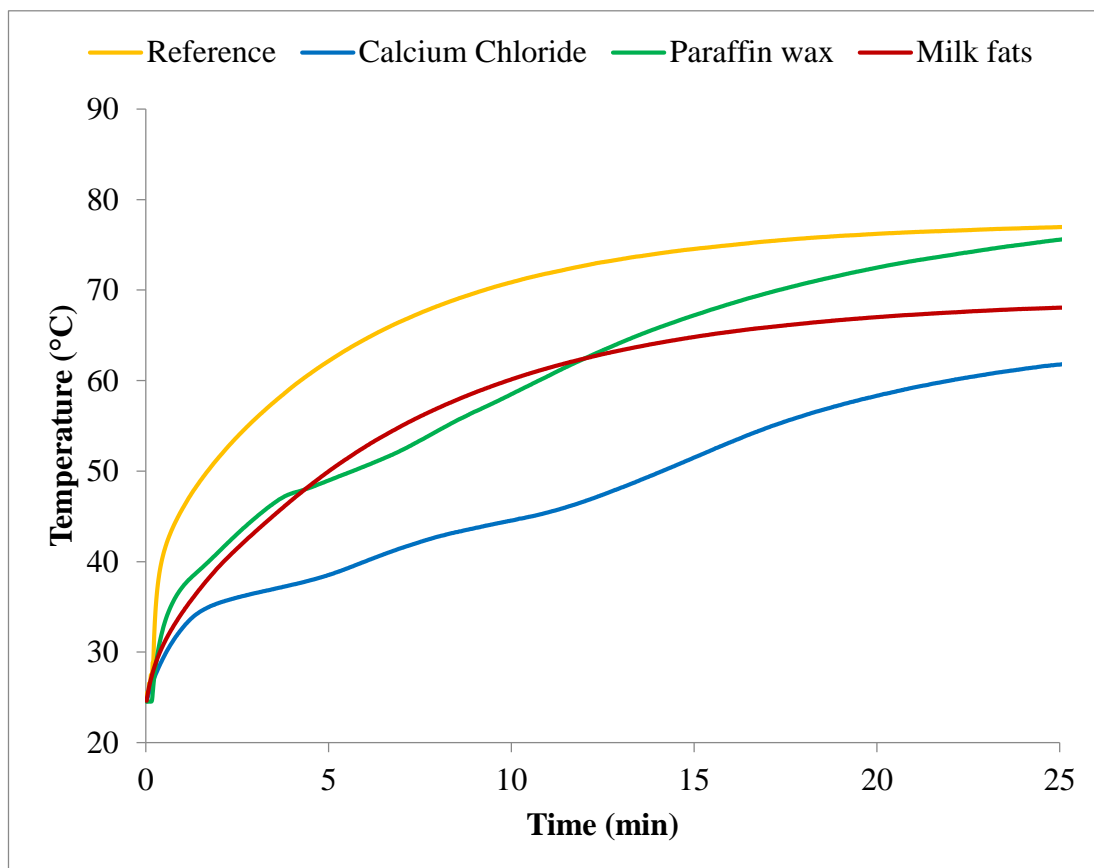
Figure 67: The heating curves for heat sink filled with three PCMs, namely Salt hydrate, Paraffin wax and Milk-fat compared to the reference case heat sink without PCM subjected to heat input 10W under forced convection